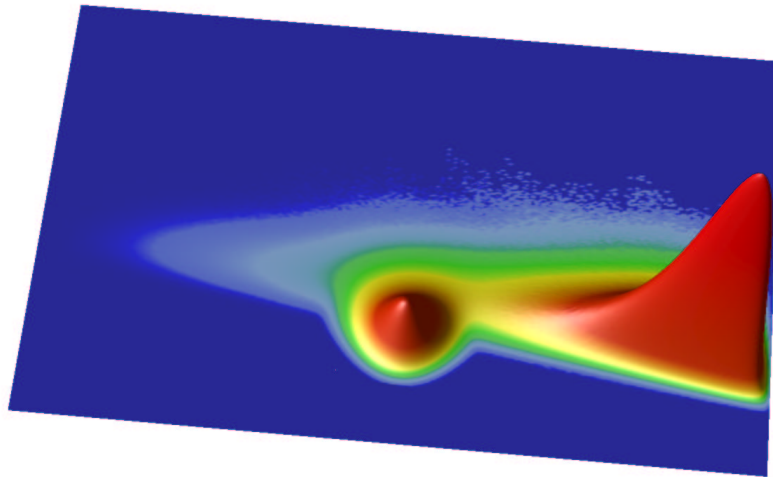


Phase transitions in magnetic clusters and other finite systems



Am Fachbereich Physik
der Universität Oldenburg
zur Erlangung des Grades eines

Doktors der Naturwissenschaften (Dr. rer. nat.)

angenommene Dissertation von

Heinrich Wilhelm Stamerjohanns

geboren am 6. Juni 1968
in Brake/Unterweser.

Erstreferent:

Prof. Dr. Dr. Eberhard R. Hilf

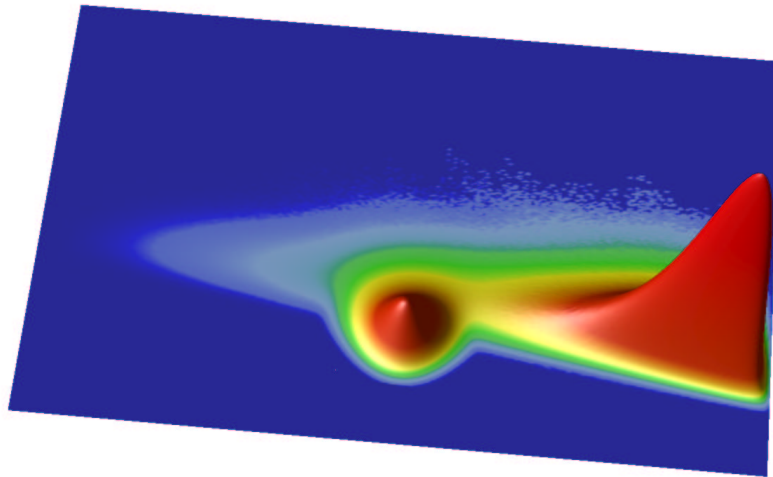
Korreferentin:

Prof. Dr. Jutta Kunz-Drolshagen

Tag der Disputation:

30. November 2001

Phase transitions in magnetic clusters and other finite systems



Am Fachbereich Physik
der Universität Oldenburg
zur Erlangung des Grades eines

Doktors der Naturwissenschaften (Dr. rer. nat.)

angenommene Dissertation von

Heinrich Wilhelm Stamerjohanns

geboren am 6. Juni 1968
in Brake/Unterweser.

Erstreferent:

Prof. Dr. Dr. Eberhard R. Hilf

Korreferentin:

Prof. Dr. Jutta Kunz-Drolshagen

Tag der Disputation:

30. November 2001

Preface

This dissertation is of cumulative type and consists of seven papers dealing with phase transitions of magnetic clusters or other finite systems which have been published in, accepted by, or submitted to major physics journals.

The main topic of all papers is the investigation and identification of thermodynamic phase transitions in various finite systems. We show that phase transitions in finite systems, which can be experimentally seen only in floppy humps of the specific heat or the magnetic susceptibility, can be quantitatively described by an analysis of an optimized estimation of the probability distribution of the system states combined with Landau free energy, or by analyzing the partition function in complex time, or other complex-time response functions such as the complex specific heat.

We show that new efficient methods, such as the Ferrenberg analysis, not applicable to infinite systems, can be applied to finite systems, even if the systems have more than one external parameter. With an Optimized Multidimensional Data Analysis of histograms produced by canonical Monte Carlo simulations, we are able to compute the phase behaviour of finite magnetic systems over a wide temperature and magnetic field range just by determining observables at a few given temperatures and magnetic fields.

Specifically, in Chapter II-1, we present a new method to determine potential and kinetic energies of atomic clusters directly from experimental scattering spectra. We use Path Integral Monte Carlo Simulations and an Optimized Data Analysis to compute pair correlation functions for ‘experimental’ scattering spectra. From the scattering functions generated in these simulations we have calculated the caloric curves and compare them with the exact results from the simulations [1].

With numerical simulations we investigate in Chapters II-2 to II-4 the phase behaviour of clusters consisting of a few magnetic nanoparticles, which are dissolved in a suspension, called ferrofluids. With a multidimensional Optimized Data Analysis we determine the potential energy surface with two stable isomers and show how the nature of a phase transition can be tuned by the variation of the external parameters, the magnetic field B and the temperature T [2–4].

We address in Chapter II-5 the classification of the phase transition of a finite number of non-interacting bosons in a power-law trap within a semi-analytic approach with

a continuous one-particle density of states $\Omega(E) \approx E^{d-1}$ [5]. We use the classification scheme based on the distribution of zeros of the canonical partition function by GROSSMANN *et al.* [8] and FISCHER *et al.* [9] which has been extended by BORRMANN *et al.* [10] as a classification scheme for small systems.

Among others GROSS *et al.* have suggested a microcanonical treatment [11–13] where phase transitions of different order can be distinguished by the curvature of the entropy $S = \ln \Omega(E)$, where $\Omega(E)$ is the density of states. In Chapter II-6, we compare these classification schemes by means of a Multiple Normal Modes model and show that transitions in these systems can only completely be understood by considering the whole complex temperature plane [6].

In Chapter II-7 we use a simple statistical model for small magnetic clusters to show that the common indicators of phase transitions like the magnetic susceptibility or the specific heat might eventually cause misleading interpretations of the underlying physics [7].

An introduction to the issues raised in the articles, which is meant to be a introduction for the more interested general reader is presented in the first Part. I will shortly discuss clusters and present some examples of the systems used in the articles. I will also give an outline of the numerical methods that have been used in these articles in Chap. 2. There I will concentrate on an Optimized Data Analysis, because this method has not been mentioned in detail in the papers dealing with phase transition of ferrofluid clusters. An overview about the identification of phase transitions in finite systems follows in Chap. 3.

All papers presented here have been written in teamwork with current and former members of the group Smallsystems of PD Dr. Peter Borrmann, three papers (the second, third and fourth one) have been done in good collaboration with the group of Prof. Dr. David Tománek at the Michigan State University. For these papers most of the numerical work has been performed in Oldenburg, while the quaternion Molecular Dynamics have been done by the group at MSU. All Monte Carlo simulations and the implementation of an Optimized Data Analysis have been done by myself.

The papers *Temperature measurement from scattering spectra of cluster. Theoretical treatment* (Z. Phys. D **40**, 190 (1997); see Chap. II-1) and *Self-assembly of magnetic nanostructures* (Z. Phys. D **40**, 539 (1997); see Chap. II-2) were included in my diploma thesis, because they had already been published by that time. The articles *Thermodynamics of finite magnetic two-isomer systems* (J. Chem. Phys. **111**, 10689 (1999); see Chap. II-3) and *Paradoxical magnetic cooling in a structural transition model* (E. Phys. J. B, **19**, 117 (2001); see Chap. II-4) are successions from that work and have been published later.

While in the paper *Classification of phase transitions of finite Bose-Einstein condensates in power-law traps by Fisher zeros* (Phys. Rev. A **64**, 013611 (2001); see Chap. II-5) my contribution to the paper is confined to a search algorithm for zeros in the com-

plex plane and support for the graphical representations of the results, my contribution to the other papers was the production, analysis and interpretation of results and its textual and graphical representation.

The calculations for the articles *The Origins of Phase Transitions in Small Systems* (Phys. Rev. E (2001) in press; see Chap. II-6) and *Deceptive Signals of phase transitions in Small Magnetic Clusters* (submitted; see Chap. II-7) have been done in equal portions by Oliver Mülken and me, the articles were written in teamwork by all authors.

I thank Ebs Hilf and Peter Borrmann for a long lasting mentorship. Their ideas, prolific discussions and useful suggestions have always been productive. Further I am grateful to my collaborators David Tománek, Habbo Heinze and especially Jens Harting and Oliver Mülken, because it is just fun to work in such an environment.

I also thank the *Regionales Rechenzentrum für Niedersachsen in Hannover* for excellent support and the possibility to use uncounted hours of CPU time on the Crays in Hannover and Berlin.

Contents

Preface	III
I Introduction	1
1 Clusters	2
1.1 Rare-Gas Clusters	3
1.2 Ferrofluid-Clusters	4
2 Numerical Methods	8
2.1 Molecular Dynamics	8
2.2 MC-Methods	9
2.3 Multiple Normal Modes Model	9
2.4 Optimized Data Analysis	11
3 Phase Transitions	17
3.1 Identification of Phase Transitions	17
3.2 Zeros of the Partition Function	19
3.3 Other classification schemes	22
4 Conclusion	26
5 Outlook	27
Bibliography	28
II Articles	35
1 Temperature measurement from scattering spectra of clusters: theoretical treatment	
H. HEINZE, P. BORRMANN, H. STAMERJOHANNIS AND E. R. HILF <i>Zeitschrift für Physik D</i> 40 , (1-4) 190-193 (1997)	36

2 Self-assembly of magnetic nanostructures D. TOMÁNEK, S. G. KIM, P. JUND, P. BORRMANN, H. STAMERJOHANN AND E. R. HILF Zeitschrift für Physik D 40, (1-4) 539-541 (1997)	41
3 Thermodynamics of finite magnetic two-isomer systems P. BORRMANN, H. STAMERJOHANN, E. R. HILF, P. JUND, S. G. KIM AND D. TOMÁNEK Journal of Chemical Physics 111, (23) 10689-10693 (1999)	45
4 Paradoxical magnetic cooling in a structural transition model P. BORRMANN, H. STAMERJOHANN, E. R. HILF AND D. TOMÁNEK European Physical Journal B 19, (1) 117-119 (2001)	51
5 Classification of phase transitions of finite Bose-Einstein condensates in power-law traps by Fisher zeros O. MÜLKEN, P. BORRMANN, J. HARTING AND H. STAMERJOHANN Physical Review A 64, 013611 (2001)	55
6 Origins of Phase Transitions in Small Systems O. MÜLKEN, H. STAMERJOHANN AND P. BORRMANN Physical Review E 64, 047105 (2001) in press	62
7 Deceptive Signals of phase transitions in Small Magnetic Clusters H. STAMERJOHANN, O. MÜLKEN AND P. BORRMANN arxiv/cond-mat 0107176 (2001), to be published in Phys. Rev. Lett.	66
Curriculum Vitae	71

I

INTRODUCTION

1 Clusters

Clusters are aggregates of atoms or molecules. The properties of clusters differ quantitatively and qualitatively from bulk matter. Clusters may be classified by their size as small, medium or large clusters. Small clusters consist of a few up to about thousand particles, their properties vary strongly with size and shape, so that no simple dependence on cluster size can normally be given. Properties of medium-sized clusters vary smoothly with size, while the properties of large clusters approach the behaviour of bulk material. Quantitative properties, like the melting point, differ from bulk values, because a large fraction of the particles are on the surface, and large energy gaps between energy states lead to different behaviour as known from the corresponding bulk. In macroscopic systems fluctuations about the mean values of fluctuating extensive variables such as the volume V or the energy E can be neglected since they are very small. In small systems though, the second moment (the square of the standard deviation) and higher moments must be taken into account [14].

Van der Waals forces, ionic forces, or metallic bonds may hold a cluster together. Molecules however are mostly bound by covalent forces, and have definite numbers and mostly specific structures, apart from isomers, while clusters may be composed of any specific number of particles. With growing cluster-size the number of stable structures and therefore the number of structural isomers rapidly increases.

Free clusters can be produced by many different methods:

- Clusters (e.g. rare-gas clusters) can be formed in a supersonic jet expansion, where a gas is expanded from high pressure through a nozzle into vacuum. The atoms which move at random speed and direction prior to expansion are almost thermalized and cooled adiabatically during the expansion process. The relative velocities are extremely reduced and clusters are formed by condensation [15].
- In gas aggregation sources atoms or molecules are blown into a rare gas flow. After cooling by collision processes with the rare gas atoms these atoms accumulate to clusters [16, 17].
- Clusters can also be produced by desorption from a solid surface by photons (laser desorption) where high power laser pulses are focused on a small surface area, so atoms, molecules or clusters are ejected, and the few ionized are extracted by an electric field and measured by time of flight. Energetic ion beams can also be used to ablate material from a solid surface, locally from the ion-impact zone [18].

In mass spectra of clusters some cluster sizes exhibit intensity peaks, because of their higher stability. This has its reason in the geometrical nature of binding as a function of the cluster size N . For metallic clusters, when all states in a shell are filled up with electrons, there is a gap in the energy difference to the next vacant state. After the production, most clusters are in an excited state (hot clusters). They can give away energy by evaporating atoms from their surface. If a cluster of some size is extremely stable (geometrically or electronically), then the evaporation of atoms is less probable than in a less stable cluster. Clusters with geometrically or electronically closed shells have therefore a higher appearance in mass spectra (magic numbers).

One goal of modern cluster-science is to use clusters to build new materials or use them for applications. Novel properties that have been found include single magnetic domains that may be used for magnetic recording [19], a small mean free path of electrons to build new special conductors (nanowires) [20] or non-linear optical properties that may be applied in photovoltaics or to produce molecular filters. Clusters may coat surfaces in order to increase the scratching and abrasion resistance or to produce highly reactive catalysts.

1.1 Rare-Gas Clusters

Rare-gas clusters are ideal for theoretical studies, since they are loosely bound. Electrons are neither exchanged nor delocalized because of the stability of the atoms in the neutral cluster. Therefore the pairwise interaction of the atoms can be modeled with a Lennard-Jones potential

$$V(r) = 4\epsilon \left[\left(\frac{\sigma}{r} \right)^{12} - \left(\frac{\sigma}{r} \right)^6 \right] \quad (1.1)$$

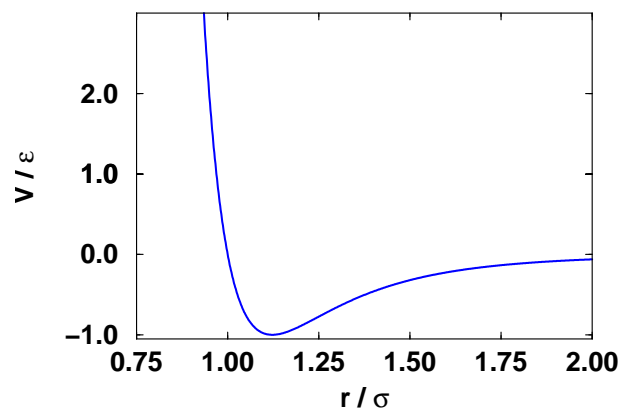


Figure 1.1: The Lennard-Jones effective pair potential.

with a long-range attractive van der Waals part and a short range repulsive part because of the overlap of the electron wave-functions. r describes the distance between two

atoms, the parameters $\sigma = 3.405 \text{ \AA}$ and $\epsilon = 10.3 \text{ eV}$ are used for Argon. The pairwise force approximation and these parameters give a good description of the properties of Argon via computer simulations because average three-body effects are included in this effective pair potential. These values thus do not apply for an isolated pair of Argon atoms nor for the bulk material because of the different number of neighbour atom pairs [21].

Rare-gas clusters have been theoretically and experimentally investigated in great detail [22–25]. Theoretical simulations indicated that Argon clusters of certain sizes, e.g. Ar_7 , Ar_{13} or Ar_{19} exhibit a well-defined temperature region where they are in equilibrium between their solid and liquid forms [26, 27]. BERRY *et al.* [23] also found unequal freezing and melting temperatures for clusters. There is a transition phase between solid and liquid phase, the so called “coexistence phase” [27]. For Ar_{55} , LABASTIE [28] found a first-order melting transition.

Ar_{13} , Ar_{55} , Ar_{147} ... can arrange themselves as complete Mackay icosahedra, which consist of twenty face-centered-cubic (fcc) tetrahedra that share a common point and have six five-fold axes of symmetry. Because of their larger number of nearest-neighbour contacts than other structures, icosahedra are here minimal in energy per atom.

Electron diffraction experiments, X-ray absorption spectroscopy or neutron beams that are normally used to investigate such structures, have found those low energetic structures in experiment. To analyze these experimental scattering spectra, theoretical scattering spectra are produced with Monte-Carlo or Molecular Dynamics methods for given cluster geometries and are then visually compared [29–31]. Many simulations had to be done in order to have a reasonable number of theoretical spectra, also the expected structures must be a priori assumed.

In Chapter II-1 we show for Argon-clusters that potential and kinetic energies and the classical temperature can be expressed as functionals of scattering spectra and an interaction potential. We use classical Monte-Carlo and Path-Integral Monte-Carlo (PIMC) simulations of Argon and Neon as “ideal experiments” and compute expectation values for the energy and classical temperature and identify coexistence phases. This result has a far reaching potential for applications to determine thermodynamic properties just from measuring structural scattering data.

1.2 Ferrofluid-Clusters

In contrast to many other finite systems like noble gas clusters, where one given parameter, e.g. the total energy or temperature determines all other properties, because the cluster relaxes its volume or structure automatically, magnetic cluster properties are determined by two external parameters, namely the Temperature T and the magnetic field B .

Ferrofluids consist of clusters of many small magnetic nanoparticles which are solved in a colloidal suspension. The experimentally realized spherical particles have a typical diameter of $\sigma \approx 10-100$ nm and are covered with a surfactant (e.g. oleic acid) in order to prevent aggregation. Ferrofluids do not exist in nature, but must be synthesized [32]. If the ferrofluid is prepared with magnetic nanoparticles of a suitable size, the fluid is stable, because of the thermal fluctuations of the particles and the inhibition of aggregation by the surfactant layer.

Most applications with commercial importance use the possibility to fix a ferrofluid in a certain position by a magnetic field, as it is used to seal the gap between a magnet and a rotating shaft in small devices. New ideas in the biomedical field have been proposed, e.g. to enclose an active drug and magnetic nanoparticles in a microcapsule, which will then burst at the preferred region of the human body by local application of a magnetic field [33]. Also the Ferromagnetic Embolization Hyperthermia (FEH), where heat is locally generated in tumor tissue by magnetically induced reorientation of the particles in an alternating magnetic field is a promising field of research for cancer treatment [34–36]. Current research also focuses on the use of magnetic nanoparticles for hard disks with limiting bit densities of 40 Gb/inch [37, 38].

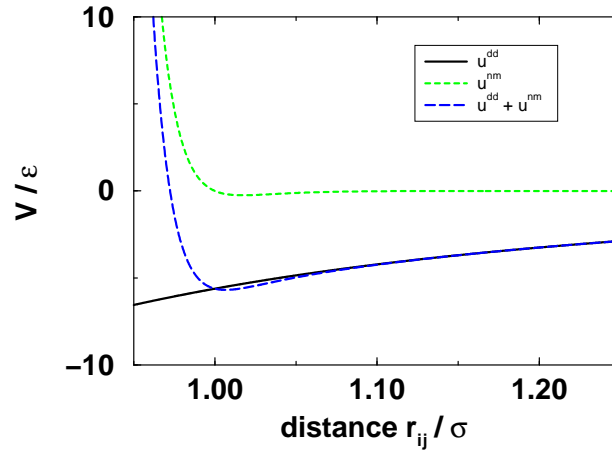


Figure 1.2: The pair potential for magnetic nanoparticles of a diameter of $\sigma = 20$ nm. The black solid line describes the magnetic dipole-dipole interaction, while the green line shows the non-magnetic interaction. The sum of these interaction is shown by the blue line.

The potential energy E_p of a system of magnetic nanoparticles in the external field \vec{B}_{ext} consists of the interaction between each particle i and the applied field, given by $u_i = -\vec{\mu}_i \cdot \vec{B}_{\text{ext}}$, and the pair-wise interaction between the particles i and j , given by [39]

$$u_{ij} = (\mu_0^2/r_{ij}^3) [\hat{\mu}_i \cdot \hat{\mu}_j - 3(\hat{\mu}_i \cdot \hat{r}_{ij})(\hat{\mu}_j \cdot \hat{r}_{ij})] + \epsilon \left[\exp\left(-\frac{r_{ij} - \sigma}{\rho}\right) - \exp\left(-\frac{r_{ij} - \sigma}{2\rho}\right) \right]. \quad (1.2)$$

The first term in Eq. (1.2) is the magnetic dipole-dipole interaction energy. The second

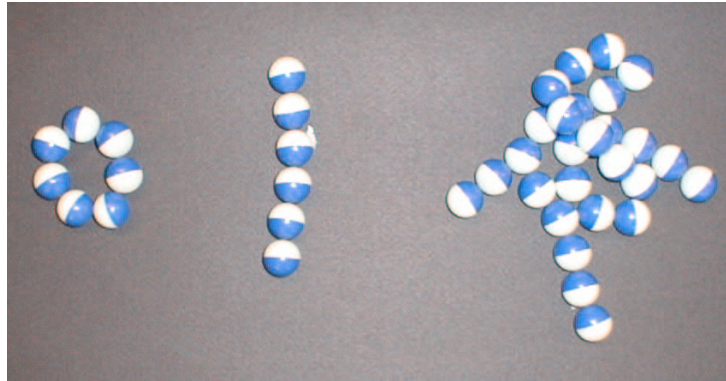


Figure 1.3: Magnetic marbles show possible structures of small ferrofluid clusters. For a few particles the most stable isomers are the chain and ring structure. More particles form complex labyrinthine patterns.

term describes a non-magnetic interaction between the surfactant covered tops in a ferrofluid that is repulsive at short range and attractive at long range [40]. The most significant part of this interaction, which we describe by a Morse-type potential with parameters $\epsilon = 0.121$ eV and $\rho = 2.5$ Å, is the short-range repulsion, since even at equilibrium distance the attractive part does not exceed 10% of the dipole-dipole attraction. For our simulations of nanoparticles we have chosen a diameter of $\sigma = 200$ Å which carries a large permanent magnetic moment $\mu_0 = 1.68 \times 10^5 \mu_B$.

Systems of 10-100 particles are known to form complex labyrinthine pattern [39] while for less particles ring and chain structures are the most thermally stable isomers. These isomers have almost equal potential energy, while the magnetic moment is very different. This behaviour has also been found for transition-metal clusters [41].

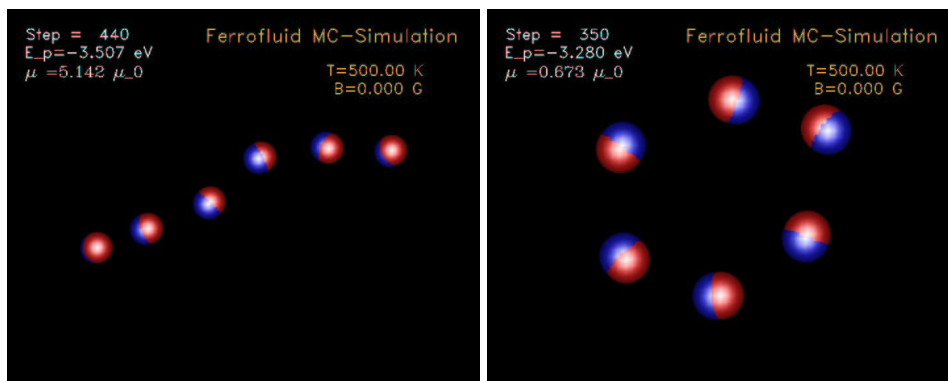


Figure 1.4: Ring and chain structures for system of six particles, visualized from a Monte-Carlo run. For a video see <http://www.smallsystems.de/~stamer/ff/>.

The ring structure is more stable at low temperatures and zero magnetic field, while at higher temperatures and increasing magnetic fields the chain structure is predominant because of its higher vibrational entropy. In Chap. II-2 we have used quaternion Molecular Dynamics to describe the magnetic and structural transitions in a microcanonical

ensemble, and show that it is possible to interconvert the chain- and ring structure with a magnetizable tip. We have also studied the magnetic nanoparticles with histogram Monte Carlo techniques combined with an improved data analysis (see Chap. 2.4) to investigate the phase-behaviour of a six-particle system.

2 Numerical Methods

Small systems can on one hand be experimentally studied, but because of the low number of particles computer simulations are also well suited to study the phase behaviour of a system. The thermodynamic ensemble of choice then depends on the system to be studied, e.g. for an isolated cluster, the microcanonical ensemble, a constant-energy system, is preferred and studied with Molecular Dynamics (MD) simulations.

2.1 Molecular Dynamics

With Molecular Dynamics solutions of the equations of Newton's second law for classical systems are determined numerically.

With given positions and momentum, Newton's equation of motion are solved to determine positions and velocities as a function of time. The resulting trajectory yields a complete description of the system in phase space. The dynamical information from MD is limited, because computer-induced, random errors destroy the reversibility of integration. Thus the simulation of slow processes is not very reliable, while for short-time dynamics it has been established as an important method to study small systems.

The group of D. Tománek has used quaternion molecular dynamics to describe the phase behaviour of magnetic nanoparticles. Here four quaternion parameters are used as generalized coordinates, in order to avoid problems with the divergence in orientational equations of motion [21, 42].

Numerical methods have to deal with progressing errors. Any two classical trajectories which are initially close will eventually diverge from another exponentially with time. A small error by finite floating point arithmetic will cause a computer generated trajectory to diverge from the true classical trajectory with which it initially overlapped.

But for the generation of states sampled from the microcanonical ensemble it is not necessary to generate exact classical trajectories, but to ensure that particle trajectories remain on the constant-energy hypersurface in phase space in order to ensure energy conservation. This must be especially obeyed with the enormous increase of computing time while dealing with soft potentials.

2.2 MC-Methods

If a cluster is treated in contact with a heat reservoir, a canonical ensemble of constant temperature is used.

The system is studied with Metropolis Monte-Carlo simulations [43], where the phase-space is sampled by Markov-chains, which yield no dynamic link from one step to the next. Detailed descriptions of the Monte Carlo method can be found in textbooks by BINDER [44–46], HAMMERSLEY [47] or KALOS [48].

Monte-Carlo methods rely, due to their stochastic nature, on the quality of the computer generated pseudo-random numbers. If there are correlations between successively generated numbers only parts of the multidimensional phase space might be explored by the generated Markov-chains. We have developed [49] a new portable pseudo-random number generator based on an improved Marsaglia-Zaman algorithm [50] and based on the work by Lüscher [51] to guarantee efficiently generated random numbers with good statistical properties, long period ($\sim 2^{100}$) and reproducibility.

After the development of the ‘Mersenne Twister’ [52], we have switched to this best-known random number generator for Monte Carlo simulations. This random number generator has a far longer period and far higher order of equidistribution than any other implemented generator. Its very long period of $2^{19937-1}$, and its 623-dimensional equidistribution property, which is especially important for the generation of Monte Carlo steps, makes it the most promising generator for numerical simulations at present time.

2.3 Multiple Normal Modes Model

For a first orientation of thermodynamic properties of clusters it is also possible to give a qualitative description of the phase behaviour by restricting the phase space to some discrete points, namely the most important potential minima. This superposition approach has been used in earliest cluster calculations [53–55], but has also been applied to larger clusters in recent years [56, 57].

With this simple statistical model only energy differences between different potential minima must be taken into account. An extension to this method is the Multiple Normal Modes (MNM) model [24, 57], where the mobility of the atoms by the determination of the normal modes is taken into account. Transitions between different isomers can be modeled simply by considering the vibrational eigenfrequencies ω_{ij} and permutational degeneracy σ_i of the isomer i . Then the partition function for M isomers of an N -particle cluster reads

$$Z(\beta) = \sum_{i=1}^M \sigma_i \exp(-\beta E_i) \prod_{j=1}^{3N-6} \frac{2\pi}{\beta \omega_{ij}}, \quad (2.1)$$

where $\beta = 1/T$. In Chap. II-6 we have used this method to investigate the validity and applicability of different classification schemes for phase transitions in small systems. In order to investigate small magnetic clusters with this model the magnetic field has to be included. For simplicity we only consider two isomers with magnetic moments μ_i and ground state energies $E_0(i)$. With the magnetic field pointing in z -direction the partition function reads [41]

$$Z(\beta) = \sum_{i=1}^2 \exp[-\beta E_0(i)] \frac{2}{\beta \mu_i H} \sinh(\beta \mu_i H). \quad (2.2)$$

This method is practical for smaller clusters, but for larger clusters an impractically larger number of minima have to be taken into account.

The simple assumption that the phase space volumes of the minima are of equal size might lead to quantitatively wrong results. In order to sum the phase space volumes for each minimum independently, it is assumed that these volumes do not overlap, which might lead to an overestimation of the density of states $\Omega(E)$ [58].

2.4 Optimized Data Analysis

For systems with large free energy barriers between low-energy states, as they occur in first order phase transitions, it is difficult to calculate low-temperature thermodynamic properties because the barriers hinder ergodicity, which is an essential necessity for successful simulations [21, 59]. At low temperatures the simulated system might get stuck in metastable states [46], so depending on the start configurations the simulations might yield different results.

With the Optimized Data Analysis method it is possible to circumvent this problem by simulating a system at temperatures where high mobility of particles is ensured. By an optimized estimate of the density of states $\Omega(E)$ which does not depend on the temperature, the phase behaviour of the system can be determined. With a histogram-reweighting method, a method which is analogous to the approach of BENNETT [60] who computed free energy differences, FERRENBURG and SWENDSEN [61] have shown that by reweighting histograms taken from Monte-Carlo simulations it is possible to describe the phase behaviour over a broader parameter range, e.g. the temperature.

Basically a probability distribution $P(E, T_0)$ which is collected in histograms for a given temperature $T_0 = 1/\beta_0$ is reweighted with $\exp(\beta_0 E)$ to obtain an estimation for the density of states $\Omega(E)$. To obtain a probability estimation of $P(E, T)$ for another temperature T this density is reweighted at the new temperature T to obtain $P(E) \exp(-\beta E)$.

The probability distribution collected in histograms is approximately a Gauss curve as a function of energy, so only few events will be counted at both wings and the statistical uncertainty is high. In these wings of the distribution the statistical errors may be greatly magnified by reweighting methods. This can be eased by combining histograms from several simulations taken at different temperatures [62]. Analogous approaches have been used in the so called *umbrella sampling* [63, 64], the *multicanonical ensemble* [65] or the *multimagnetic ensemble* [66, 67] or in *simulated tempering* [68].

We have extended this method in a way that multiple multidimensional histograms can be used for systems which depend on two or more external parameters, thus the temperature T and external magnetic field B may be varied. With this method it is possible to describe the phase behaviour of e.g. magnetic nanoparticles in a magnetic field, because with some Monte Carlo simulations being run at just a few parameter points one is able to obtain all thermodynamic functions of interest in a broad region of the (T, B) plane.

We will elaborate this method in greater detail, because the knowledge on these new methods is not well distributed and in use yet, although they have the potential of to be applied to cover a huge spectrum of quite different small systems.

In the case of the magnetic nanoparticles, the canonical partition function, from which

all thermodynamical quantities can be derived, is given by

$$Z(B_{\text{ext}}, T) = (2\pi\beta)^{-6N/2} \int \left[\prod_{i=1}^N d\vec{x}_i d\phi_i d\theta_i d\psi_i \right] \times \exp \left(-\beta \left(\sum_{i<j}^N u_{ij} - \sum_i^N \mu_{i,z} B_{\text{ext}} \right) \right), \quad (2.3)$$

where $\beta = T^{-1}$ and where the field \vec{B}_{ext} is aligned with the z -axis. The pre-exponential factor addresses the fact that each particle has three rotational and three center-of-mass degrees of freedom. The key quantities are the formation enthalpy of the isolated system, $E^* = \sum_{i<j} u_{ij} = E_p + \mu_z B_{\text{ext}}$, and the z -component of the total magnetic moment of the aggregate, μ_z , both of which are functions of T and B_{ext} . The energy E^* is the appropriate thermodynamic potential describing the present system; its definition is analogous to the enthalpy of a (p,V,T)-ensemble.

For each Monte-Carlo Simulation which we carry out for given external parameters, the temperatures T_k and the external magnetic fields $B_{\text{ext},m}$, we measure the two-dimensional histograms $G_{k,m}(E^*, \mu_z)$, the number of configurations with energy E^* and the magnetic moment μ_z in one run with $n_{k,m}$ Monte-Carlo steps.

The probability $P(E^*, \mu_z; \beta_k, B_m)$ that the system has the energy E^* and the magnetic moment μ_z at the external parameters $\beta_k = 1/T_k$ and $\vec{B}_{\text{ext}} = B_m$ is proportional to the histogram $G_{k,m}(E^*, \mu_z)$, so the density of states can be written as

$$\rho(E^*, \mu_z) = \frac{G_{k,m}(E^*, \mu_z)}{n_{k,m}} \exp(\beta_k(E^* - \mu_z B_m) - f_{k,m}), \quad (2.4)$$

with $f_{k,m} = \beta_k F(\beta_k, B_m)$.

The free energy F of the system is defined by $F = 1/\beta \ln Z$. The density of states of all simulations can be estimated by a weighted sum of the density of states of each simulation [62],

$$\rho(E^*, \mu_z) = \sum_{k,m} \frac{p_{k,m}(E^*, \mu_z) G_{k,m}(E^*, \mu_z)}{n_{k,m}} \times \exp[-f_{k,m} + \beta_k(E^* + \mu_z B_m)]. \quad (2.5)$$

where the sum runs over all simulations at $T = T_k$ and $\vec{B}_{\text{ext}} = B_m$, and the number of Monte Carlo steps $n_{k,m}$ is defined by $\min(1, n_{k,m})$, so we can just sum over all points in the parameter space even if we have not simulated at the particular point. If we have not simulated at the external parameters β_k and B_m , $G_{k,m}$ is just zero. The addend is then zero, because $G_{k,m}$ is zero.

Inserting the histograms and minimizing the error in the estimate for $\rho(E^*, \mu_z)$ we find for the weighting-function

$$p_{k,m}(E^*, \mu_z) = \frac{n_{k,m} \exp[-\beta_k(E^* - \mu_z B_m) + f_{k,m}]}{\sum_{k,m} n_{k,m} \exp[-\beta_k(E^* - \mu_z B_m) + f_{k,m}]}. \quad (2.6)$$

With the unnormalized probability density

$$D(E^*, \mu_z; \beta, B) = \rho(E^*, \mu_z) \exp[-\beta(E^* - \mu_z B)] \quad (2.7)$$

we find by inserting equation (2.5) and (2.6) in (2.7)

$$D(E^*, \mu_z; \beta, B) = \frac{\sum_{k,m} G_{k,m}(E^*, \mu_z) \exp[-\beta(E^* - \mu_z B)]}{\sum_{k,m} n_{k,m} \exp[-\beta_k(E^* - \mu_z B_m) + f_{k,m}]}, \quad (2.8)$$

where

$$\exp(-f_{k,m}) = \sum_{E^*, \mu_z} D(E^*, \mu_z, \beta_k, B_m). \quad (2.9)$$

The expectation value of an arbitrary function of E^* can be calculated by

$$\langle A(E^*, \mu_z) \rangle(\beta, B) = \sum_{E^*, \mu_z} A(E^*, \mu_z) P(E^*, \mu_z; \beta, B), \quad (2.10)$$

where the normalized probability density is determined by

$$P(E^*, \mu_z, \beta, B) = \frac{D(E^*, \mu_z; \beta, B)}{\sum_{E^*, \mu_z} D(E^*, \mu_z; \beta, B)}. \quad (2.11)$$

By self-consistent iteration over (2.8) and (2.9) the free energy can be computed.

Implementation

The probability function $P(E^*, \mu_z, \beta, B)$ depends on four parameters, thus the above equations cannot be directly used to determine thermodynamic functions because it consumes too much memory. But the exponential term in (2.8) is independent of β_k und B_m , so all histograms $G_{k,m}(E^*, \mu_z)$ can be combined in $\tilde{G}(E^*, \mu_z) = \sum_{k,m} G_{k,m}$.

The free energy (2.9) needs only to be determined by self-consistent iteration for the discrete external parameters β_k, B_m , at which the simulations have actually been carried out. The partition function at these points is given by

$$Z(\beta_k, B_m) = \sum_{E^*, \mu_z, i, j} n_{i,j} \exp\left[(-\beta_k - \beta_i)E^* + \mu_z(\beta_i B_j - \beta_k B_m) + f_{i,j}\right] \quad (2.12)$$

and the $f(\beta_k, B_m)$ can be calculated by

$$f(\beta_k, B_m) = -\ln Z(\beta_k, B_m). \quad (2.13)$$

By self-consistent iteration of these two equations we determine $f(\beta_k, B_m)$.

With these free energies we store the denominator in (2.8) as a function of E^*, μ_z as $\tilde{D}_{\text{den}}(E^*, \mu_z)$ defined as $\sum_{k,m} n_{k,m} \exp[-\beta_k(E^* - \mu_z B_m) + f_{k,m}]$, therefore the sum

over all histograms only needs to be computed once. The unnormalized probability distribution $D_{E^*, \mu_z, \beta, B}$ is calculated for all E^*, μ_z, β, B ,

$$D_{E^*, \mu_z, \beta, B} = \tilde{G}(E^*, \mu_z) \exp[-\beta E^* + \beta \mu_z B] \times \tilde{D}_{\text{den}}(E^*, \mu_z), \quad (2.14)$$

where the partition function $Z(\beta, B)$ and arbitrary thermodynamic values like $\langle E^* \rangle(\beta, B)$ can be determined by continuous summation.

With this method many Monte Carlo Simulations in a multi-dimensional parameter space can be combined and evaluated on workstations, where the computing cost neither depends on the number of histograms to be evaluated nor depends on the chosen interval size for the thermodynamic functions. The additional cpu time and amount of memory is negligible. It is also possible to determine the probability density $P(E_p, \mu_z)$,

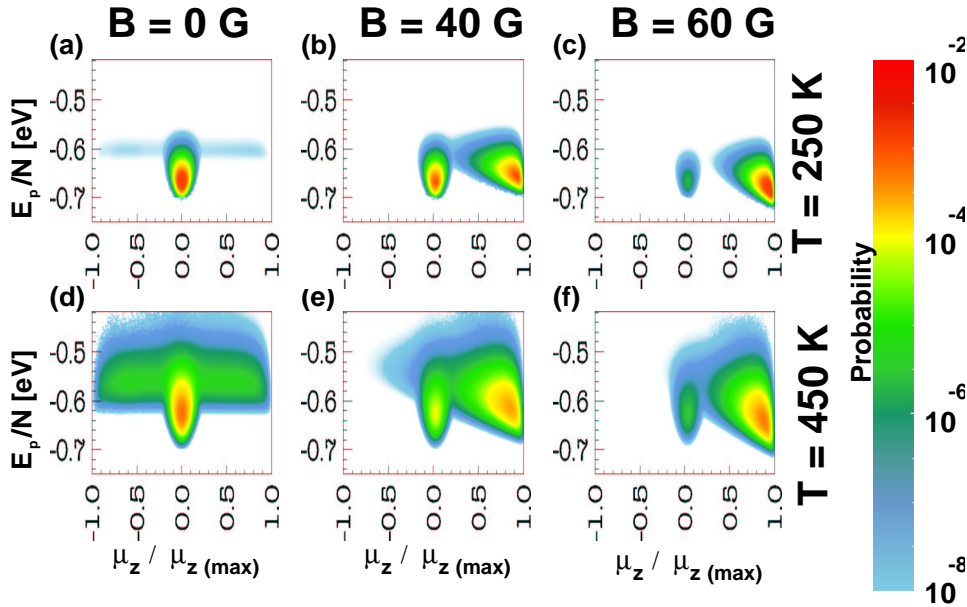


Figure 2.1: Monte Carlo results for the probability to find an aggregate in a state with its magnetic moment in the field direction μ_z and potential energy E_p . The individual contour plots show our results for the temperature $T = 250$ K at the field values (a) $B_{\text{ext}} = 0$ G, (b) $B_{\text{ext}} = 40$ G, (c) $B_{\text{ext}} = 60$ G, and $T = 450$ K at the field values (d) $B_{\text{ext}} = 0$ G, (e) $B_{\text{ext}} = 40$ G, (f) $B_{\text{ext}} = 60$ G.

with $E_p = E^* - \mu_z B_{\text{ext}}$, at fixed parameters T and B_{ext} by corresponding subsummation, The configuration space of the system can be easily calculated and represented (see Fig. 2.1). These plots nicely reveal the two different phases and its transition.

We have used the Optimized Data Analysis in order to determine the phase behaviour of the magnetic nanoparticles. For the Metropolis Monte Carlo simulations, we chose

the temperature to be low enough so that the particles do not evaporate, but at the same time high enough so there is enough mobility to explore the configuration space.

When particles evaporate, which means that the distance in between them is so large, that the interaction is negligible, the simulation is stopped. The physical meaning is of course also a phase transition to a lower $(N - 1)$ -particle cluster, which we have not further investigated here.

We carry out some simulations at high enough temperature ($T = 400$ to 450 K) and different external magnetic fields B_{ext} . Then with the Optimized Data Analysis we determine the approximate phase behaviour of the system by calculating the specific heat (2.15), the susceptibility and (2.16) and the maxima of the functions. The specific heat per particle in a canonical ensemble is given by $c_B = d\langle E/N \rangle / dT$, where the total energy is given by $E = \frac{6}{2} N k_B T + E_p$. Correspondingly, we define the magnetic susceptibility per particle as $\chi = d\langle \mu_z / N \rangle / dB_{\text{ext}}$.

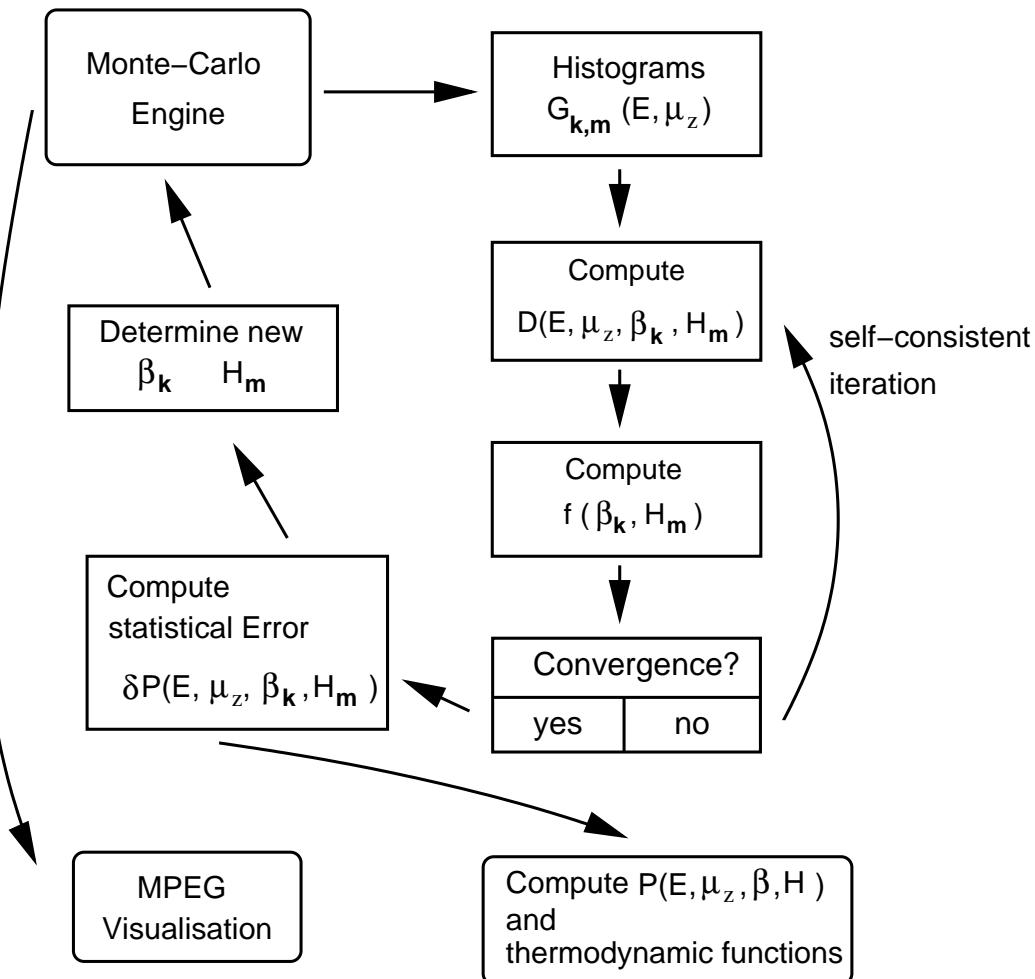


Figure 2.2: Schema for self-correcting, self-consistent MC.

These response functions are related to the fluctuations of E_p and μ_z by

$$c_B = \left[\frac{6N}{2} k_B + k_B \beta^2 (\langle E^2 \rangle - \langle E \rangle^2) \right] / N, \quad (2.15)$$

$$\chi = [\beta (\langle \mu_z^2 \rangle - \langle \mu_z \rangle^2)] / N. \quad (2.16)$$

The data generated from the Optimized Data Analysis can be fed back into the input data for the Monte-Carlo simulations so the simulations can be carried out at critical field at high enough temperature to ensure ergodicity. A scheme (cmp. Fig. 2.2) illustrates this self-correcting self-consistent Monte Carlo method. A simulation generates histograms $G_{k,m}(E^*, \mu_z)$ from which the free energy is computed by self-consistent iteration.

From this the probability distribution $P(E^*, \mu_z, \beta, H)$, other thermodynamic functions and the statistical error [62]

$$\delta P(E^*, \mu_z, \beta, B) = \frac{P(E^*, \mu_z, \beta, B)}{\sqrt{\sum_{k,m} G_{k,m}(E^*, \mu_z)}} \quad (2.17)$$

is obtained, and new parameters β_k and H_m to reduce the statistical error are determined. These parameters are then fed back into the Monte Carlo engine and are used as input parameters for further simulations.

Additionally the pseudo-dynamics of the magnetic nanoparticles are visualized in an animated film (see Fig. 1.4). One has to keep in mind though that Monte Carlo simulations compute only (correlated) states in the configurational phase space which do not yield true dynamics [45, 59], although at least for Lennard-Jones fluids it has been recently shown, that Monte Carlo simulations can be used to describe dynamical processes [69].

3 Phase Transitions

One of the most interesting events in nature are transitions between different states of matter. The classical phase transitions between solid, fluid and gaseous phases have been investigated extensively. In recent years a rich world with a variety of phenomena including superfluidity, superconductivity, liquid crystals, surface melting or magnetic ordering have been investigated.

3.1 Identification of Phase Transitions

In the bulk a phase transition occurs, when the free energy or one of its derivatives exhibits a singularity. If there is a discontinuity in a first derivative of the appropriate thermodynamic potential the transition is called *first-order*. If the first derivative is continuous, but the second derivative are discontinuous or infinite the transitions is termed to be of *second* or *higher* order or called a *continuous* phase transition. Originally phase transitions have been classified by EHRENFEST including third and fourth order, but FISHER has proved this classification to be to inappropriate and nowadays *second-order* and *continuous* transitions are mostly used synonymously. Another classification scheme by PIPPARD [70] varies the classification of EHRENFEST and orientates on physical systems. PIPPARD distinguishes between second and third order transitions and classifies the superconducting transition, the Weiss model of ferromagnetism and the order-disorder transitions in many solids as to be of second order, while the Curie transition the transition in the 2D Ising model and the Bose-Einstein condensation of liquid ^4He are classified to be of third order.

Singularities in the free energy or one of its derivatives are caused by fluctuations, which persist not only at the microscopic level, but cover all length scales. WILSON [71] has shown in his renormalizations groups theory that phase behaviour of many different systems can be divisioned into universality classes, which are determined by fundamental properties of the system such as the spatial dimension or range of interaction.

For finite systems these correlations are of course finite which lead to rounded curves in the derivatives of thermodynamic potentials. Thus there are no singularities, the derivatives are continuous, so that the phase transitions of finite systems cannot be classified on the basis of discontinuities of the derivatives of the appropriate thermodynamic potential. The specific heat exhibits finite peaks in the transition regions and

can therefore not be used to classify phase transitions non-ambiguously, which has led to many discussions and considerable confusion. The absence of singularities has led to the thesis that finite systems do not even exhibit phase transitions. Some authors like BERRY [72] rather use the term *phase changes* to distinguish from phase transitions in bulk systems because they cannot be classified according to ‘order’ in the Ehrenfest sense. However, because of many analogies to the bulk most authors also use the term *phase transitions* for finite systems.

We have investigated and classified phase transitions in finite systems by two different approaches. In Chap. II-2 to II-4 we have calculated the partition function and appropriate thermodynamic functions. By inspection of the probability distribution and the free energy, we have determined that the system of magnetic nanoparticles undergoes a phase transition of first order.

In Chap. II-5 to II-7 we have calculated the complex partition function for non-interacting bosons in a power law trap, and simple model clusters and have classified the transitions according to the scheme which has been proposed by BORRMANN *et al.* [10] and will be explained in the next Section.

With the finite-size scaling theory, which has been developed by FERDINAND and FISHER [73] it is possible to extrapolate finite-system properties found by e.g. Monte Carlo simulations to the thermodynamic limit. For the system of magnetic nanoparticles finite-size scaling cannot be applied, because the transition between rings and chains can only be observed for very small systems. Other characteristics must be investigated in order to classify the type of transition.

A solid-liquid transition of argon-clusters bears a coexistence of two phases [26, 27], which cannot be occupied at the same time, because due to their finite size the clusters can be only in one state or the other. This transition is identified to be of first-order, because the free energy of the system has two minima at the critical temperature. Since the barrier between two minima of the free energy of a finite system can only be finite, there is a finite probability for the system to cross the barrier. The system cannot only cross from a metastable to a stable state but also vice versa. This is called the *coexistence phase*.

In order to distinguish between different phases, we introduce an order parameter Φ [74, 75]. For the system of magnetic nanoparticles the order parameter is given by the sum of the magnetic moments of all particles. With $\Phi = \mu_z / \mu_z^{max}$, the order parameter Φ is close to zero for a ring, while for chains Φ is close to 1, because the chains align along the field. At a continuous phase transition the order parameter approaches continuously zero. While approaching the critical point, the probability distribution $P(\Phi)$ will show only one maximum, because no metastable states exist. On the other hand the existence of metastable phases is an indicator of first order phase transitions. If convergence of the simulation is guaranteed, $P(\Phi)$ will then show (at least) two maxima. With

$$F(\Phi) = -\frac{1}{\beta} \ln P(\Phi) \quad (3.1)$$

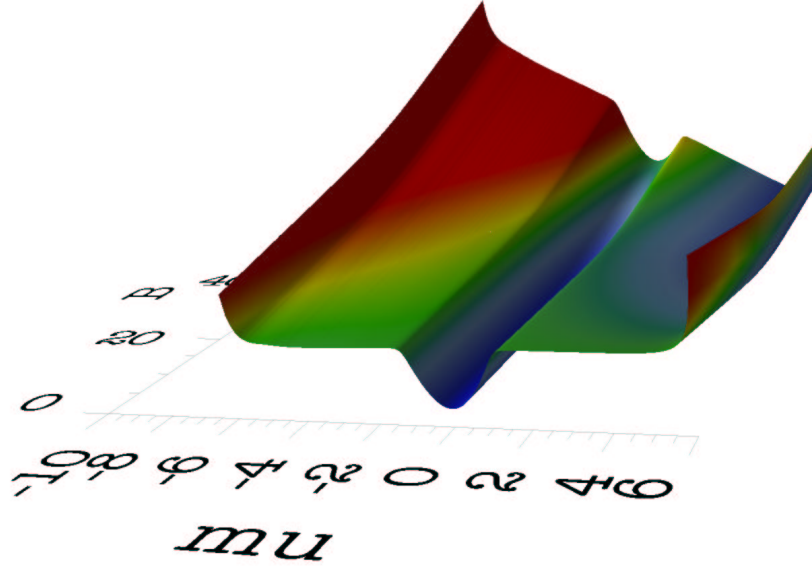


Figure 3.1: The Landau free energy $F(\Phi)$ as a function of the applied magnetic field at $T = 300$ K. At zero magnetic field the only minimum can be found at $\Phi = 0$. With increasing field the free energy exhibits a second minimum.

we determine the Landau free energy as a function of the order parameter [59, 76, 77]. With the Optimized Data Analysis we determine $F(\Phi; \beta, B)$ by

$$F(\Phi; \beta, B) = -\frac{1}{\beta} \ln \frac{\sum_{E^*} D(E^*, \mu_z; \beta, B)}{\sum_{E^*, \mu_z} D(E^*, \mu_z; \beta, B)}. \quad (3.2)$$

At a first-order transition $F(\Phi)$ shows (at least) two minima [75]. By plotting the probability density P in dependence of E_p or Φ the coexistence phase can be determined. The distribution must be bimodal, if there is coexistence.

3.2 Zeros of the Partition Function

YANG and LEE [78, 79] have shown that the grand canonical partition function can be written as a function of its zeros in the complex fugacity plane. They are e.g. located on a unit circle in the case of hard-core interactions for the Ising model.

GROSSMANN *et al.* [8, 80–82] have extended this approach to the canonical ensemble by analytic continuation of the inverse temperature to the complex plane $\beta \rightarrow \mathcal{B} = \beta + i\tau$. BORRMANN and MÜLKEN and HARTING [10] have extended this scheme to classify phase transitions in finite systems, where the distribution of zeros is discrete and the zeros of $Z(\mathcal{B})$ do not lie dense on lines in the complex temperature plane and do not approach the real temperature axis infinitely close.

The canonical partition function

$$Z(\beta) = \left(\frac{1}{2\pi\beta} \right)^{3N/2} \int dx^{3N} \exp[-\beta V(x)], \quad (3.3)$$

can be factored into a product of the kinetic part and a product depending on the zeros $\mathcal{B}_k = \beta_k + i\tau_k$, with $\mathcal{B}_{-k} = \mathcal{B}_k^*$ of the integral function in the complex temperature plane.

$$Z(\beta) = \left(\frac{1}{2\pi\beta} \right)^{3N/2} \prod_{k=-M}^M \left(1 - \frac{\beta}{\mathcal{B}_k} \right) \exp\left(\frac{\beta}{\mathcal{B}_k} \right), \quad (3.4)$$

where $2M$ is the number of its complex conjugate zeros.

All thermodynamic quantities can then be derived from the distribution of the zeros of the partition function. The internal energy $U(\mathcal{B})$ or the specific heat $C_V(\mathcal{B})$ can be determined by standard differentiation. The interaction part of the specific heat, e.g. yields

$$C_V(\mathcal{B}) = -\mathcal{B}^2 \sum_{k=-M}^M \left(\frac{1}{(\mathcal{B}_k - \mathcal{B})^2} \right). \quad (3.5)$$

Zeros of the partition function $Z(\mathcal{B})$ are poles in $U(\mathcal{B})$ and $C_v(\mathcal{B})$. Zeros close to the real axis contribute most to the specific heat, a zero that approaches the real axis infinitely close will result in divergence of the specific heat.

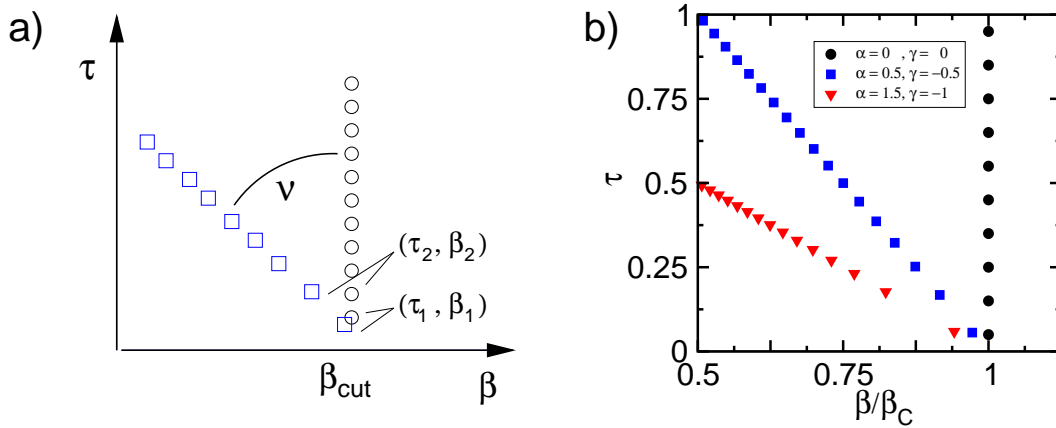


Figure 3.2: a) Schematic illustration of the zeros in the complex temperature plane, b) The black circles illustrate a typical distribution of zeros for $\alpha = 0$ and $\gamma = 0$, which is identified as a first order transition. The blue squares illustrate a distribution of zeros for $\alpha = 0.5$ which indicate a transition of second order, while the red triangles show a transition of higher order with $\alpha > 1$.

The distribution of zeros close to the real axis can approximately be described by three parameters, where two of them, namely α and γ , reflect the order of the transition while the third τ merely describes the size of the system.

According to the Grossmann scheme they assume the zeros to lie on straight lines. with a discrete density of zeros given by

$$\phi(\tau_k) = \frac{1}{2} \left(\frac{1}{|\mathcal{B}_k - \mathcal{B}_{k-1}|} + \frac{1}{|\mathcal{B}_{k+1} - \mathcal{B}_k|} \right). \quad (3.6)$$

with $k = 2, 3, 4, \dots$, and approximate for small τ the density of zeros by a simple power law $\phi(\tau) \sim \tau^\alpha$. By considering only the first three zeros the exponent α can be estimated as

$$\alpha = \frac{\ln \phi(\tau_3) - \ln \phi(\tau_2)}{\ln \tau_3 - \ln \tau_2}. \quad (3.7)$$

The second parameter describes the distribution of zeros, which is given by $\gamma = \tan(\nu) \sim (\beta_2 - \beta_1)/(\tau_2 - \tau_1)$ where ν is the crossing angle of the line of zeros with the real axis. With these parameters they give a distinct characterization of phase transitions in small systems:

- *1st order*: $\alpha \leq 0$ and $\gamma = 0$,
- *2nd order*: $\begin{cases} 0 < \alpha < 1 \text{ and } \gamma = 0 \\ \gamma \neq 0 \end{cases}$
- *higher order*: $\alpha > 1$ and arbitrary γ ,

The discreteness of the system is reflected in the imaginary part τ_1 of the zero closest to the real axis. While α describes the density increase of the zeros, γ describes the angle of the zeros to the real axis. A first-order transition will thus have always equally or increasingly spaced zeros perpendicular to the real axis.

A calculation of the distribution of zeros for the system of magnetic nanoparticles (see Fig. 3.3) backs the conclusion that the chain-ring transition is of first order. The zeros are equally spaced on a line perpendicular to the real axis at $T \approx 180$ K. The parameters α and γ are zero, therefore the transition can be regarded as to be of first order. The large bright area at higher temperatures reflects the order-disorder transition of the system. In this region the numerical data taken from the Monte-Carlo simulations are not reliable enough to classify the order of transition.

In 1995 ANDERSON *et al.* observed Bose-Einstein condensation in vapor of Rubidium, where atoms were confined in a magnetic trap. Bose-Einstein condensation has also been realized in Natrium [83] and in Lithium [84, 85]. The trapped Bose gases are finite systems, the number is typically between hundreds and a few millions of atoms.

In Chap. II-5 we determine the order of the phase transition of a finite number of non-interacting bosons in a power-law trap. We calculate the canonical partition function for N non-interacting bosons by a recursion formula found by BORRMANN and FRANKE [86].

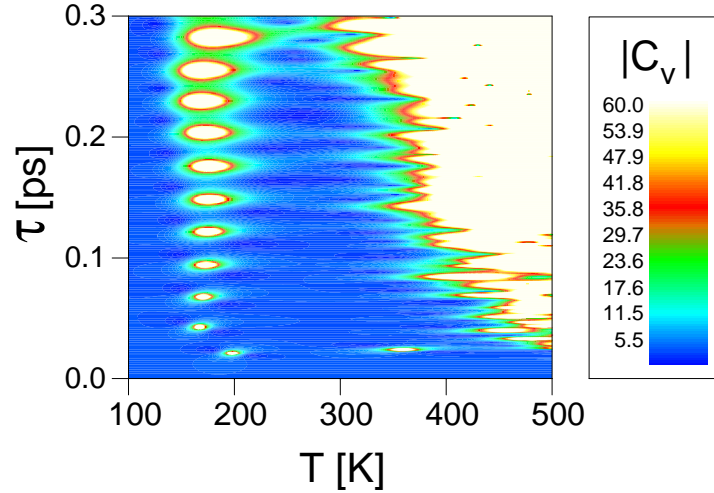


Figure 3.3: Distribution of zeros for a system of six magnetite particles at $B = 40G$. Here the specific heat is computed in the complex temperature plane. Bright spots indicate the location of zeros.

For the investigated dimensions equal to one to six, one can deduce that there is no transition in the one-dimensional case as it is expected. With the parameters α and γ , the transitions can be classified in a non-ambiguous way to be of higher order in the two-dimensional case and to be of second-order for the dimensions $d = 3 - 6$. The distance of the imaginary part τ_1 of the zero closest to the real axis can be used to measure the finiteness of the system or equivalently the distance of a phase transition from being a true phase transition in the Ehrenfest sense.

3.3 Other classification schemes

GROSS *et al.* have suggested another classification of phase transitions in small systems [11–13]. They classify phase transitions by the topological properties of the determinant $D(E, N)$ of the microcanonical entropy surface $S(E, N)$. The determinant is defined by

$$D(E, N) = \left\| \begin{array}{cc} \frac{\partial^2 S}{\partial E^2} & \frac{\partial^2 S}{\partial N \partial E} \\ \frac{\partial^2 S}{\partial E \partial N} & \frac{\partial^2 S}{\partial N^2} \end{array} \right\|, \quad (3.8)$$

where N is the number of particles and E is the energy of the system. The transitions are classified as follows:

- The system is considered to be in a single phase if the determinant $D(E, N) > 0$.
- A first order transition for $D(E, N) < 0$. The depth of the intruder is supposed to be a measure of the intra-phase surface tension. This corresponds to a back bending in the microcanonical caloric curve.

- That region is bounded by a line with $D(E, N) = 0$, where the transition is supposedly continuous, with no convex intruder in $S(E, N)$.

From classical statistical mechanics it is clear that the back bending is forbidden in the thermodynamic limit by the van Hove concavity condition [87]. However, in finite systems the microcanonical caloric curve may exhibit such a negative slope which results in negative heat capacities. Such a negative heat capacity has been observed in several numerical simulations [28, 88, 89] and has even been found indirectly in experiments with sodium clusters [90]. However, by comparing microcanonical and canonical caloric curves based on simple model systems BIXON and JORTNER [88] have shown that in a canonical ensemble a negative slope is impossible because it is proportional to the mean squared energy fluctuation.

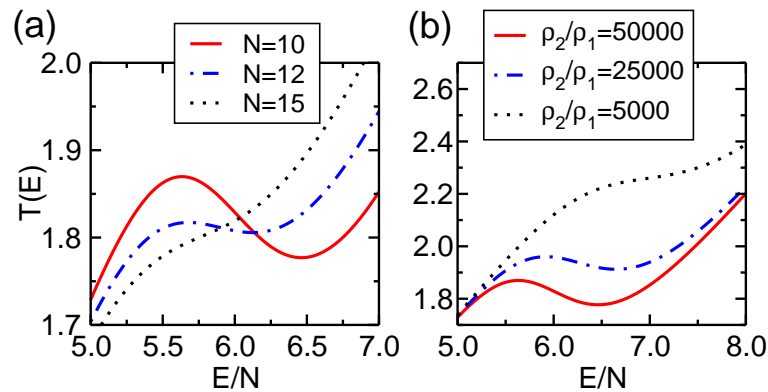


Figure 3.4: Microcanonical caloric curves for the Multiple Normal Modes model with an energy difference $\Delta E = 20$ between two isomers. a) With constant $\rho_2/\rho_1 = 50000$ and increasing particle number the back bending can be easily tuned out. b) With constant $N = 10$ and decreasing ratio ρ_2/ρ_1 the back bending can also be tuned out.

In Chapter II-6 we show that the back bending of the microcanonical caloric curve can be easily tuned by variation of the particle number N and the ratio ρ_2/ρ_1 , thus we infer that the back bending which can be only seen in the microcanonical treatment of a system might not be sufficient to classify phase transitions in finite systems, see Fig. 3.4. By using the Multiple Normal Modes model (see Chap. 2.3) we have also shown that the classification of finite systems by the zeros of its complex partition function is robust against variations of the particle number N , as long as the assumption of the model for the structure of the cluster is suited.

As it has been discussed in Chap. 3.1, the investigation of the specific heat or the magnetic susceptibility is not sufficient to determine the order of transition. For a simple system of magnetic clusters (see Chap. 2.3), we also demonstrate that even signals of the specific heat in the positive temperature range may have their origin at complex negative temperatures. Thus one may find for a commonly used indicator such as the specific heat, a deceptive signal for a phase transition at positive temperatures, although the phase transition takes place at negative temperatures.

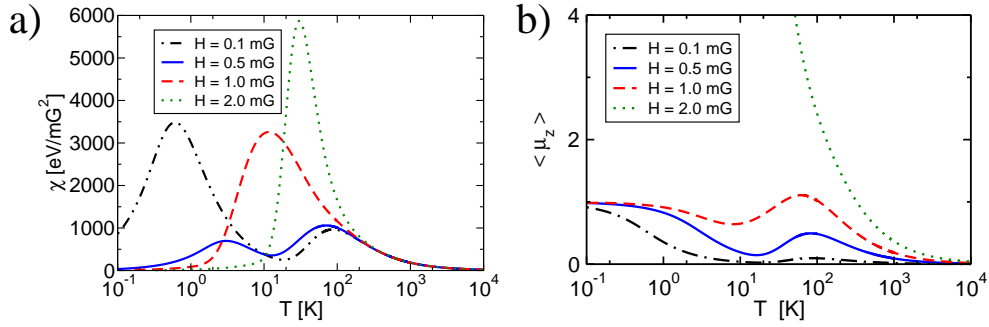


Figure 3.5: a) the magnetic susceptibility versus temperature and b) the absolute value of the average magnetic moment for different magnetic fields.

For example, at 0.5 mGauss (see Fig. 3.5) this simple system exhibits many humps in the magnetic susceptibility, but a strong difference in the magnetization can only be found for magnetic fields above 1.1 mGauss.

Finite systems with finite energy range may show an inverse change of entropy. With the canonical definition for the inverse temperature $\beta = \partial_E S(E) = \partial_E \ln \Omega(E)$, the system can be regarded as in a state of negative temperature. LiF-crystals have been found in negative temperature states by decoupling the spin-temperature from the kinetic energy contribution [91–93].

The inspection of the zeros of the average magnetic moment and the specific heat

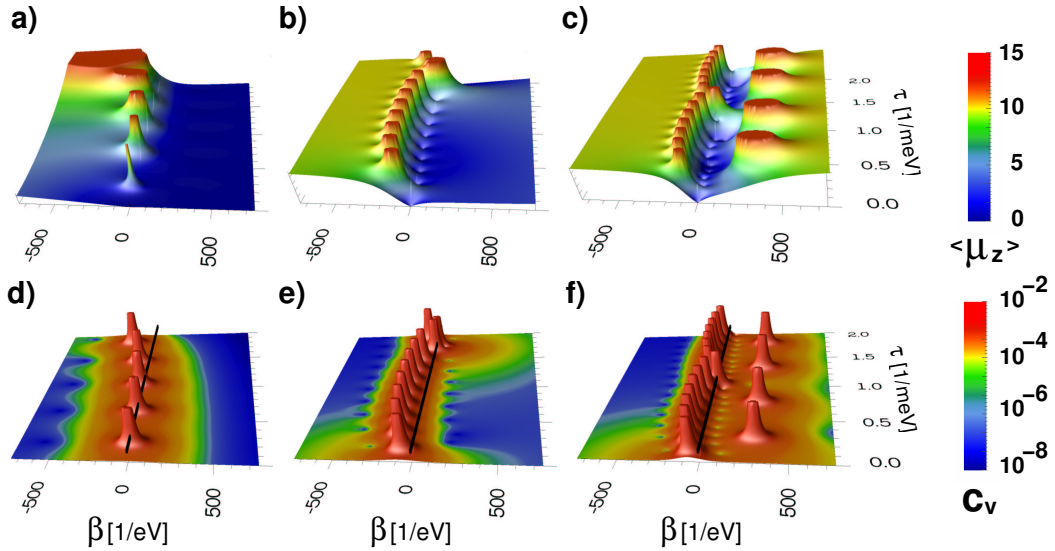


Figure 3.6: The absolute value of the average magnetic moment in the complex temperature plane for (a) 0.1 mGauss, (b) 1.2 mGauss, and (c) 2.0 mGauss and the specific heat in the complex temperature plane for (d) 0.1 mGauss, (e) 1.2 mGauss, and (f) 2.0 mGauss.

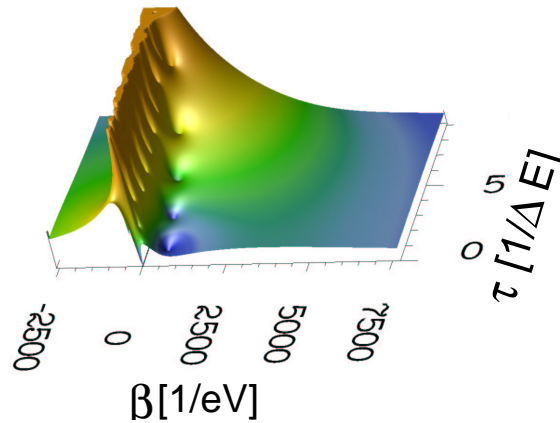


Figure 3.7: The magnetic susceptibility χ over the complex inverse temperature plane for $\chi = 0.5$ mGauss. The z -axis has a logarithmic scale and coloring to better illustrate the radiation of the poles onto the real axis.

reveal a very different formation of the zeros in the complex inverse temperature plane, see Fig. 3.6. The poles of $|\langle \mu_z \rangle|$ coincide with the zeros of the canonical partition function $Z(\mathcal{B})$. With increasing magnetic field the distribution changes and for higher fields a second distribution appears which corresponds to a structural transformation between the two isomers. The classification parameters are $\alpha = 0$ and $\gamma = 0$, therefore this transition is of first order.

By a closer investigation of the complex inverse temperature plane we demonstrate that the origin for the first maximum of $H = 0.5$ mGauss at $T = 40$ K in Fig. 3.5 has its origin in the distribution of zeros in the complex negative temperature plane. The zeros “radiate” onto the real axis. Also the hump in χ at $T \approx 3$ K ($\beta \approx 3800$ 1/eV) has its origin in the distribution of zeros at negative temperatures. Figure 3.7 illustrates the radiation of the poles onto the real axis.

4 Conclusion

In the early days of cluster science many people were doubtful whether phase transitions for small systems even exist. With the strict definition of EHRENFEST for bulk material in mind, they denied the existence of phase transitions in small systems since divergencies and discontinuities in typical thermodynamic response functions were absent. With the advances in numerical simulation and investigation of small systems, many effects such as cluster melting or structural transformations in clusters have been found and are now fairly well understood. But the determination of phase changes involved great numerical effort, because simulations had to be run at many parameter points to extract the thermodynamical properties in order to describe the phase behaviour of the system.

With a few simulations for given temperature and magnetic field, and subsequent multidimensional data analysis we have been able to describe the phase behaviour of magnetic nanoparticles over a broad parameter range. We successfully determined the preferred structures of the magnetic system and identified the order of the transition by different methods, such as the investigation of the Landau free energy and the distribution of zeros of the partition function in the complex temperature plane.

The method of determining the order of a transition by the zeros of the partition function has also been applied to other small systems, such as non-interacting bosons trapped in a small volume, where we have found a dependence of the order on the dimensionality, a property which is also known from Ising-models.

We have also compared the classification scheme with other propositions for the determination of the order of transitions in small systems. We have clearly shown that the proposed equivalence of microcanonical back bending in the caloric curve and first-order phase transitions is not suitable, although in the microcanonical treatment the resulting negative heat capacity might be a sufficient, but not necessary condition.

The commonly used indicators like specific heat or magnetic susceptibility are not only unsuitable to be able to assign an order to a phase transition in small systems, but might also show misleading signals. By the investigation of the whole complex inverse temperature plane we were able to show that the origins of such signals might be in the negative temperature region, although the peak is found in the positive temperature range.

5 Outlook

Clusters offer the opportunity to understand more precisely how nanoscale structures lead to physical and chemical properties of macroscopic phases.

The numerical methods which have been used to ease the investigation of the phase behaviour of small systems, such as the Optimized Data Analysis have interesting prospectives to be applied to other small systems, for instance social and financial networks. Especially the exploration of phase transitions in such systems may give new insights and yield new applications in the future. A good theoretical framework on phase transitions in small systems will support and ease the investigation.

The finding of equivalent conditions for first-order transitions such as the bimodality in probability distributions or the existence of two minima in the Landau free energy or equally spaced zeros perpendicular to the real axis in the complex temperature plane are such steps towards a common view on phase transitions in finite systems.

The classification by the zeros of the complex partition function has been successfully applied to many systems, but in order to spread these ideas further, standard models like the Ising model or the Potts model should be taken into account, since these models have been intensively studied and there are numerous results that can be used to compare with our findings.

Bibliography

- [1] H. H. Heinze, P. Borrmann, H. Stamerjohanns, E. R. Hilf. Temperature measurement from scattering spectra of clusters: theoretical treatment: *Z. Phys. D* **40**, (1-4) 190 (1997).
- [2] D. Tománek, S. G. Kim, P. Jund, P. Borrmann, H. Stamerjohanns, E. R. Hilf. Self-assembly of magnetic nanostructures: *Z. Phys. D* **40**, (1-4) 539 (1997).
- [3] P. Borrmann, H. Stamerjohanns, E. R. Hilf, P. Jund, S. G. Kim, D. Tománek. Thermodynamics of finite magnetic two-isomer systems: *J. Chem. Phys.* **111**, (23) 10689 (1999).
- [4] P. Borrmann, H. Stamerjohanns, E. R. Hilf, D. Tománek. Paradoxical magnetic cooling in a structural transition model: *Eur. Phys. J. B* **19**, (1) 117 (2001).
- [5] P. Borrmann, J. Harting, O. Mülken, H. Stamerjohanns. Classification of phase transitions of finite Bose-Einstein condensates in power-law traps by Fisher zeros: *Phys. Rev. A* **64**, 013611 (2001).
- [6] O. Mülken, H. Stamerjohanns, P. Borrmann. Origins of phase transitions in small systems: *Phys. Rev. E* **64**, 047105 (2001). in press.
- [7] H. Stamerjohanns, O. Mülken, P. Borrmann. Deceptive Signals of phase transitions in Small Magnetic Clusters: *arxiv:cond-mat* page 0107176 (2001).
- [8] S. Grossmann, W. Rosenhauer. Temperature Dependence Near Phase Transition: *Z. Phys.* **207**, 138 (1967).
- [9] M. E. Fisher. The nature of critical points, Statistical Physics, Weak Interactions, Field Theory. In W. E. Brittin, editor, *Lectures in Theoretical Physics*, volume 7c, pages 1–159, University of Colorado Press, Boulder, (1965).
- [10] P. Borrmann, O. Mülken, J. Harting. Classification of phase transitions in small systems: *Phys. Rev. Lett.* **84**, 3511 (2000).
- [11] D. H. E. Gross. Microcanonical thermodynamics and statistical fragmentation of dissipative systems the topological structure of the n-body phase space.: *Phys. Rep.* **279**, 119 (1997).

- [12] D. H. E. Gross, M. Madjet, O. Schapiro. Fragmentation phase transition in atomic clusters I. Microcanonical thermodynamics: *Z. Phys. D* **39**, 75 (1997).
- [13] D. H. E. Gross, E. Votyakov. Phase transitions in "small" systems: *Eur. Phys. J. B* **15**, 115 (2000).
- [14] T. L. Hill. *Thermodynamics of Small Systems Parts I and II*. W. A. Benjamin, Inc, New York, (1963).
- [15] O. Echt, K. Sattler, E. Recknagel. Magic Numbers for Sphere Packings: Experimental Verification in Free Xenon Clusters: *Phys. Rev. Lett.* **47**, 1121 (1981).
- [16] K. Sattler, E. Recknagel, J. Mühlbach. Generation of Metal Clusters Containing from 2 to 500 Atoms: *Phys. Rev. Lett.* **45**, 821 (1980).
- [17] S. Sugano, H. Koizumi. *Microcluster Physics*, volume 20 of *Materials Science*. Springer Verlag, Berlin, Heidelberg, New York, 2nd edition, (1998).
- [18] H. Pauly. *Atom, Molecule and Cluster Beams I*, volume 28 of *Atomic, Optical, and Plasma Physics*. Springer Verlag, Berlin, Heidelberg, New York, (2000).
- [19] J. Lohau, A. Moser, C. T. Rettner, M. E. Best, B. D. Terris. Writing and reading perpendicular magnetic recording media patterned by a focused ion beam: *Appl. Phys. Lett.* **78**, (7) 990 (2001).
- [20] U. Landman, R. N. Barnett, A. G. Scherbakov, P. Avouris. Metal-Semiconductor Nanocontacts: Silicon Nanowires: *Phys. Rev. Lett.* **85**, (4) 1958 (2000).
- [21] M. P. Allen, D. J. Tildesley. *Computer Simulations of Liquids*. Clarendon, Oxford, (1987).
- [22] R. S. Berry, J. Jellinek, G. Natanson. Melting of clusters and melting: *Phys. Rev. A* **30**, 919 (1984).
- [23] R. S. Berry, J. Jellinek, G. Natanson. Unequal freezing and melting temperatures for clusters: *Chem. Phys. Lett.* **107**, 227 (1984).
- [24] G. Franke. *Struktur und Thermodynamik kleiner Edelgascluster*. PhD thesis, University of Oldenburg, Februar 1990.
- [25] P. Borrmann. How should thermodynamics for small systems be done: *Comp. Mat. Sci.* **2**, 593 (1994).
- [26] R. S. Berry, J. Jellinek, G. Natanson. Solid-liquid phase behaviour in microclusters: *Adv. Chem. Phys.* **90**, 75 (1988).
- [27] D. J. Wales, R. S. Berry. Coexistence in Finite Systems: *Phys. Rev. Lett.* **73**, (21) 2875 (1994).

- [28] P. Labastie, R. L. Whetten. Statistical thermodynamics of the cluster solid-liquid transition: *Phys. Rev. Lett.* **65**, 1567 (1990).
- [29] J. Farges, M. F. de Feraudy, B. Raoult, G. Torchet. Noncrystalline structure of argon clusters. i. Polyicosahedral structure of Ar_n clusters, $20 < n < 50$.: *J. Chem. Phys.* **78**, 5067–5080 (1983).
- [30] J. Farges, M. F. de Feraudy, B. Raoult, G. Torchet. Noncrystalline structure of argon clusters. ii. multilayer icosahedral structure of Ar_n clusters, $50 < n < 750$.: *J. Chem. Phys.* **84**, 3491–3501 (1986).
- [31] J. Farges, M. F. de Feraudy, B. Raoult, G. Torchet. Structural models for clusters produced in a free jet expansion.: *Adv. Chem. Phys.* **70**, 45–74 (1988).
- [32] R. E. Rosensweig. *Ferrohydrodynamics*. Cambridge Univ. Press, Cambridge, (1985).
- [33] P. Borrmann, P. Jund, P. Tománek, S. G. Kim. Verfahren und Behältnis zur planmässigen Freisetzung einer Wirksubstanz: *Patent application No. 196 06 804.5, Deutsches Patentamt München* (1996).
- [34] A. Jordan, R. Scholz, P. Wust, H. Faehling, R. Felix. Magnetic fluid hyperthermia (MFH): Cancer treatment with AC magnetic field induced excitation of biocompatible superparamagnetic nanoparticles: *J. Magnetism and Magnetic Materials* **201**, 413 (1999).
- [35] R. Hiergeist et al. Application of magnetite ferrofluids for hyperthermia: *J. Magnetism and Magnetic Materials* **201**, 420 (1999).
- [36] P. Moroz, S. K. Jones, J. Winter, B. N. Gray. Targeting Liver Tumours with Hyperthermia: Ferromagnetic Embolization in a Rabbit Liver Tumour Model: *J. Surg. Oncology* **77**, 1 (2001).
- [37] S. Sun, C. B. Murray, D. Weller, L. Folks, A. Moser. Monodisperse FePt Nanoparticles and Ferromagnetic FePt Nanocrystal Superlattices: *Science* **12**, 1989 (2000).
- [38] D. A. Thompson, J. S. Best. The future of magnetic data storage technology: *IBM J. Res. Develop.* **44**, (3) 311 (2000).
- [39] P. Jund, S. G. Kim, D. Tománek, J. Hetherington. Formation and fragmentation of complex structures in ferrofluids: *Phys. Rev. Lett.* **74**, 3049 (1995).
- [40] H. Wang, Y. Zhu, C. Boyd, W. Luo, A. Cebers, R. E. Rosensweig. Periodic Branched Structures in Phase-Separated Magnetic Colloid: *Phys. Rev. Lett.* **72**, (12) 1929 (1994).
- [41] P. Borrmann, B. Diekmann, E. R. Hilf, D. Tománek. Magnetism of small transition metal clusters and effects of isomerisation: *Surf. Rev. Lett.* **3**, 463 (1996).

- [42] D. J. Evans. On the representation of orientation in space: *Mol. Phys.* **34**, 317–325 (1977).
- [43] N. Metropolis, A. Rosenbluth, M. N. Rosenbluth, A. H. Teller, E. Teller. Equation of State Calculations by Fast Computing Machines: *J. Chem. Phys.* **21**, 1087 (1953).
- [44] K. Binder, editor. *Monte Carlo Methods in Statistical Physics*, volume 7 of *Topics in Current Physics*. Springer Verlag, Berlin, Heidelberg, New York, (1979).
- [45] K. Binder, D. W. Heermann. *Monte Carlo Simulation in Statistical Physics*, volume 80 of *Solid-State Sciences*. Springer Verlag, Berlin, Heidelberg, New York, (1988).
- [46] K. Binder, editor. *The Monte Carlo Method in Condensed Matter Physics*, volume 71 of *Topics in Applied Physics*. Springer Verlag, Berlin, Heidelberg, New York, 2nd corrected edition, (1995).
- [47] J. M. Hammersley, D. C. Handscomb. *Monte Carlo Methods*. Methuen & Co Ltd., London, (1975).
- [48] M. H. Kalos, P. A. Whitlock. *Monte Carlo Methods*. John Wiley & Sons, New York, (1986).
- [49] P. Borrmann. A 53-bit Random number generator. unpublished.
- [50] F. James. A Review of Pseudorandom Number Generators: *Comput. Phys. Commun.* **60**, 329–340 (1990).
- [51] M. Lüscher. A portable high-quality random number generator for lattice field theory simulations: *Comput. Phys. Commun.* **79**, 100–110 (1994).
- [52] M. Matsumoto, T. Nishimura. Mersenne Twister: A 623-dimensionally equidistributed uniform pseudorandom number generator: *ACM Trans. on Modeling and Computer Simulation* **8**, 3–30 (1998).
- [53] D. J. McGinty. Vapor Phase Homogeneous Nucleation and the Thermodynamic Properties of Small Clusters of Argon Atoms: *J. Chem. Phys.* **55**, 580 (1971).
- [54] J. J. Burton. Vibrational Frequencies and Entropies of Small Clusters of Atoms: *J. Chem. Phys.* **56**, 3123 (1972).
- [55] M. R. Hoare. Structure and dynamics of simple microclusters: *Adv. Chem. Phys.* **40**, 49 (1979).
- [56] D. J. Wales. Coexistence in Small Inert Gas Clusters: *Mol. Phys.* **78**, 151 (1993).
- [57] G. Franke, E. R. Hilf, P. Borrmann. The structure of small clusters: Multiple normal-modes model: *J. Chem. Phys.* **98**, 3496 (1993).

- [58] D. J. Wales. Energy Landscapes. In C. Guet, editor, *Atomic Clusters and Nanoparticles*, Les Houches Session LXXIII, Springer Verlag, Berlin, Heidelberg, New York, (2001).
- [59] O. G. Mouritsen. *Computer Studies of Phase Transitions and Critical Phenomena*. Springer Verlag, Berlin, Heidelberg, New York, (1984).
- [60] C. H. Bennet. Efficient Estimation of Free Energy Differences from Monte Carlo Data: *J. Comp. Phys.* **22**, 245 (1976).
- [61] A. M. Ferrenberg, R. H. Swendsen. New Monte Carlo Technique for Studying Phase Transitions: *Phys. Rev. Lett.* **61**, (23) 2635 (1988).
- [62] A. M. Ferrenberg, R. H. Swendsen. Optimized Monte Carlo Data Analysis: *Phys. Rev. Lett.* **63**, (12) 1195 (1989).
- [63] J. P. Valleau, D. N. Card. Monte Carlo Estimation of the Free Energy by Multistage Sampling: *J. Chem. Phys.* **57**, (12) 5457 (1972).
- [64] G. M. Torrie, J. P. Valleau. Monte Carlo Free Energy Estimates using Non-Boltzmann Sampling: Application to the Sub-critical Lennard Jones Fluid: *Chem. Phys. Lett.* **28**, (4) 578 (1974).
- [65] B. A. Berg, T. Neuhaus. Multicanonical ensemble: A new approach to simulate first-order phase transitions: *Phys. Rev. Lett.* **68**, 9 (1992).
- [66] B. A. Berg, U. Hansmann, T. Neuhaus. Simulation of an Ensemble with varying magnetic Field: a Numerical Determination of the Order-Order Interface Tension in the D=2 Ising Model: *Phys. Rev. B* **47**, 229 (1993).
- [67] U. Hansmann, B. A. Berg, T. Neuhaus. Recent Results from Multimagnetical Simulations of the Ising Model: *Intl. Mod. Phys. C* **3**, 1155 (1992).
- [68] E. Marinari, Parisi G. Simulated Tempering: A New Monte Carlo Scheme: *Europhys. Lett.* **68**, 9 (1992).
- [69] H. E. A. Huitema, J. P. van der Eerden. Can Monte Carlo simulations describe dynamics? A test on Lennard-Jones systems: *J. Chem. Phys.* **110**, (7) 3267 (1998).
- [70] A. B. Pippard. *Elements of Classical Thermodynamics*. Cambridge University Press, Cambridge, (1957).
- [71] Wilson. The Renormalization Group and the Critical Phenomena: *Rev. Mod. Phys.* **55**, 583 (1983).
- [72] R. S. Berry, H. Haberland. Introduction. In H. Haberland, editor, *Cluster of Atoms and Molecules I*, volume 52 of *Chemical Physics*, page 1, Springer Verlag, Berlin, Heidelberg, New York, (1995).

- [73] A. E. Ferdinand, M. E. Fisher. Bounded and Inhomogenous Ising Models. I. Specific Heat Anomaly of a Finite Lattice: *Phys. Rev.* **185**, (2) 185 (1969).
- [74] L. D. Landau, E. M. Lifshitz. *Statistische Physik*, volume I. Akademie-Verlag, Berlin, (1976).
- [75] K. Binder. Theory of first-order phase transitions: *Rep. Prog. Phys.* **50**, 783 (1987).
- [76] M. Glosli, J. Plischke. A Monte Carlo and Renormalization Group Study of the Ising Model with Nearest and Next Nearest Neighbor Interactions on the Triangular Lattice: *Can. J. Phys.* **61**, 1515 (1983).
- [77] Y. Zhou, C. K. Hall, M. Karplus. A first-order disorder-to-order transition in an isolated homopolymer model: *Phys. Rev. Lett.* **77**, 2822 (1996).
- [78] C. N. Yang, T. D. Lee. Statistical Theory of Equations of State and Phase Transitions, I. Condensation: *Phys. Rev.* **97**, 404 (1952).
- [79] C. N. Yang, T. D. Lee. Statistical Theory of Equations of State and Phase Transitions, II. Lattice Gas and Ising Model: *Phys. Rev.* **87**, 410 (1952).
- [80] S. Grossmann. Phase Transitions and Distribution of Zeros in the Complex Temperature Plane: *Phys. Lett.* **28A**, (2) 162 (1968).
- [81] S. Grossmann, W. Rosenhauer. Phase Transition and the Distribution of Temperature Zeros of the Partition Function, I. General Relations: *Z. Phys.* **218**, 437 (1969).
- [82] S. Grossmann, V. Lehmann. Phase Transition and the Distribution of Temperature Zeros of the Partition Function, II. Applications and Examples: *Z. Phys.* **218**, 449 (1969).
- [83] K. B. Davis, M.-O. Mewes, M. R. Andrews, N. J. Van Druten, D. S. Durfee, D. M. Kurn, W. Ketterle. Bose-Einstein Condensation in a Gas of Sodium Atoms: *Phys. Rev. Lett.* **75**, (22) 3969 (1995).
- [84] C. C. Bradley, C. A. Sackett, J. J. Tollett, R. G. Hulet. Evidence of Bose-Einstein Condensation in an Atomic Gas with Attractive Interactions: *Phys. Rev. Lett.* **75**, (9) 1687 – 1690 aug 1995.
- [85] C. C. Bradley, C. A. Sackett, R. G. Hulet. Bose-Einstein Condensation of Lithium: Observation of Limited Condensate Number: *Phys. Rev. Lett.* **78**, (Phys. Rev. Lett.) 985 (1997).
- [86] P. Borrmann, G. Franke. Recursion formulas for quantum statistical partition functions: *J. Chem. Phys.* **98**, 2484 (1993).
- [87] L. van Hove. Quelques propriétés générales de l'intégrale de configuration d'un système de particules avec interaction: *Physica* **15**, 951 (1949).

-
- [88] M. Bixon, J. Jortner. Energetic and thermodynamics size effects in molecular clusters: *J. Chem. Phys.* **91**, (1631) (1989).
- [89] D. H. E. Gross. Statistical decay of very hot nuclei: *Phys. Rep.* **53**, 605 (1990).
- [90] M. Schmidt, R. Kusche, T. Hippler, J. Donges, W. Kronmüller, B. von Issendorf, H. Haberland. Negative Heat Capacity for a Cluster of 147 Sodium Atoms: *Phys. Rev. Lett.* **86**, 1191 (2001).
- [91] A. Abragam, W. G. Proctor. Spin Temperature: *Phys. Rev.* **109**, 1441 (1958).
- [92] E. Purcell, R. Pund. A Nuclear Spin System at Negative Temperature: *Phys. Rev.* **81**, 279 (1951).
- [93] N. Ramsey. Thermodynamics and Statistical Mechanics at Negative Absolute Temperatures: *Phys. Rev.* **103**, 20 (1956).

II

ARTICLES

1 Temperature measurement from scattering spectra of clusters: theoretical treatment

**H. Heinze, P. Borrmann, H. Stamerjohanns
and E. R. Hilf**

Zeitschrift für Physik D **40**, (1-4) 190-193 (1997)

Temperature measurement from scattering spectra of clusters: theoretical treatment

H. Heinze, P. Borrmann, H. Stamerjohanns, E.R. Hilf

Fachbereich Physik, Carl-von-Ossietzky-Universität, D-26111 Oldenburg, Germany

Received: 4 July 1996 / Final version: 14 September 1996

Abstract. Scattering spectra from X-ray, electron or neutron diffraction experiments are sufficient to describe the phase behaviour of noble gas clusters and to determine their temperature. Using classical Monte Carlo simulations combined with optimized data analysis and Path Integral Monte Carlo calculations as “idealized experiments” we obtain scattering spectra of Ar- and Ne-clusters. Starting from the classical and quantum mechanical hypervirial theorems we devise a method to estimate the temperature and the caloric curves (which describe the phase behaviour of the noble gas clusters) directly from these scattering spectra using an interatomic potential function as input. As applications we studied for Ar-clusters the effect of different model potentials on the temperature estimate thus contributing to the intricate question of what experimentally is the temperature of an isolated cluster. For Ne-clusters we investigate the differences between classical and quantum mechanical treatment.

PACS: 36.40.+d; 05.20.Gg; 05.30.-d

1 Introduction

Although in the last few years the thermodynamics of small clusters have been a research topic of steadily increasing interest [1–9], there is relatively little progress in connecting experimental and theoretical results. The most crucial experimental task in determining the thermodynamic properties of small clusters is the measurement of the temperature itself.

Early attempts have been made by Farges et al. [10] in 1980 to determine the temperature of clusters produced from free jet expansion by comparison of experimental and theoretical electron diffraction spectra.

This method has two major drawbacks: First, theoretical diffraction spectra have to be calculated for each individual cluster size and several temperatures by time consuming Monte Carlo or Molecular Dynamics simulations. Second, the determination of the experimental temperature has to be done by visual comparison of the theoretical and experimental spectra. A new method is presented here to determine the

kinetic energy of a cluster directly from experimental scattering spectra. If the cluster behaves *almost* classically the canonical ensemble temperature is directly related to the internal kinetic energy by $E_{\text{kin}} = 3/2(N - 1)k_{\text{B}}T$. The kinetic energy is a simple functional of the scattering spectra and an assumed interatomic potential and can be evaluated by a simple one dimensional integration.

In Sect. 2 we derive the necessary quantum mechanical equations for calculating the temperature and the kinetic energy. To test the applicability of our method we use classical Monte Carlo and Path Integral Monte Carlo simulations of small Argon and Neon clusters as idealized experiments (Sect. 3). From the scattering functions generated in these simulations we then calculate the caloric curves and compare them with the exact results from the simulations (Sect. 4).

2 Theoretical method

From kinematic scattering theory it is well known [11] that the real-space pair correlation function

$$\Gamma(r) = \frac{2}{N(N-1)} \left\langle \sum_{1 \leq i < j \leq N} \delta(|\mathbf{x}_i - \mathbf{x}_j| - r) \right\rangle \quad (1)$$

is directly related to the 3-dimensional Fourier transform

$$\Gamma(r) = \int_0^\infty ds \left(\frac{I(s)}{N|f(s)|^2} - 1 \right) 4\pi s^2 \frac{\sin(sr)}{sr} \quad (2)$$

of the scattering intensity $I(s)$ of X-ray, electron or neutron diffraction experiments, respectively. Here the \mathbf{x}_j denote particle positions and $f(s)$ is the atomic structure factor. This function can be determined experimentally and is tabulated for most cases [12].

The pair correlation function is the probability distribution of all possible 2-particle distances r in the clusters. The basic idea of our method is to express quantum mechanical expectation values of the kinetic energy E_{kin} and the potential energy E_{pot} in terms of $\Gamma(r)$.

To accomplish this goal we recall the *hypervirial theorem* of Hirschfelder [13], which is a generalization of the well known virial theorem of Clausius:

Theorem Let \mathbf{H} be a nonrelativistic, time-independent Hamiltonian and \mathbf{W} be a linear operator that is time-independent. If the expectation value of \mathbf{W} for stationary energy eigenstates Ψ of \mathbf{H} is not infinite, then the expectation value of the commutator $[\mathbf{H}, \mathbf{W}]$ for the same eigenstates vanishes: $\langle \Psi | [\mathbf{H}, \mathbf{W}] | \Psi \rangle = 0$.

For a large number of experiments the thermodynamics of noble gas clusters of N identical atoms can be described [14] by a canonical ensemble with a Hamiltonian of the form

$$\mathbf{H} = \left(\sum_{i=1}^N \frac{\mathbf{p}_i^2}{2m} - \frac{\mathbf{P}^2}{2M} \right) + \sum_{i < j} V(r_{ij}), \quad (3)$$

with $r_{ij} = |\mathbf{x}_i - \mathbf{x}_j|$. Here we subtracted the center of mass motion of the system to indicate that only the internal degrees of freedom are of interest.

In coordinate representation the expectation value of the internal kinetic energy is given by

$$E_{\text{kin}} = \frac{1}{Z} \sum_k e^{-\beta E_k} \langle k | \mathbf{H}_{\text{kin}} | k \rangle. \quad (4)$$

where the sum runs over all energy eigenstates, $|k\rangle = |\Psi_k(\mathbf{x}_1, \dots, \mathbf{x}_N)\rangle$ is the N -particle eigenfunction corresponding to energy eigenvalue E_k and $Z = \sum_k \exp(-\beta E_k)$ is the canonical partition function.

As our final goal is the evaluation of the kinetic energy in terms of $\Gamma(r)$ we use the hypervirial theorem to find an expression which is related to $\Gamma(r)$. Choosing the operator \mathbf{W} as

$$\mathbf{W} = \sum_{i=1}^N \mathbf{x}_i \cdot \nabla_i, \quad (5)$$

the hypervirial theorem for this system reduces to

$$\begin{aligned} \langle k | \left(\sum_{i=1}^N \frac{\mathbf{p}_i^2}{2m} - \frac{\mathbf{P}^2}{2M} \right) | k \rangle \\ = \langle k | \frac{1}{2} \sum_{i=1}^N \mathbf{x}_i \cdot \nabla_i \sum_{m < n} V(r_{mn}) | k \rangle \\ = \langle k | \frac{1}{2} \sum_{i < j} r_{ij} V'(r_{ij}) | k \rangle \end{aligned} \quad (6)$$

Equation (6) can be interpreted as the quantum mechanical version of Clausius' virial theorem of classical mechanics.

Now the potential as well as the kinetic energy can be represented as expectation values of functions depending only on the interparticle distances r_{ij} :

$$E_{\text{kin}} = \frac{1}{Z} \sum_k e^{-\beta E_k} \langle k | \frac{1}{2} \sum_{i < j} r_{ij} V'(r_{ij}) | k \rangle, \quad (7)$$

$$E_{\text{pot}} = \frac{1}{Z} \sum_k e^{-\beta E_k} \langle k | \sum_{i < j} V(r_{ij}) | k \rangle. \quad (8)$$

Since the pair correlation function (1) gives the probability of finding two particles at distance r we easily derive

$$E_{\text{kin}} = \frac{N(N-1)}{4} \int_0^\infty dr \Gamma(r) r V'(r), \quad (9)$$

and

$$E_{\text{pot}} = \frac{N(N-1)}{2} \int dr \Gamma(r) V(r). \quad (10)$$

In the classical limit it is possible to express the temperature T in terms of the internal kinetic energy as

$$T = \frac{2}{3(N-1)k_B} E_{\text{kin}} = \frac{N}{6k_B} \int_0^\infty dr \Gamma(r) r V'(r). \quad (11)$$

In a typical experimental situation with a normalized size distribution $\sigma(N)$ of clusters (e.g. in a cluster beam produced by supersonic jet expansion) we find

$$T = \frac{1}{6k_B} \frac{\int dr \tilde{\Gamma}(r) r V'(r)}{\int dN \sigma(N) N^{-1}} \quad (12)$$

where $\tilde{\Gamma}(r)$ is the Fourier transform (2) of the measured intensity. Note that (12) is obviously only valid if the clusters of different sizes are in thermal equilibrium.

3 Numerical experiments

Neon clusters are expected to show distinct quantum effects. This makes a comparison between a quantum mechanical and a classical treatment reasonable. Argon clusters are very well investigated clusters and can, somehow, be regarded as a reference system. We therefore decided to take both, Argon and Neon clusters, as test systems for the temperature measurement method presented above.

To obtain appropriate scattering spectra we performed classical and Path Integral Monte Carlo calculations [15] for Argon and Neon clusters of different sizes up to $N=56$. We used a Lennard-Jones (12-6) potential to model the interaction between the atoms

$$V(r) = 4\epsilon \left[\left(\frac{\sigma}{r} \right)^{12} - \left(\frac{\sigma}{r} \right)^6 \right] \quad (13)$$

with parameters $\sigma = 3.405 \text{ \AA}$ and $\epsilon = 10.3 \text{ eV}$ for Argon and $\sigma = 2.745 \text{ \AA}$ and $\epsilon = 3.068 \text{ eV}$ for Neon. With this potential choice all classical results for Neon clusters can be inferred from those for Argon clusters by means of simple scalings. For Argon clusters the classical treatment is almost appropriate. For Neon clusters it is not and only made for comparison with the full quantum mechanical treatment.

The scattering spectra are obtained from canonical ensemble Metropolis [16] samplings with 2×10^7 steps per temperature combined with a subsequently applied data analysis similar to the method of Ferrenberg et.al. [17].

Since we carefully checked all our results for convergence and obtained error estimates well below 0.3 % we regard the results of our very demanding computer experiments, which took e.g. for the quantum mechanical calculation of Ne_{13} about 10 days on a Convex SPPUX parallel computer with 16 processors, as quasi exact. A more detailed account of our simulation techniques will be given in a subsequent publication.

As an example Fig. 1 displays some scattering spectra and the corresponding pair correlations functions for Ar_{13} , Ar_{14} , Ar_{55} , Ar_{56} , and Ne_{13} . For simplicity we have set the atomic structure factor $f(s)$ appearing in (2) to 1.

192

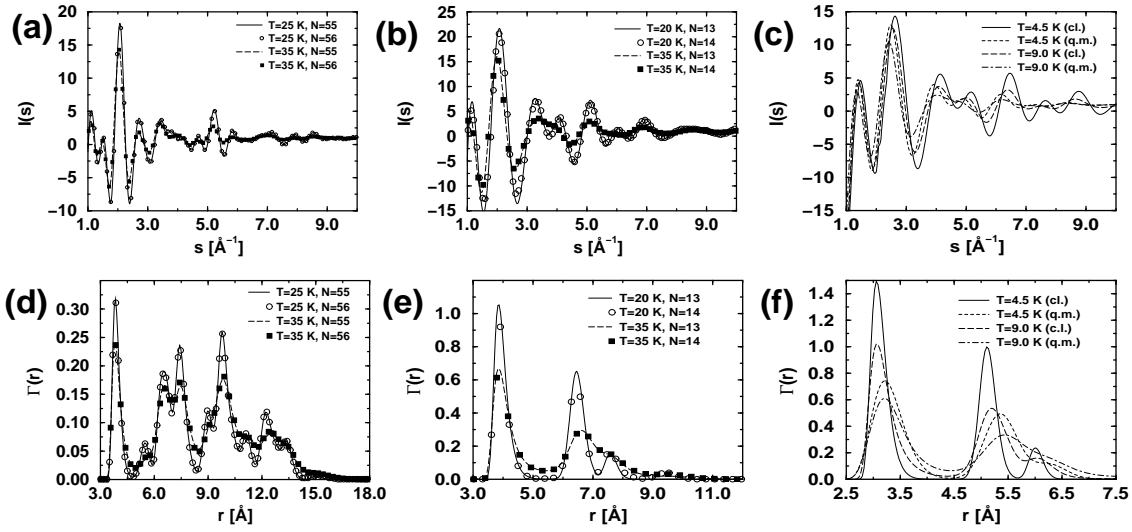


Fig. 1a-f. Scattering spectra $I(s)$ and the corresponding pair correlation functions $\Gamma(r)$ of **a** Ar_{55} and Ar_{56} , **b** Ar_{13} and Ar_{14} , and **c** Ne_{13} and **d-f.** The results for Argon are from classical Monte Carlo calculations only, while for Neon classical (cl.) and quantum mechanical (q.m.) results are plotted

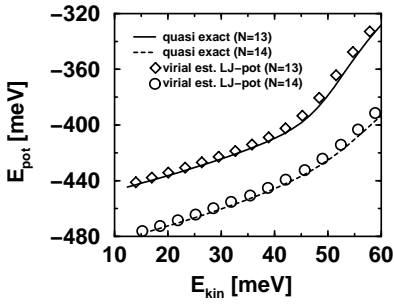


Fig. 2. Caloric curves of Ar_{13} clusters: exact curve (solid line), virial estimate (diamonds), and Ar_{14} clusters: exact curve (dashed line), virial estimate (circles)

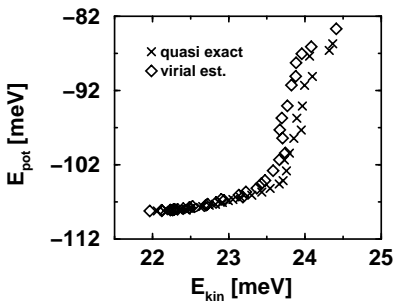


Fig. 3. Quantum mechanical caloric curves of Ne_{13} clusters

4 Results

Since in canonical (Path Integral) Monte Carlo simulations the temperature T acts as an external parameter and E_{kin} , E_{pot} , and C_V can easily be evaluated on the fly, these (as quasi exact regarded) values can be compared to those obtained from scattering spectra.

Figure 2 displays the caloric curves for Ar_{13} and Ar_{14} clusters. The scattering spectra for Argon are results of classical MC simulation. For both cluster sizes the agreement

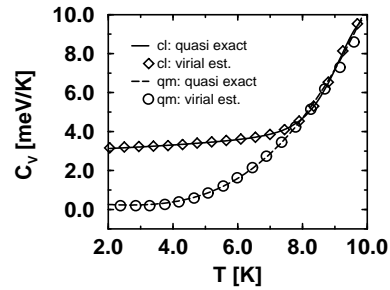


Fig. 4. Identification of phase transitions from scattering functions: Constant volume heat capacity C_V of Ne_{13}

between the exact curves and those derived using the hyper-virial method is almost perfect.

For Ne_{13} we utilized Path Integral Monte Carlo simulations to calculate the caloric curves shown in Fig. 3. Although there are slight deviations of the virial estimate curve from the exact curve in the well known coexistence phase of different cluster isomers at about 23.7 meV the phase behaviour of the clusters can be judged very accurately from this curve.

Figure 4 shows the specific heat C_V of Ne_{13} as a function of temperature as obtained by numerical differentiation of the caloric curves. Again the agreement between the exact and the curve based on the virial estimate is almost perfect.

The absolute error of the temperature estimate based on (11) for Ar_{12-14} turns out to be less than 2 K in the whole examined region from 10-40 K (see Fig. 5). Since (11) is exact in the classical case the source of the error is easily identified to be the noise in the scattering spectra.

Some tests on the influence of the interatomic potential functions on the temperature estimates revealed that all commonly used realistic potentials give similar results with only slight deviations.

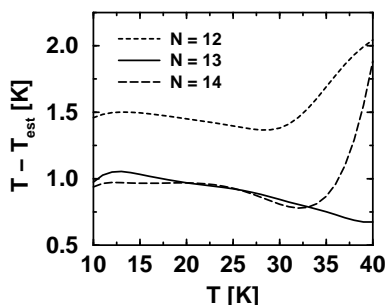


Fig. 5. Absolute error of the temperature estimate of Ar_{12-14} using the hypervirial method

5 Conclusion

We presented a method to determine the kinetic energy and the temperature directly from scattering spectra. This method is superior in its numerical effort as compared to others since only one Fourier transform and one integration have to be performed. Numerical tests for Argon and Neon clusters have shown that it is applicable for classical and quantum mechanical systems. From (12) we infer that this computational technique is quite useful even in experimental situations with broad distributions of cluster sizes.

References

1. C.L. Briant, J.J. Burton, *J. Chem. Phys.* **63**, 2045 (1975).
2. M.R. Hoare, *Adv. Chem. Phys.* **40**, 49 (1979).

3. G. Natanson, F. Amar, R.S. Berry, *J. Chem. Phys.* **78**, 399 (1983); R.S. Berry, J. Jellinek, G. Natanson, *Chem. Phys. Lett* **107**, 227 (1984).
4. H.L. Davis, J. Jellinek, S. Berry, *J. Chem. Phys.* **86**, 6456 (1987).
5. F.G. Amar, R.S. Berry, *J. Chem. Phys.* **85**, 5943 (1986); J. Jellinek, T.L. Beck, S. Berry, *J. Chem. Phys.* **84**, 2783 (1986); T.L. Beck, J. Jellinek, S. Berry, *J. Chem. Phys.* **87**, 545 (1987); T.L. Beck, S. Berry, *J. Chem. Phys.* **88**, 3910 (1988); R.S. Berry, *Z. Phys. D* **12**, 161 (1989).
6. R. Stephen Berry, *Phys. Rev. Lett.* **71**, 3987 (1993); R. Stephen Berry, *Phys. Rev. Lett.* **73**, 2875 (1993).
7. G. Franke, E. R. Hilf, L. Polley, *Z. Phys. D* **9**, 343 (1988); G. Franke, J. Schulte, *Z. Phys. D* **12**, 65 (1989).
8. G. Franke, E.R. Hilf, P. Borrmann, *J. Chem. Phys.* **98**, 3496 (1993).
9. P. Borrmann, D. Gloski, E.R. Hilf, *Surface Review and Letters* **3**, 103 (1996).
10. J. Farges, M.F. de Feraudy, B. Raoult, and G. Torchet, *J. Phys. (Paris) C 3, No. 4*, **41**, (1980); *Surf. Sci.* **106**, 95 (1981).
11. L.E. Sutton, in *Molecular Structure by Diffraction Methods - Volume 1*, Spec. Period. Rep., (The Chemical Society, 1973).
12. L.S. Bartell, *Chem. Rev.* **86**, 491 (1986) and references therein.
13. J.O. Hirschfelder, *J. Chem. Phys.* **33**, 1462 (1960).
14. R.S. Berry, in *Atomic and Molecular Clusters I*, edited by H. Haberland (Springer, Berlin Heidelberg, 1994).
15. P. Borrmann, *COMMAT* **2**, 593 (1994); P. Borrmann, Ph.D. thesis, Carl von Ossietzky University Oldenburg (1995).
16. N. Metropolis, A.W. Rosenbluth, M.N. Rosenbluth, A.H. Teller and E. Teller, *J. Chem. Phys.* **21**, 1087 (1953).
17. A.M. Ferrenberg, R.H. Swendsen, *Phys. Rev. Lett.* **61**, 2635 (1988); **63**, 1195 (1989).

This article was processed by the author using the L^AT_EX style file *pljour2* from Springer-Verlag.

2 Self-assembly of magnetic nanostructures

**D. Tománek, S. G. Kim, P. Jund, P. Borrmann,
H. Stamerjohanns and E. R. Hilf**

Zeitschrift für Physik D **40**, (1-4) 539-541 (1997)

Self-assembly of magnetic nanostructures

David Tománek¹, Seong Gon Kim¹, Philippe Jund¹, Peter Borrmann², Heinrich Stamerjohanns², Eberhard R. Hill²

¹ Department of Physics and Astronomy, Michigan State University, East Lansing, MI 48824-1116, USA

² Department of Physics, University of Oldenburg, D-26111 Oldenburg, Germany

Received: 5 July 1996 / Final version: 23 October 1996

Abstract. We use Monte Carlo and quaternion molecular dynamics simulations to study the self-assembly of intriguing structures which form in colloidal suspensions of small magnetite particles. We show that the only stable isomers with few particles, a ring and a chain, can be efficiently interconverted using a magnetizable tip. We propose to use the oscillating dipole field of the tip to locally anneal the aggregates to either a ring in zero field or a chain in nonzero applied field.

PACS: 75.50.Mm

Given the present advanced stage of miniaturization, the most promising way to significantly reduce the dimension of devices involves a transition from micro-manufacturing to self-assembly of nanostructures [1]. Inspired by the richness of structures observed in aggregates of magnetic nanoparticles [2, 3] and the possibility of their structural transformation [4, 5], we propose a hybrid thermodynamic self-assembly technique capable of producing magnetic patterns of unprecedented packing density [6]. The key ingredients are a system of magnetic nanoparticles in a colloidal suspension, resonant magnetic heating on the nanometer scale that we postulate, and the possibility to manipulate individual nanostructures using a local magnetic field. In the following, we prove our technique to work using realistic Monte Carlo and Molecular Dynamics simulations addressing the self-assembly, the field-assisted interconversion, and the long-term stability of the magnetic nanostructures.

In the following, we will describe microscopically the structural and magnetic transitions in microcanonical and canonical ensembles of few magnetic particles. Commercially available spherical nanoparticles of magnetite are covered by a thin surfactant layer to inhibit irreversible coalescence in a viscous liquid at room temperature [2]. Such colloidal suspensions, called ferrofluids, have recently become a focus of experimental and theoretical attention due to their interesting behavior in applied magnetic fields [2, 3, 7–12]. We will discuss the effect of field and temperature on the stability of the individual isomers, which – for few particles – are known to be either a chain or a ring [4]. More important, we will show how to locally modify their equilibrium

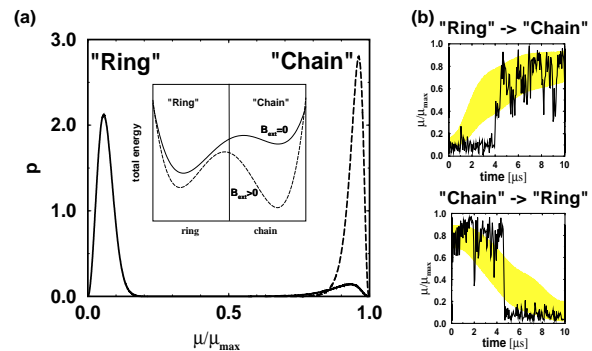


Fig. 1. **a** Magnetic moment distribution p at $B_{\text{ext}} = 0$ (solid line) and $B_{\text{ext}} = 100$ Gauss (dashed line), both at $T = 300$ K. **b** Temporal evolution of the total magnetic moment of the aggregate during the assembly causing the transformation from a ring to a chain, and transformation from a chain to a ring. The solid lines illustrate successful trajectories and the gray shaded areas statistical ensemble averages

structure by changing the field and temperature (assembly of nanostructures) and how to distinguish magnetically between the different isomers (detection of nanostructures).

The Hamiltonian describing our model system of six [13] magnetic particles has been described in [4] and can be easily parametrized [14]. Depending on the magnetic field, the equilibrium geometry of this system at low temperatures is either a ring with zero total magnetic moment or a chain with the magnetic moment $\mu = \mu_{\max} = N\mu_0$. As illustrated in the inset of Fig. 1a, rings are more stable in zero field, whereas chains are more stable in high magnetic fields B_{ext} [4]. The large minimum potential energy barrier per particle $\Delta E \approx 0.16$ eV, corresponding to a “melting” temperature $T_M \approx 630$ K, prevents metastable chains in zero field from closing to rings at room temperature. On the other hand, rings do not fragment into chains, unless exposed to high magnetic fields $B_{\text{ext}} \gtrsim 600$ Gauss [4, 5], and hence are not disturbed by the low fields generated by aggregates in neighboring cells. This establishes the required stability of the magnetic structure [15].

Next, we studied the efficiency of the field-assisted assembly process. Results of a room temperature Monte Carlo simulation in applied fields $B_{\text{ext}} = 0$ and $B_{\text{ext}} = 100$ Gauss

are presented in Fig. 1a. These data indicate that upon the application of a high magnetic field for sufficiently long time, the majority of the systems will form a chain. In absence of a field, after careful annealing, the majority of the systems will form a ring. Both isomers can be easily distinguished by separate peaks in the distribution of magnetic moments. Consequently, we will use the magnetic moment as the single characteristic of the nanostructure.

In order to estimate the time needed to assemble a nanostructure, we performed Molecular Dynamics simulations of the transition between a ring and a chain in a microcanonical ensemble of six magnetite particles. We made use of the quaternion formalism [16–18] to avoid divergencies in the orientational equations of motion which would otherwise occur in this system of magnetic spherical tops (with a nonvanishing mass and inertia) due to discontinuities in Euler angle coordinates. We used time steps $\Delta t = 5 \times 10^{-11}$ s and integrated the equations of motion numerically using a fourth-order Runge-Kutta algorithm, since this method proved to be more stable and to better conserve the energy than alternate integration schemes.

These and our above Monte Carlo studies suggest that heating up the system 100 K above room temperature reduces the average time for a structural transformation by one order of magnitude and hence significantly accelerates the assembly. On the other hand, the higher vibrational entropy of the chain in zero field (as compared to the ring) plays an increasingly important role at these higher temperatures. This has no adverse effect on the ring-to-chain conversion in nonzero fields, but reduces the fraction of rings in zero field and hence the efficiency of the chain-to-ring conversion.

The feasibility of a high packing density of nanostructures depends on the availability of an extremely localized source of magnetic field and heat. As a promising technical realization, we suggest to use a soft magnetic nanotip, surrounded by a coil, as the source of localized static and oscillating magnetic field. This nanoscopic electromagnet assembly can be suspended on a cantilever using the technology developed for the Atomic Force Microscope (AFM) [19]. The capability to assist in the assembly and detection of magnetic nanostructures with a precision of 100 – 1000 Å might be relatively simple to achieve in view of the AFM's success to obtain atomic resolution [19].

For field assisted assembly, a sharp magnetic tip has several advantages. (i) The field inhomogeneity guarantees that neighboring structures are not disturbed and that magnetite particles aggregate faster in the tip region. (ii) The tip can be used to generate a locally large static field to assemble a chain. (iii) Fast field reversal can be used to detach any aggregate from the tip. (iv) An oscillating high-frequency field, generated by the tip, can be used to excite preferentially the transverse bending modes of the chain, hence accelerating ring closure in a cooling environment [20].

The sharp tip, suspended on the cantilever of a Magnetic Force Microscope, can also be used to investigate the magnetic structures. The detection process is initiated by applying a weak inhomogeneous magnetic field which will attract only magnetic aggregates (chains, but *not* nonmagnetic rings) to the tip. The presence of a chain attached to the tip will lead to a lowering of the mechanical resonance frequency of the cantilever-tip system that can be detected.

This allows for a discrimination between a chain and a ring in a nondestructive way.

We model the magnetic tip by a nonmagnetic cone with an opening angle of 60° , which is rounded off at the end and terminated by a magnetizable sphere (see Fig. 2). The diameter of this sphere, $\sigma_{tip} = 400$ Å, is twice that of the magnetite particles in the colloidal suspension, and its magnetic moment is aligned with the cone axis. The nonmagnetic part of the interaction between the tip and the magnetite particles is assumed to be purely repulsive. In analogy to the nonmagnetic interaction between the particles [14], it is given by $u_r = \epsilon \exp(-d/\rho_1)$, where d is the minimum distance between the surfaces of the tip and the magnetite particle in the colloid. The inhomogeneous magnetic field produced by this tip attracts magnetic aggregates and aligns their magnetic moment with the cone axis.

The dynamics of the structural transformation, assisted by the local field of a sharp magnetic tip, is illustrated in Fig. 1b. To accelerate a ring-to-chain conversion, we first heated the system locally. We found that an oscillating dipole field of frequency $\nu = 1$ MHz, generated by changing periodically the direction of the dipole moment at the tip $\mu_{tip} = 7 \times 10^5 \mu_B$, was most efficient in heating up the system by exciting resonantly its low-frequency eigenmodes, such as the bending mode. The system, which had reached an average temperature of 500 K after 5 μ s, was subsequently cooled down during the next 5 μ s in the *static* field of the tip dipole $\mu_{tip} = 7 \times 10^5 \mu_B$ by extracting stepwise the energy doses of 15 meV, each followed by 1 μ s equilibration time. The same annealing schedule has been used for a chain-to-ring conversion, with the exception of using a smaller value for the oscillating tip dipole moment $\mu_{tip} = 4 \times 10^5 \mu_B$ during the annealing process and $\mu_{tip} = 0$ during the cooling process. As seen in Fig. 1b, the average time needed to convert a ring to a chain or vice versa lies close to 5 μ s [21].

The field-assisted assembly process with a sharp magnetic tip is illustrated in Fig. 2 by snapshots from a Molecular Dynamics simulation. At the starting point of our simulation, shown in Fig. 2a, the magnetite particles are randomly distributed and oriented in zero field. The assembly of a chain is initiated by a static magnetization of the tip. This causes the particles to aggregate in the region of strongest B_{ext} -field and to form a chain aligned with the field lines that is attached to the tip, as shown in Fig. 2b. Subsequent reversal of the magnetization of the tip causes the chain to detach from the tip, as shown in Fig. 2c. At this point, a stable chain is formed. As illustrated in Fig. 2d, applying a high-frequency dipole field excites the bending mode of the chain efficiently, facilitating closure to a ring. Figure 2e shows the spontaneous self-assembly of the ring structure after the field had been switched off. The stability of this structure increases as it cools down in the suspending liquid.

In conclusion, we proposed and modeled a hybrid self-assembly technique for aggregates consisting of magnetite nanoparticles, that is capable of producing magnetic patterns with unprecedented density. When viewed as information, this data density would by far exceed that of conventional magnetic and protein-based memories [22]. The key to tailored magnetic nanopatterns are the substantially different magnetic moments of the only stable isomers with few magnetite particles which are a ring and a chain. We proposed an

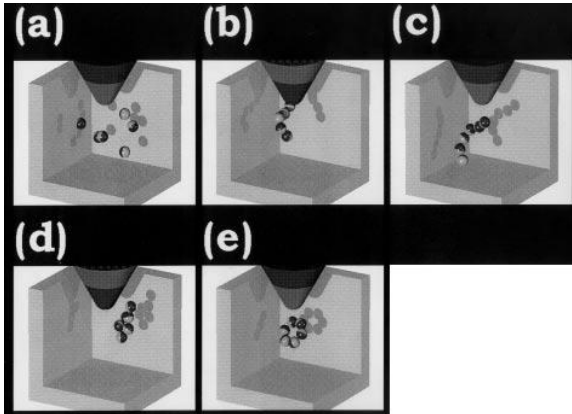


Fig. 2a–e. Snapshots of the nanostructure assembly process. The spheres represent the magnetite dipoles and the shading of the hemispheres the dipole orientation. The cone in the *upper part* of the cell represents the magnetic tip as source of the localized magnetic field. Grey shading shows the polarity of the tip when a field is applied. **a** Initial random configuration in zero field. **b** In a static dipole field, particles form a chain attached to the tip. **c** Field reversal causes the intact chain to detach from the tip. **d** Local magnetic “heating” of the system by a high-frequency field of the tip excites predominantly the bending mode of the chain. **e** Spontaneous aggregation in zero field in the suspending liquid concludes the assembly to a ring

efficient process to assemble and to detect individual nanostructures using the localized static and oscillating dipole field of a sharp magnetic tip. We believe that the technique proposed here may bring us closer to nanopatterning on the atomic scale.

DT, PJ and SGK acknowledge financial support by the National Science Foundation under Grant Number PHY-92-24745 and the Office of Naval Research under Grant Number N00014-90-J-1396. Our extensive computer simulations have been performed on the CRAY-T3D/192 of the *Konrad-Zuse-Institute* in Berlin and the S400 supercomputer of the *Regionales Rechenzentrum für Niedersachsen (RRZN)* in Hannover.

References

- George M. Whitesides: *Scientific American* (September 1995), p. 146; Kaigham J. Gabriel: *Scientific American* (September 1995), p. 150
- Hao Wang, Yun Zhu, C. Boyd, Weili Luo, A. Cebers, R.E. Rosensweig: *Phys. Rev. Lett.* **72**, 1929 (1994)
- Akiva J. Dickstein, Shyamsunder Erramilli, Raymond E. Goldstein, David P. Jackson, Stephen A. Langer: *Science* **261**, 1012 (1993)
- P. Jund, S.G. Kim, D. Tománek, J. Hetherington: *Phys. Rev. Lett.* **74**, 3049 (1995)
- Peter Borrmann, Heinrich Stamerjohanns, Eberhard R. Hilf, Seong Gon Kim, Philippe Jund, David Tománek: (submitted for publication)
- In contrast to the current definition of self-assembly, we discuss a technique to externally direct the self-assembly of ordered, thermodynamically stable structures
- H. Zhang, M. Widom: *Phys. Rev. E* **49**, R3591 (1994); *J. Mag. Mag. Mat.* **122**, 119 (1993)
- J.J. Weis, D. Levesque: *Phys. Rev. E* **48**, 3728 (1993); D. Levesque, J.J. Weis: *Phys. Rev. E* **49**, 5131 (1994)
- A.S. Clarke, G.N. Patey: *J. Chem. Phys.* **100**, 2213 (1994)
- Holly B. Lavender, Karthik A. Iyer, Sherwin J. Singer: *J. Chem. Phys.* **101**, 7856 (1994)
- Thomas C. Halsey, Will Toor: *Phys. Rev. Lett.* **65**, 2820 (1990); Thomas C. Halsey, James E. Martin, Douglas Adolf: *Phys. Rev. Lett.* **68**, 1519 (1992); Thomas C. Halsey: *Phys. Rev. E* **48**, R673 (1993)
- R. Tao, J.M. Sun: *Phys. Rev. Lett.* **67**, 398 (1991)
- The exact number of particles in the system is not critical, since all systems with $4 \lesssim N \lesssim 14$ are known to have only the “ring” or the “chain” as their equilibrium structure [4, 8], and hence show the same physical phenomena
- Our system contains spherical magnetite particles with a diameter $\sigma = 200 \text{ \AA}$, mass $m = 1.31 \times 10^7 \text{ amu}$, inertia $I = 5.25 \times 10^7 \text{ amu \AA}^2$, and a permanent magnetic moment $\mu_0 = 1.68 \times 10^5 \mu_B$. Besides considering the interaction of the magnetic dipoles with the external magnetic field and their mutual dipole-dipole interaction, we introduce a pairwise nonmagnetic interaction between the particles, given by $u(r) = \epsilon \left[\exp\left(-\frac{r_{ij}-\sigma}{\rho_1}\right) - \exp\left(-\frac{r_{ij}-\sigma}{\rho_2}\right) \right]$, with $\rho_1 = 5.0 \text{ \AA}$, $\rho_2 = 2\rho_1 = 10.0 \text{ \AA}$, and $\epsilon = 64 \times 10^{-3} \text{ eV}$
- The stability of the nanostructure can be independently increased by increasing the viscosity of the suspending liquid. This would make a creation of permanent devices possible
- Herbert Goldstein: *Classical Mechanics*, 2nd edn., Reading Mass: Addison-Wesley 1980
- D.J. Evans: *Mol. Phys.* **34**, 317 (1977); D.J. Evans, S. Murad: *Mol. Phys.* **34**, 327 (1977)
- Michael P. Allen: *Mol. Phys.* **52**, 717 (1984)
- G. Binnig, C.F. Quate, Ch. Gerber: *Phys. Rev. Lett.* **56**, 930 (1986); *Appl. Phys. Lett.* **40**, 178 (1982)
- The oscillating external magnetic field may be used not only to excite the internal modes of chains and rings, but also to accelerate these aggregates back and forth, eventually causing an impact-induced fragmentation of the aggregate at the tip
- We found that after $10 \mu\text{s}$, $\approx 95\%$ rings have converted successfully to chains, and $\approx 90\%$ chains have converted to rings. A higher success rate can be achieved by a corresponding extension of the interconversion time
- Robert R. Birge: *Scientific American* (March 1995), p. 90

3 **Thermodynamics of finite magnetic two-isomer systems**

**P. Borrmann, H. Stamerjohanns, E. R. Hilf,
P. Jund, S. G. Kim and D. Tománek**

Journal of Chemical Physics **111**, (23) 10689-10693
(1999)

Thermodynamics of finite magnetic two-isomer systems

Peter Borrmann, Heinrich Stamerjohanns,^{a)} and Eberhard R. Hilf
Department of Physics of the University Oldenburg, D-26111 Oldenburg, Germany

Philippe Jund,^{b)} Seong Gon Kim,^{c)} and David Tománek
Department of Physics and Astronomy, Michigan State University, East Lansing, Michigan 48824-1116

(Received 28 June 1999; accepted 23 September 1999)

We use Monte Carlo simulations to investigate the thermodynamical behavior of aggregates consisting of few superparamagnetic particles in a colloidal suspension. The potential energy surface of this classical two-isomer system with a stable and a metastable “ring” and “chain” configuration is tunable by an external magnetic field and temperature. We determine the complex “phase diagram” of this system and analyze thermodynamically the nature of the transition between the ring and the chain “phase.” © 1999 American Institute of Physics.
 [S0021-9606(99)51747-9]

I. INTRODUCTION

With progressing miniaturization of devices,¹ there is a growing interest in the thermodynamical behavior of finite-size systems. A central question in this respect is, whether small systems can exhibit well-defined transitions that could be interpreted as a signature of phase transitions which, strictly speaking, are well defined only in infinite systems.² So far, reproducible features of the specific heat have been interpreted as indicators of “melting” transitions in small rare gas clusters.^{3,4} While most of the computational studies of cluster thermodynamics have considered only one external variable, namely either the temperature or the energy, there is only one study by Cheng *et al.*,⁵ where the pressure p entered as a second variable.

Here, we investigate the thermodynamical behavior of a finite system which is also controlled by *two* external variables, namely the temperature T and the magnetic field B_{ext} . The system of interest consists of few near-spherical, superparamagnetic particles with a diameter of ≈ 10 – 500 Å in a colloidal suspension. Such systems, covered by a thin surfactant layer, are readily available in macroscopic quantities, are called ferrofluids, and are known to form complex labyrinth⁶ or branched structures⁷ as many-particle systems, whereas the only stable isomers for systems with few particles ($N < 14$) are the “ring” and the “chain.”⁸

The existence of two environmental variables, yet still only two isomer states, gives rise to a rich thermodynamic behavior, as compared to that of other small clusters such as the noble gas clusters.^{3,4} This classical, externally tunable finite two-isomer system is quite different from finite spin lattices, where magnetic interactions between fixed sites are parametrized.^{2,9} The magnetic tops in our system are free to move in three-dimensional space and their magnetic dipole–

dipole interaction has a nontrivial spatial dependence.

We will show that the system exhibits a phase transition between *two* ordered phases, one magnetic and the other nonmagnetic, as well as phase transitions between these ordered phases and a disordered phase. Whereas the system is not susceptible to small magnetic fields, it shows a strong paramagnetic response when exposed to larger magnetic fields.

II. MODEL

Our model system consists of six spherical magnetite particles with a diameter of $\sigma = 200$ Å and a large permanent magnetic moment $\mu_0 = 1.68 \times 10^5 \mu_B$. The potential energy E_p of this system in the external field \mathbf{B}_{ext} consists of the interaction between each particle i and the applied field, given by $u_i = -\boldsymbol{\mu}_i \times \mathbf{B}_{\text{ext}}$, and the pair-wise interaction between the particles i and j , given by⁸

$$u_{ij} = (\mu_0^2 / r_{ij}^3) [\hat{\boldsymbol{\mu}}_i \times \hat{\boldsymbol{\mu}}_j - 3(\hat{\boldsymbol{\mu}}_i \times \hat{r}_{ij})(\hat{\boldsymbol{\mu}}_j \times \hat{r}_{ij})] + \epsilon \left[\exp\left(-\frac{r_{ij} - \sigma}{\rho}\right) - \exp\left(-\frac{r_{ij} + \sigma}{2\rho}\right) \right]. \quad (1)$$

The first term in Eq. (1) is the magnetic dipole–dipole interaction energy. The second term describes a nonmagnetic interaction between the surfactant covered tops in a ferrofluid that is repulsive at short range and attractive at long range.⁷ We note that the most significant part of this interaction, which we describe by a Morse-type potential with parameters $\epsilon = 0.121$ eV and $\rho = 2.5$ Å, is the short-range repulsion, since even at equilibrium distance the attractive part does not exceed 10% of the dipole–dipole attraction. The thermal equilibrium structures of small clusters are either rings or chains, which can be easily distinguished by their mean magnetic moment $\langle \mu \rangle$.

III. NUMERICAL METHOD

The canonical partition function, from which all thermodynamical quantities can be derived, is given by

^{a)} Author to whom correspondence should be addressed. Electronic mail: stamer@uni-oldenburg.de

^{b)} Present address: Laboratoire des Verres, Université de Montpellier 2, Case 069 - Place Eugene Bataillon, F-34095 Montpellier Cedex 5, France.

^{c)} Present address: Code 6690, Complex Systems Theory Branch, Naval Research Laboratory, Washington, DC 20375-5320.

$$Z(B_{\text{ext}}, T) = (2\pi\beta)^{-6N/2} \int \left[\prod_{i=1}^N d\mathbf{x}_i d\phi_i d\theta_i d\psi_i \right] \times \exp\left(-\beta\left(\sum_{i<j}^N u_{ij} - \sum_i^N \mu_{i,z} B_{\text{ext}}\right)\right), \quad (2)$$

where $\beta = (k_B T)^{-1}$ and where the field \mathbf{B}_{ext} is aligned with the z -axis. The pre-exponential factor addresses the fact that each particle has three rotational and three center-of-mass degrees of freedom. The key quantities are the formation enthalpy of the isolated system, $E^* = \sum_{i<j} u_{ij} = E_p + \mu_z B_{\text{ext}}$, and the z -component of the total magnetic moment of the aggregate, μ_z , both of which are functions of T and B_{ext} . E^* is the appropriate thermodynamic potential describing the present system; its definition is analogous to the enthalpy of a (p, V, T) -ensemble.

We studied the thermodynamical behavior of the system in a set of 32 extensive Metropolis Monte Carlo simulations,¹⁰ each of which consisted of 6×10^9 steps. We used the multiple histogram method of Ferrenberg *et al.*^{11,12} to combine the results of all simulations and to calculate the normalized density of states $\rho(E^*, \mu_z)$ with a minimized statistical error.¹³ In order to cover the $6N$ -dimensional configuration space properly and to eliminate any potential dependencies on the starting configurations, we based our data analysis on simulations performed with B and T close to the ‘‘phase boundary’’ between rings and chains.

With the density of states $\rho(E^*, \mu_z)$ at hand, the partition function Z can be rewritten as

$$Z(B_{\text{ext}}, T) = (2\pi\beta)^{-6N/2} \int dE^* d\mu_z \rho(E^*, \mu_z) \times \exp(-\beta(E^* - \mu_z B_{\text{ext}})), \quad (3)$$

and the field- and temperature-dependence of the expectation value of any function $F(E^*, \mu_z)$ can be obtained from

$$\begin{aligned} \langle F(E^*, \mu_z; B_{\text{ext}}, T) \rangle &= Z^{-1}(B_{\text{ext}}, T) \int d\mu_z \int dE^* F(E^*, \mu_z) \rho(E^*, \mu_z) \\ &\times \exp(-\beta(E^* - \mu_z B_{\text{ext}})). \end{aligned}$$

IV. RESULTS

In order to obtain a rough idea of the stable and metastable states of the system, we plotted in Fig. 1 the probability of finding the aggregate in a state with potential energy E_p and total magnetic moment in the field direction μ_z . This is the projection of the probability to find the system in a specific state in the high-dimensional configuration space onto the (E_p, μ_z) subspace. High probability regions in this subspace indicate not only the energetic preference of the corresponding states, but also their entropic preference due to a large associated phase space volume.

Rings always have an absolute magnetic moment $|\mu/\mu^{\text{max}}|$ that is close to zero. Consequently, the z -component of the magnetic moment of rings is also near zero, as seen in Fig. 1. Even though the absolute magnetic moment $|\mu/\mu^{\text{max}}|$ of chains is close to 1, these aggregates

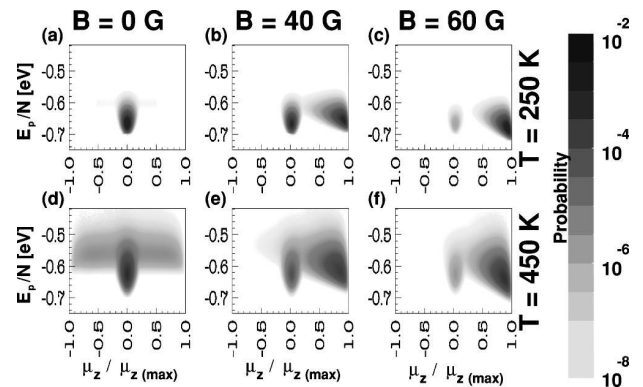


FIG. 1. Monte Carlo results for the probability to find an aggregate in a state with its magnetic moment in the field direction μ_z and potential energy E_p . The individual contour plots show our results for the temperature $T = 250$ K at the field values (a) $B_{\text{ext}} = 0$ G, (b) $B_{\text{ext}} = 40$ G, (c) $B_{\text{ext}} = 60$ G, and $T = 450$ K at the field values, (d) $B_{\text{ext}} = 0$ G, (e) $B_{\text{ext}} = 40$ G, (f) $B_{\text{ext}} = 60$ G.

cannot be distinguished easily from rings in the absence of a field. In the zero field, chains have no orientational preference and the z -component of their magnetic moment μ_z/μ_z^{max} averages to zero. Of course, this is not a serious complication within our simulations but in an experimental situation the measurement of one component of the magnetic moment μ would not be sufficient to determine the dominant structure of an ensemble of clusters.

Chains—unlike rings—do align with a nonzero magnetic field and, especially at low temperatures, show a magnetic moment $\mu_z/\mu_z^{\text{max}} \approx 1$ in the field direction.

The relative stability of an aggregate is reflected in its potential energy E_p . We find E_p to increase (corresponding to decreasing stability) with increasing temperature. On the other hand, applying a magnetic field destabilizes rings in favor of field-aligned chains. With increasing field, chains are confined to a gradually decreasing fraction of the configurational space which sharpens their distribution in the (E_p, μ_z) subspace, as seen when comparing Figs. 1(a)–1(c) and Figs. 1(d)–1(f).

Under all conditions, we find two more or less pronounced local maxima in the probability distribution P , corresponding to a ring with $0 \leq \mu_z/\mu_z^{\text{max}} \ll 1$, and a chain with $0 \ll \mu_z/\mu_z^{\text{max}} \leq 1$. At zero field we observe a predominant occupation of the more stable ring state. Due to the relatively small energy difference with respect to the less favorable chain $\Delta E_p^{\text{cr}}/N = (E_p^{\text{chain}} - E_p^{\text{ring}})/N = 0.06$ eV, both states become more evenly occupied at higher temperatures. At fields as low as $B_{\text{ext}} = 40$ G, the energy difference between chains and rings drops significantly to $\Delta E_p^{\text{cr}}/N = 0.02$ eV. As seen in Fig. 1(b), this results in an equal occupation of both states even at low temperatures. At the much higher field value $B_{\text{ext}} = 60$ G, chains are favored with respect to the rings by a considerable amount of energy $\Delta E_p^{\text{cr}}/N = -0.2$ eV. This strongly suppresses the occurrence of rings, as seen in Figs. 1(c) and 1(f).

A first-order phase transition in an infinite system can be identified by a discontinuous change of the energy at the critical point.

In corresponding finite systems, this critical point ex-

J. Chem. Phys., Vol. 111, No. 23, 15 December 1999

pands to a “critical region.” Even though the energy changes continuously in the finite system, such a transition may still be classified as a first-order transition or a higher-order phase transition, like in the work of Proykova and Berry,¹⁴ due to its physical similarity to those in infinite systems. We investigated the nature of the transition in our system by inspecting the temperature dependence of the bimodal distribution, shown in Fig. 1, following a procedure outlined in Refs. 15–17. This analysis revealed the transition between rings and chains, which is a transition between two ordered phases being “first-order like”. We have to emphasize that this classification is drawn by analogy. Unlike other small systems like those considered by Cheng *et al.*,⁵ it does not make sense to ask if the “transition” observed would become a true first-order phase transition in the limit of large particle numbers. Here, we discuss explicitly a finite magnetic two-isomer system. With increasing system size the number of different isomers (complex labyrinth⁶ or branched structures⁷) will increase dramatically and features like the bimodal probability distribution will probably disappear. For this reason, methods like finite-size scaling cannot be applied for the system under consideration. The ring–chain transition observed for small ferrofluid clusters will definitely disappear for larger clusters. Thus, the *traditional* way to classify phase transitions by studying the behavior of the probability distribution as a function of N cannot be used here. There is also some experimental evidence that this way might not be suitable for other clusters types, e.g., sodium clusters which exhibit a transition from molecular-like to jellium-like clusters with increasing particle number.¹⁸ In such cases it is easy to imagine that the type of phase transition as extracted from the probability function changes from first to higher order by going from N to $N+1$ or $N-1$. The phase behavior of a small sodium cluster might be more similar to that of a large argon cluster than to that of a large sodium cluster. There is apparently a growing need for a systematic definition of phase transitions in finite systems. Recently, an attempt to solve this problem has been made by analyzing the distribution of zeros of the canonical partition function in the complex temperature plane.¹⁹

Figure 1 shows not only the stable and metastable states under the given conditions, but also the states found along the preferential transition pathway between a ring and a chain in the projected (E_p, μ_z) subspace. During this transition each aggregate must undergo a *continuous* change of E_p and μ_z . The favored transition pathways are then associated with high-probability trajectories in the (E_p, μ_z) subspace. The value of the activation barrier ΔE_p^{act} is then given by the smallest increase of E_p along the optimum transition path which connects the stable and metastable ring and chain islands. In our simulations we found that the activation barrier always occurred at $\mu_z/\mu_z^{\text{max}} \approx 0.22$. Consequently, we concluded that the field dependence of the activation energy follows the expression $\Delta E_p^{\text{act}}(B_{\text{ext}}) = \Delta E_p^{\text{act}}(B_{\text{ext}}=0) - 0.22 \mu_z^{\text{max}} B_{\text{ext}}$.

In order to quantitatively describe the phase transitions occurring in this system, we focused our attention on the specific heat and the magnetic susceptibility. The specific heat per particle in a canonical ensemble is given by c_B

Thermodynamics of magnetic two-isomer systems 10691

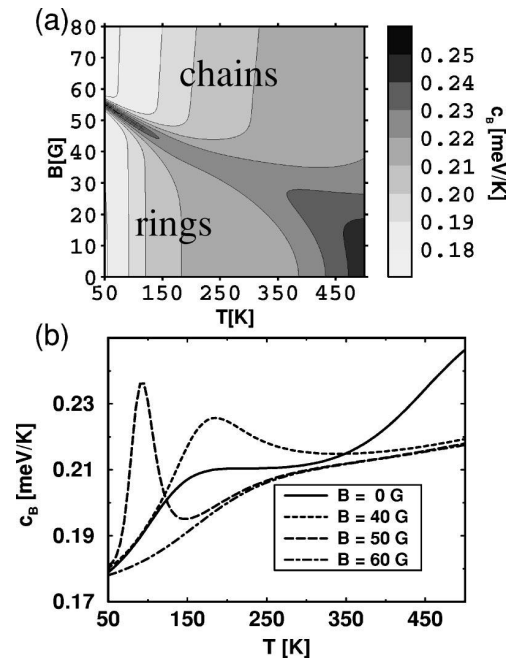


FIG. 2. Specific heat per particle c_B of the system as a function of temperature T and the external magnetic field B_{ext} . Results for the entire temperature and field range investigated here are presented as a contour plot in (a). The temperature dependence of c_B for selected values of B_{ext} is presented in (b).

$=d\langle E/N \rangle/dT$, where the total energy is given by $E = (6/2)Nk_B T + E_p$. Correspondingly, we define the magnetic susceptibility per particle as $\chi = d\langle \mu_z/N \rangle/dB_{\text{ext}}$. These response functions are related to the fluctuations of E_p and μ_z by

$$c_B = \left[\frac{6N}{2} k_B + k_B \beta^2 (\langle E^2 \rangle - \langle E \rangle^2) \right] / N, \quad (4)$$

$$\chi = [\beta (\langle \mu_z^2 \rangle - \langle \mu_z \rangle^2)] / N. \quad (5)$$

As already mentioned, transitions in finite systems are gradual.² Still, it makes physical sense to compare them to phase transitions in infinite systems. There, first-order phase transitions are associated with a diverging specific heat at the phase boundary. In the $T-B_{\text{ext}}$ “phase diagram” in Fig. 2(a), a well-defined yet not sharp “crest line” separates the ring and the chain phase. Similar phase diagrams, albeit for nonmagnetic systems, have been discussed in Refs. 3 and 20. Our results illustrate how the critical magnetic field for the ring–chain transition decreases with increasing temperature. At high temperatures, the “line” separating the phases broadens significantly into a region where rings and chains coexist.

The line plot in Fig. 2(b) is the respective constant-field cut through the contour plot in Fig. 2(a). As can be seen in Fig. 2(b), there is no transition from chains to rings, indicated by a peak in c_B at fields exceeding 50 G which is close to the critical field value at which chains become favored over rings at zero temperature. At fields $B_{\text{ext}} \ll 40$ G, on the other hand, there is no region where chains would be thermodynamically preferred over the rings, and we observe

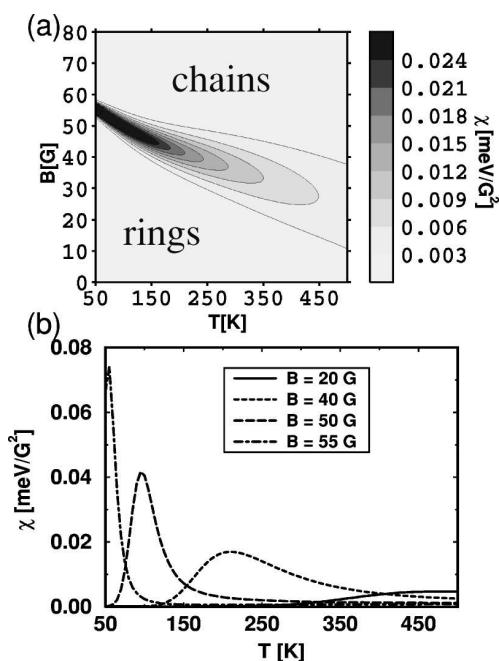


FIG. 3. Magnetic susceptibility per particle χ of the system as a function of temperature T and the external magnetic field B_{ext} . Results for the entire temperature and field range investigated here are presented as a contour plot in (a). The temperature dependence of χ for selected values of B_{ext} is presented in (b).

only a gradual transition from the ring phase into the coexistence region with increasing temperature. The specific heat behavior at zero field resembles that of a small system with a gradual *melting* transition close to 150 K and an onset of disorder at about 350 K.²¹ As seen in Fig. 2(b), the critical temperature and the width of the transition region can be externally tuned by the second thermodynamical variable, the external magnetic field B_{ext} .

Figure 3 displays the magnetic susceptibility χ , another prominent indicator of phase transitions in magnetic systems, as a function of T and B_{ext} . Like the specific heat in Fig. 2(a), the crest line in χ separates the chain phase from the ring phase in this T – B_{ext} phase diagram. Moreover, Fig. 3 reveals the fundamentally different magnetic character of these phases. Whereas the system is nonmagnetic in the ring phase found below 40 G, it behaves like a ferromagnet consisting of Langevin paramagnets in the chain phase at higher fields. The transition between these states is again gradual. The line plot in Fig. 3(b) is the respective constant-field cut through the contour plot in Fig. 3(a). When the system is in the chain phase, it behaves like a paramagnet obeying the Curie–Weiss law, as can be seen in Fig. 3(b).²²

At relatively low temperatures, where the aggregates are intact, the expectation value of the magnetic moment first increases with increasing magnetic fields. This is due to the gradual conversion from nonmagnetic rings to paramagnetic chains. According to Fig. 3(b), this uncommon behavior persists up to $T=200$ K at $B_{\text{ext}}=40$ G. This trend is reversed at higher temperatures, where all aggregates eventually fragment into single paramagnetic tops. In this temperature range the magnetic moment as well as the susceptibility decrease

with increasing temperature. Snapshots from our simulations at temperatures in the melting region indicate that rings and chains break up to form a number of different isomers. Single particles leave the chain and ring structures and attach at arbitrary positions. We interpret this as the onset of disordering or melting. For computational reasons the dissociation process has not been studied in detail.

Since the transition probability between both states is extremely low at low temperatures and fields, magnetically distinguishable metastable states can be frozen. A chain configuration, which is metastable in zero field, can be prepared by first annealing the system to $T \geq 350$ K and subsequent quenching in a strong field. Similarly a frozen-in ring configuration is unlikely to transform to a chain at low temperatures, unless exposed to very large fields. Thus, the above-described phase diagrams can be used to externally manipulate the self-assembly of magnetic nanostructures.

In conclusion, we have studied the thermodynamic behavior of a finite two-isomer system, which is externally tunable by two independent variables, namely the temperature and the magnetic field. Much of the behavior encountered in this system such as transitions between different states has a well-defined counterpart in infinite systems. The reason for the encountered richness of the thermodynamic and magnetic properties is the relative ease of structural transformations which is typical for finite systems. Consequently, we expect other finite magnetic systems, e.g., small transition metal clusters, where a small number of structural isomers with substantially different magnetic moments could coexist,²³ to follow this behavior. Moreover, we expect that our results can also be transferred to nanocrystalline material, such as magnetic clusters encapsulated in the supercages of zeolites, which will likely retain some of the intriguing properties of the isolated finite systems.

¹K. Gabriel, *Sci. Am.* **273**(3), 150 (1995).

²T. Hill, *Thermodynamics of Small Systems* (Parts I and II) (W.A. Benjamin, New York, 1963 and 1964).

³R. E. Kunz and R. S. Berry, *Phys. Rev. Lett.* **71**, 3987 (1993); D. J. Wales and R. S. Berry, *ibid.* **73**, 2875 (1994).

⁴P. Borrmann, *COMMAT* **2**, 583 (1994); G. Franke, E. R. Hilf, and P. Borrmann, *J. Chem. Phys.* **98**, 3496 (1993).

⁵H.-P. Cheng, X. Li, R. L. Whetten, and R. S. Berry, *Phys. Rev. A* **46**, 791 (1992).

⁶A. J. Dickstein *et al.*, *Science* **261**, 1012 (1993).

⁷H. Wang, Y. Zhu, C. Boyd, W. Luo, A. Cebers, and R. E. Rosensweig, *Phys. Rev. Lett.* **72**, 1929 (1994).

⁸P. Jund, S. G. Kim, D. Tománek, and J. Hetherington, *Phys. Rev. Lett.* **74**, 3049 (1995).

⁹A. E. Ferdinand and M. E. Fisher, *Phys. Rev.* **185**, 832 (1969).

¹⁰N. Metropolis, A. Rosenbluth, M. N. Rosenbluth, A. H. Teller, and E. Teller, *J. Chem. Phys.* **21**, 1087 (1953).

¹¹A. M. Ferrenberg and R. H. Swendsen, *Phys. Rev. Lett.* **61**, 2635 (1988).

¹²A. M. Ferrenberg and R. H. Swendsen, *Phys. Rev. Lett.* **63**, 1195 (1989).

¹³We extended the Ferrenberg analysis in a straightforward way to deal with a two-dimensional density of states.

¹⁴A. Proykova and R. S. Berry, *Z. Phys. D: At., Mol. Clusters* **40**, 215 (1997).

¹⁵M. Glosli and J. Plischke, *Can. J. Phys.* **61**, 1515 (1983).

¹⁶O. G. Mouritsen, *Computer Studies of Phase Transitions and Critical Phenomena* (Springer, Berlin, 1984).

¹⁷Y. Zhou, C. K. Hall, and M. Karplus, *Phys. Rev. Lett.* **77**, 2822 (1996).

¹⁸C. Ellert, M. Schmidt, T. Reiners, and H. Haberland, *Z. Phys. D: At., Mol. Clusters* **39**, 317 (1997).

¹⁹P. Borrmann and O. Muelken, eprint: cond-mat/9909184 1999.

J. Chem. Phys., Vol. 111, No. 23, 15 December 1999

Thermodynamics of magnetic two-isomer systems 10693

²⁰S. Sugano and S. Sawada, Z. Phys. D: At., Mol. Clusters **12**, 189 (1989).

²¹R. S. Berry, J. Jellinek, and G. Natanson, Chem. Phys. Lett. **107**, 227 (1984); G. Natanson, F. Amar, and R. S. Berry, J. Chem. Phys. **78**, 399 (1983).

²²Our numerical approach did not allow us to investigate the temperature

region below 50 K. The onset of the Curie–Weiss behavior, indicated by a maximum in χ at nonzero temperature, can be seen whenever the system is in the chain phase.

²³P. Borrmann, B. Diekmann, E. R. Hilf, and D. Tománek, Surf. Rev. Lett. **3**, 103 (1996).

4

Paradoxical magnetic cooling in a structural transition model

**P. Borrmann, H. Stamerjohanns, E. R. Hilf
and D. Tománek**

European Physical Journal B **19**, (1) 117-119 (2001)

Eur. Phys. J. B **19**, 117–119 (2001)

THE EUROPEAN
PHYSICAL JOURNAL B

EDP Sciences
© Società Italiana di Fisica
Springer-Verlag 2001

Paradoxical magnetic cooling in a structural transition model

P. Borrmann¹, H. Stamerjohanns^{1,a}, E.R. Hilf¹, and D. Tománek²

¹ Department of Physics, Carl von Ossietzky University, 26111 Oldenburg, Germany

² Department of Physics and Astronomy, Michigan State University, East Lansing, Michigan 48824-1116, USA

Received 5 September 2000

Abstract. In contrast to the experimentally widely used isentropic demagnetization process for cooling to ultra-low temperatures we examine a particular classical model system that does not cool, but rather heats up with isentropic demagnetization. This system consists of several magnetite particles in a colloidal suspension, and shows the uncommon behavior of disordering structurally while ordering magnetically in an increasing magnetic field. For a six-particle system, we report an uncommon structural transition from a ring to a chain as a function of magnetic field and temperature.

PACS. 05.70.Fh Phase transitions: general studies – 75.10.-b General theory and models of magnetic ordering – 75.50.Mm Magnetic liquids

1 Introduction

Cooling to ultra-low temperatures is presently experimentally achieved using the isentropic demagnetization process suggested in 1926 by Debye and Giauque [1,2]. Here we study the thermal and magnetic properties of a particular model system consisting of six magnetite nanoparticles in a colloidal suspension. Our calculations indicate that changing the temperature or magnetic field leads to a transition from a ring-like to a chain-like structure. We demonstrate that such a model system, that could be realized in a ferrofluid, would not cool but rather heat up during an isentropic demagnetization. The system of magnetic nanoparticles shows the uncommon behavior of disordering structurally, *i.e.* increasing its volume in phase space, while ordering magnetically in an increasing magnetic field. This behavior, associated with the break-up of the relatively rigid rings to floppy chains, occurs once the energy gain upon aligning a chain of dipoles with the field exceeds the energy cost of breaking up a ring. Thus systems that disorder structurally in high fields may be used as coolants based on isentropic magnetization instead of demagnetization. So far, only ferrofluid systems with a large number of particles have been discussed as candidates for use in magneto-caloric heat engines [3]. Here we report a paradoxical magnetic cooling phenomenon that is unique to systems with only few particles.

Both the conventional and paradoxical process utilize the energy change associated with particular structural changes for cooling. The *conventional* isentropic demagnetization process uses the fact that a magnetic system, such as a spin system, orders magnetically and thus lowers its entropy in presence of an external magnetic field.

Removal of the external magnetic field at constant temperature leads to an increase in entropy due to magnetic disordering, which requires energy. Decreasing the external magnetic field at constant entropy consequently leads to a temperature lowering. With this method, systems such as copper have been cooled down to temperatures as low as 50 nK [4].

In the following we address model systems consisting of a finite number of magnetic particles that may undergo structural transitions. Both the structural and magnetic degrees of freedom are important in this system and can not be decoupled. Applying a sufficiently high magnetic field causes the system to order magnetically while disordering structurally, at the cost of internal energy. Consequently, such a system will exhibit the paradoxical phenomenon of cooling by isentropic magnetization.

The transformation from a ring to a chain is associated with freeing up a structural degree of freedom, with a corresponding increase in entropy. Such a transformation can be induced by a magnetic field in a system of magnetic dipoles, where the energetics is governed by dipole-dipole interactions between the particles and an interaction of each particle with the external field. In small fields, the ring is stabilized with respect to the chain structure if the gain in dipole-dipole interaction upon connecting the chain ends energetically outweighs the dipole misalignment energy in a bent structure. The energy gain upon aligning all individual dipoles with a sufficiently high applied field, on the other hand, stabilizes the chain structure.

One system that satisfies all the requirements on a paradoxical magnetic coolant consists of a few ($4 \leq N \leq 14$) super-paramagnetic particles of magnetite. Such particles are the key constituents of ferrofluids, which

^a e-mail: stamer@uni-oldenburg.de

have attained rapidly increasing interest during the past few years [5,6]. Recently we have shown that such systems exhibit intriguing phase transitions between the ordered ring and chain phases and one disordered phase [7]. We also pointed out that self-assembly in these systems could be used to store information [8].

2 The model

In the following, we study the thermodynamic behavior of a six-particle system, where the chain and the ring are the dominant stable structural isomers. We chose this particular system as it allows a simple discussion of the two thermodynamical features characteristic of isomer transitions in finite systems, namely the isomeric phase space and the transition probability that is linked to the transition time. It is true that such ring and chain isomers are also stable at much larger sizes. Nevertheless, the thermodynamical behavior becomes more complex in larger systems, where the number of relevant structural isomers grows rapidly with increasing N .

Here we calculate the entropy and the dependence of temperature on an external magnetic field at constant entropy $(\partial T/\partial B)_S$ for a model system of six magnetite particles with a radius $\sigma = 50 \text{ \AA}$ and a permanent magnetic moment of $\mu = 2.63 \times 10^3 \mu_B$. The total potential energy U of this system is given by [6]

$$U = \sum_{i < j}^N \{ (\mu_0^2 / r_{ij}^3) [\hat{\mu}_i \hat{\mu}_j - 3(\hat{\mu}_i \hat{r}_{ij})(\hat{\mu}_j \hat{r}_{ij})] \quad (1)$$

$$+ \epsilon \left[e\left(-\frac{r_{ij}-\sigma}{\rho}\right) - e\left(-\frac{r_{ij}+\sigma}{2\rho}\right) \right] \} + \sum_{i=1}^N \mu_z^i B_{\text{ext}}.$$

The pairwise interaction energy is given by the dipole-dipole and a non-magnetic interaction energy. The latter is dominated by a repulsion between the spherical particles, but contains also a weak attractive part due to the van der Waals interaction. It is modelled by the above Morse-type potential with parameters [10] $\epsilon = 15.1 \mu\text{eV}$ and $\rho = 2.5 \text{ \AA}$. The second sum reflects the interaction between the magnetite particles and the external magnetic field B_{ext} that is aligned with the z -axis.

We would like to point out that the finite ferrofluid systems undergo all the intriguing transitions described below occur independent of these parameter values. Our particular choice has been taken to bring the transition into an experimentally accessible and interesting region [9].

All thermodynamic quantities can be derived from the canonical partition function $Z(B, T)$ by appropriate differentiation. We determined Z using the Metropolis Monte Carlo method [11], which we combined with a special type of optimized data analysis [12] to calculate all thermodynamic properties as functions of the temperature T and the magnetic field B_{ext} as external variables [7]. The entropy S is given by

$$S = k_B \left(\ln(Z) - \beta \frac{\partial \ln(Z)}{\partial \beta} \right), \quad (2)$$

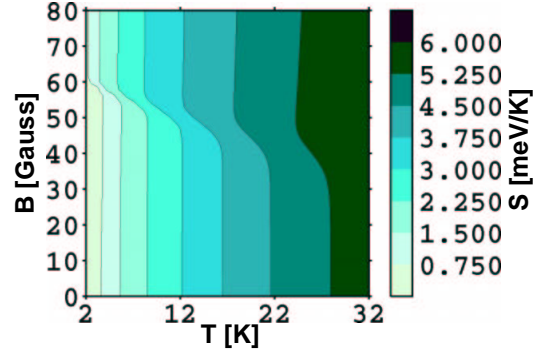


Fig. 1. Contour plot of the entropy S as a function of the external magnetic field B_{ext} and temperature T . The model system discussed here shows a temperature decrease of up to few degrees Kelvin as the field B is increased at constant entropy.

where $\beta = 1/k_B T$. The fundamental thermodynamic expression $dE = TdS - \mu_z dB$ yields immediately the Maxwell relation

$$\left(\frac{\partial T}{\partial B} \right)_S = \frac{- (\partial S / \partial B)_T}{(\partial S / \partial T)_B} \quad (3)$$

that describes the temperature response to the external field in isentropic processes. We calculate this quantity using the expectation values of the potential energy U and the z -component of the magnetic moment μ_z of the whole system as

$$\left(\frac{\partial T}{\partial B} \right)_S = -\beta \frac{\langle U \mu_z \rangle - \langle U \rangle \langle \mu_z \rangle}{\frac{6}{2} N k_B + k_B \beta^2 (\langle U^2 \rangle - \langle U \rangle^2)}. \quad (4)$$

3 Results

Our results for S and $(\partial T/\partial B)_S$ as a function of B_{ext} and T are represented by contour plots in Figure 1 and Figure 2, respectively [13]. The steps in the isentropes displayed in Figure 1 indicate a temperature decrease with increasing magnetic field at constant entropy. For example, an increase of the field from 45 to 55 Gauss cools the system down from $T = 12 \text{ K}$ to $T \approx 8 \text{ K}$. The narrow region in the $B_{\text{ext}} - T$ space, where these kinks occur, separates the chain and ring phases. It is only in this narrow region of the $B_{\text{ext}} - T$ space that $(\partial T/\partial B)_S$ shows a nonzero value and hence a potential for magnetic cooling, indicated in Figure 2. A closer inspection of Figure 1 shows that the $S = \text{const.}$ lines change their slope in the chain phase at high fields, which also corresponds to a positive value of $(\partial T/\partial B)_S$ in Figure 2. This behavior is simply related to the fact that chains behave like a *conventional* magnetic system, since their magnetic and structural order increases with increasing external magnetic field. In the six-particle system discussed above, the conventional cooling mechanism by isentropic demagnetization in high fields is about one order of magnitude less important than the paradoxical magnetic cooling that is related to the ring-chain transition.

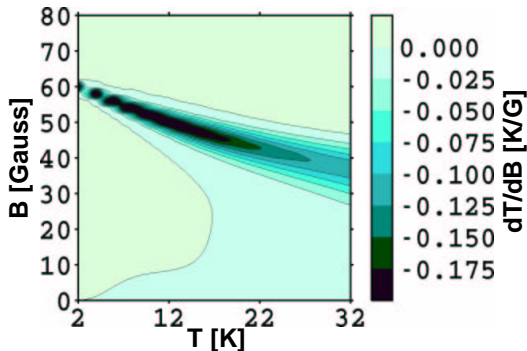


Fig. 2. Contour plot of $(\partial T/\partial B)_S$ as a function the external magnetic field B_{ext} and temperature T .

Let us now discuss some details related to a possible realization of the system. In our simulations we disregarded the internal degrees of freedom of the magnetic particles and the colloidal suspension. Obviously, the cooling efficiency of this particular composite system is highest when the magnetic degrees of freedom of the particles dominate. A potential candidate paradoxical cooling system is a dilute gas consisting of both magnetic particles, which could aggregate, and non-magnetic particles of similar size. The actual thermal transition is initiated by vibrational excitations that lead either to the breakup of rings into chains or a reconnection of chain ends to a ring. Let us now consider a mixture of chains, rings, and other isomers exposed to an oscillating magnetic field. Whereas the breakup energy increases as the neighboring dipoles gradually line up in the larger rings, the vibrational excitation spectrum gets dense especially in the range of low frequencies that drop with $1/N^2$. Hence it is preferentially the larger rings that are broken up to chains by a low-frequency external field. Also the chain structures experience an analogous softening of the vibrational spectrum with the factor of $1/N^2$. Yet due to the larger phase space volume, the likelihood of two chain ends to reconnect to a ring decreases drastically in larger systems.

The chain ends (which are to meet for a chain-to-ring transition) not only move more slowly with larger N but have to explore a much larger space in which the other end can be. The time required for the two ends to reconnect rises dramatically with N , so that chain-to-ring transitions can not be realized in a reasonable time in an ensemble of long chains.

In a realistic experiment, we also have to consider that the average size of the ferrofluid aggregates depends not only on the initial conditions, but increases as a function of time due to further aggregation. To prevent this gradual size increase, we propose to expose the ferrofluid suspension to a low frequency magnetic field that should preferentially break apart the larger aggregates and to stabilize the mixture of prevalent isomers in the region of five to seven particles per aggregate.

Paradoxical magnetic cooling is by no means restricted to the model system discussed here. We believe that the same effect should also occur in other nanostructures, such as transition metal clusters, and even in bulk matter consisting of finite-size substructures. We hope that our results will stimulate a search for experimentally realizable systems that may find application in the fascinating field of ultra-low temperature physics.

References

1. P. Debye, *Ann. Physik* **81**, 1154 (1926).
2. W.F. GIAUQUE, *J. Am. Chem. Soc.* **49**, 1864 (1927).
3. R.E. Rosensweig, *Sci. Am.* **247**, 124 (1984).
4. G.J. Ehnholm *et al.*, *Phys. Rev. Lett.* **42**, 1702 (1979).
5. Hao Wang, Yun Zhu, C. Boyd, Weili Luo, A. Cebers, R.E. Rosensweig, *Phys. Rev. Lett.* **72**, 1929 (1994).
6. P. Jund, S.G. Kim, D. Tománek, J. Hetherington, *Phys. Rev. Lett.* **74**, 3049 (1995).
7. P. Borrmann, H. Stamerjohanns, E.R. Hilf, D. Tománek, S.G. Kim, P. Jund, *J. Chem. Phys.* **111**, 10689 (1999).
8. D. Tománek, S.G. Kim, P. Jund, P. Borrmann, H. Stamerjohanns, E.R. Hilf, *Z. Phys. D* **40**, 190 (1997).
9. Particles of different materials and sizes can be used as constituents of ferrofluids. The present choice of parameters, different from the choice in reference [6], represents a system with a convenient transition temperature.
10. We note that in the present system of magnetic particles, the temperature scales with the magnetic moment of the particles.
11. N. Metropolis, A. Rosenbluth, M.N. Rosenbluth, A.H. Teller, E. Teller, *J. Chem. Phys.* **21**, 1087 (1953).
12. A.M. Ferrenberg, R.H. Swendsen, *Phys. Rev. Lett.* **61**, 2635 (1988); A.M. Ferrenberg, R.H. Swendsen, *Phys. Rev. Lett.* **63**, 1195 (1989).
13. We chose $T = 2$ K as the lower temperature limit for computational reasons that are related to the slow equilibration of a cold system.

5 **Classification of phase transitions of finite Bose-Einstein condensates in power-law traps by Fisher zeros**

**O. Mülken, P. Borrmann, J. Harting
and H. Stamerjohanns**

Physical Review A **64**, 013611 (2001)

Classification of phase transitions of finite Bose-Einstein condensates in power-law traps by Fisher zeros

Oliver Mülken, Peter Borrmann, Jens Harting, and Heinrich Stamerjohanns
Department of Physics, Carl von Ossietzky University Oldenburg, D-26111 Oldenburg, Germany
 (Received 20 June 2000; revised manuscript received 27 November 2000; published 5 June 2001)

We present a detailed description of a classification scheme for phase transitions in finite systems based on the distribution of Fisher zeros of the canonical partition function in the complex temperature plane. We apply this scheme to finite Bose systems in power-law traps within a semi-analytic approach with a continuous one-particle density of states $\Omega(E) \sim E^{d-1}$ for different values of d and to a three-dimensional harmonically confined ideal Bose gas with discrete energy levels. Our results indicate that the order of the Bose-Einstein condensation phase transition sensitively depends on the confining potential.

DOI: 10.1103/PhysRevA.64.013611

PACS number(s): 03.75.Fi, 05.30.Jp, 05.20.-y, 64.60.-i

I. INTRODUCTION

In 1924, Bose and Einstein predicted that in a system of bosons at temperatures below a certain critical temperature T_C , the single-particle ground state is macroscopically occupied [1]. This effect is commonly referred to as Bose-Einstein condensation, and a large number of phenomena, such as the condensation phenomena in alkali-metal atoms, the superfluidity of ^4He , and the superconductivity, are identified as signatures of this effect. However, the physical situation is very intricate in most experiments.

Recent experiments with dilute gases of alkali-metal atoms in magnetic [2] and optical [3] traps are in some sense the best experimental approximation up to now of the ideal noninteracting Bose-Einstein system in an external power-law potential. The achievement of ultralow temperatures by laser cooling and evaporative cooling provides the opportunity to study Bose-Einstein condensation under systematic variation of adjustable external parameters, e.g., the trap geometry, the number of trapped atoms, the temperature, and by the choice of the alkali-metal atoms the effective interparticle interactions. Even in the approximation of noninteracting particles, an explanation of these experiments requires some care, because the number of bosons in these novel traps is finite and fixed and the standard grand-canonical treatment is not appropriate. The effect of the finite particle numbers on the second moments of the distribution function, e.g., the specific heat and the fluctuation of the ground-state occupation number, has been addressed in a number of publications [4,5]. In [4,6], we have presented a recursion method to calculate the canonical partition function for non-interacting bosons, and we investigated the dependency of the thermodynamic properties of the condensate on the trap geometry.

The order of the phase transition in small systems sensitively depends on finite-size effects. Compared to the macroscopic system, even for systems as simple as the three-dimensional ideal gas, the order of the phase transition might change for mesoscopic systems where the number of particles is finite or for trapped gases with different trap geometries.

In this paper, we address the classification of the phase transition of a finite number of noninteracting bosons in a

power-law trap with an effective one-particle density of states $\Omega(E) = E^{d-1}$ being formally equivalent to a d -dimensional harmonic oscillator or a $2d$ -dimensional ideal gas. We use a classification scheme based on the distribution of zeros of the canonical partition function initially developed by Grossman *et al.* [7] and Fisher *et al.* [8], which has been extended by us [9] as a classification scheme for finite systems. On the basis of this classification scheme, we are able to extract a qualitative difference between the order of the phase transition occurring in Bose-Einstein condensates in three-dimensional traps [10,11] and in two-dimensional traps that was recently discovered by Safonov *et al.* in a gas of hydrogen atoms absorbed on the surface of liquid helium [12]. Since we do not consider particle interactions, this difference is only due to the difference in the confining potential.

We give a detailed review of the classification scheme in Sec. II. In Sec. III, we present a method for the calculation of the canonical partition function in the complex plane and describe details of the numerical implementation. Our results for $d = 1 - 6$ and particle numbers varying from 10 to 300 are presented in Sec. III as well as calculations for a three-dimensional parabolically confined Bose gas.

II. CLASSIFICATION SCHEME

In 1952, Yang and Lee showed that the grand-canonical partition function can be written as a function of its zeros in the complex fugacity plane, which, for systems with hardcore interactions and for the Ising model, lie on a unit circle [13].

Grossmann *et al.* [7] and Fisher [8] extended this approach to the canonical ensemble by analytic continuation of the inverse temperature to the complex plane $\beta \rightarrow \mathcal{B} = \beta + i\tau$. Within this treatment, all phenomenologically known types of phase transitions in macroscopic systems can be identified from the properties of the distribution of zeros of the canonical partition function.

In [9], we presented a classification scheme for finite systems that has its macroscopic equivalent in the scheme given by Grossmann. As usual, the canonical partition function reads

$$Z(\mathcal{B}) = \int dE \Omega(E) \exp(-BE), \quad (2.1)$$

which we write as a product $Z(\mathcal{B}) = Z_{\text{lim}}(\mathcal{B})Z_{\text{int}}(\mathcal{B})$, where $Z_{\text{lim}}(\mathcal{B})$ describes the limiting behavior of $Z(\mathcal{B})$ for $T \rightarrow \infty$, imposing that $\lim_{T \rightarrow \infty} Z_{\text{int}}(\mathcal{B}) = 1$. This limiting partition function will only depend on the external potential applied to the system, whereas $Z_{\text{int}}(\mathcal{B})$ will depend on the specific interaction between the system particles. For example, for an N -particle system in a d -dimensional harmonic trap, $Z_{\text{lim}}(\mathcal{B}) = \mathcal{B}^{-dN}$ and thus the zeros of $Z(\mathcal{B})$ are the same as the zeros of $Z_{\text{int}}(\mathcal{B})$. Since the partition function is an integral function, the zeros $\mathcal{B}_k = \mathcal{B}_{-k}^* = \beta_k + i\tau_k$ ($k \in \mathbb{N}$) are complex conjugate and the partition function reads

$$Z(\mathcal{B}) = Z_{\text{lim}}(\mathcal{B})Z_{\text{int}}(0) \exp(\mathcal{B} \partial_{\mathcal{B}} \ln Z_{\text{int}}(0)) \times \prod_{k \in \mathbb{N}} \left(1 - \frac{\mathcal{B}}{\mathcal{B}_k} \right) \left(1 - \frac{\mathcal{B}}{\mathcal{B}_k^*} \right) \exp\left(\frac{\mathcal{B}}{\mathcal{B}_k} + \frac{\mathcal{B}}{\mathcal{B}_k^*} \right). \quad (2.2)$$

The zeros of $Z(\mathcal{B})$ are the poles of the Helmholtz free energy $F(\mathcal{B}) = -(1/\mathcal{B}) \ln Z(\mathcal{B})$, i.e. The free energy is analytic everywhere in the complex temperature plane except at the zeros of $Z(\mathcal{B})$.

Different phases are represented by regions of holomorphy that are separated by zeros lying dense on lines in the complex temperature plane. In finite systems, the zeros do not squeeze on lines, which leads to a more blurred separation of different phases. We interpret the zeros as boundary posts between two phases. The distribution of zeros contains the complete thermodynamic information about the system, and all thermodynamic properties are derivable from it. Within this picture, the interaction part of the specific heat is given by

$$C_{V,\text{int}}(\mathcal{B}) = -k_B \mathcal{B}^2 \sum_{k \in \mathbb{N}} \left[\frac{1}{(\mathcal{B}_k - \mathcal{B})^2} + \frac{1}{(\mathcal{B}_k^* - \mathcal{B})^2} \right]. \quad (2.3)$$

The zeros of the partition function are poles of $C_V(\mathcal{B})$. As can be seen from Eq. (2.3), a zero approaching the real axis infinitely close causes a divergence at real temperature. The contribution of a zero \mathcal{B}_k to the specific heat decreases with increasing imaginary part τ_k . Thus, the thermodynamic properties of a system are governed by the zeros of Z close to the real axis.

The basic idea of the classification scheme for phase transitions in small systems presented in [9] is that the distribution of zeros close to the real axis can be described approximately by three parameters, where two of them reflect the order of the phase transition and the third merely the size of the system.

We assume that the zeros lie on straight lines (see Fig. 1) with a discrete density of zeros given by

$$\phi(\tau_k) = \frac{1}{2} \left(\frac{1}{|\mathcal{B}_k - \mathcal{B}_{k-1}|} + \frac{1}{|\mathcal{B}_{k+1} - \mathcal{B}_k|} \right), \quad (2.4)$$

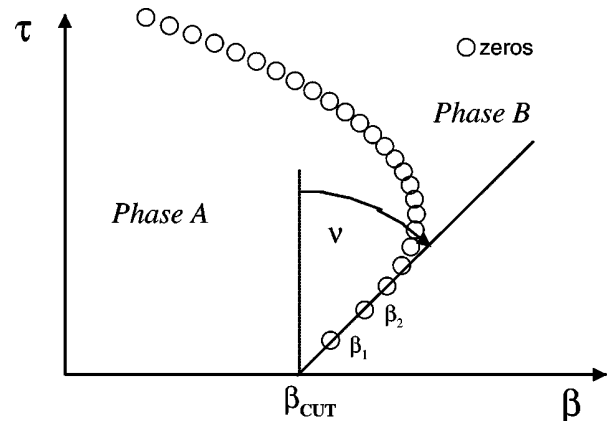


FIG. 1. Schematic illustration of the zeros in the complex temperature plane.

with $k = 2, 3, 4, \dots$, and we approximate for small τ the density of zeros, by a simple power law $\phi(\tau) \sim \tau^\alpha$. Considering only the first three zeros the exponent α can be estimated as

$$\alpha = \frac{\ln \phi(\tau_3) - \ln \phi(\tau_2)}{\ln \tau_3 - \ln \tau_2}. \quad (2.5)$$

The second parameter to describe the distribution of zeros is given by $\gamma = \tan \nu \sim (\beta_2 - \beta_1) / (\tau_2 - \tau_1)$, where ν is the crossing angle of the line of zeros with the real axis (see Fig. 1). The *discreteness* of the system is reflected in the imaginary part τ_1 of the zero closest to the real axis.

In the thermodynamic limit, we have always $\tau_1 \rightarrow 0$. In this case, the parameters α and γ coincide with those defined by Grossmann *et al* [7], who have shown how different types of phase transitions can be attributed to certain values of α and γ . They claimed that $\alpha = 0$ and $\gamma = 0$ correspond to a first-order phase transition, second-order transitions correspond to $0 < \alpha < 1$ with $\gamma = 0$ or $\gamma \neq 0$, third-order transitions to $1 \leq \alpha < 2$ with arbitrary values of γ , and that all higher order phase transition correspond to $\alpha > 1$. For macroscopic systems (with $\tau_1 \rightarrow 0$), α cannot be smaller than zero, because this would cause a divergence of the internal energy. However, in small systems with a finite τ_1 this is possible.

In our classification scheme, we therefore define phase transitions in small systems to be of first order for $\alpha \leq 0$, while second- and higher-order transitions are defined in complete analogy to the Grossmann scheme augmented by the third parameter τ_1 . The definition of a critical temperature β_c in small systems is crucial and ambiguous since no thermodynamic properties diverge. Thus, different definitions are possible. We define the critical temperature as $\beta_{\text{cut}} = \beta_1 - \gamma \tau_1$, i.e., the crossing point of the approximated line of zeros with the real temperature axis. An alternative definition is the real part of the first complex zero β_1 . In the thermodynamic limit, both definitions coincide.

Comparing the specific heats calculated for different discrete distributions of zeros shows the advantages of this classification scheme. Figure 2 shows (a) three distributions of zeros lying on straight lines corresponding to a first-order transition ($\alpha = 0$ and $\gamma = 0$), a second-order transition (α

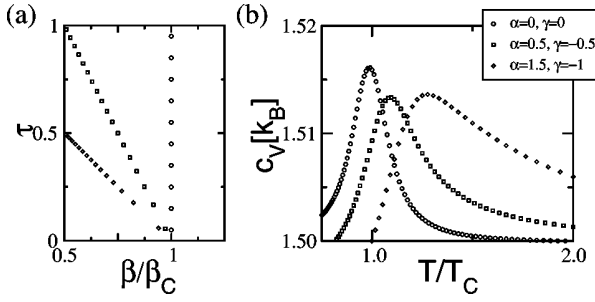


FIG. 2. Plot of (a) generated zeros lying on straight lines to simulate first- ($\alpha=0$ and $\gamma=0$), second-, ($\alpha=0.5$ and $\gamma=-0.5$), and third- ($\alpha=1.5$ and $\gamma=-1$) order phase transitions and (b) the appropriate specific heats per particle.

$=0.5$ and $\gamma=-0.5$), and a third-order phase transition ($\alpha=1.5$, and $\gamma=-1$) and (b) the pertinent specific heats. In all cases the specific heat exhibits a hump extending over a finite-temperature region and cannot be used to classify the phase transition. In contrast, even for very small systems (large τ_1), the order of the phase transition is extractable from the distribution of zeros.

The zeros of the canonical partition function have a distinct geometrical interpretation, which explains the smoothed curves of the specific heat and other thermodynamic properties in finite systems.

Figure 3 shows (a) the ground-state occupation number $|\eta_0(\mathcal{B})|/N$ in the complex temperature plane and (b) the ground-state occupation number at real temperatures for a finite ideal Bose gas of $N=120$ particles, where $\eta_0(\mathcal{B})$ is given by the derivative of the logarithm of the canonical partition function $Z(\mathcal{B})$ with respect to the ground-state energy ϵ_0 , i.e., $\eta_0(\mathcal{B}) = -(1/\mathcal{B})\partial_{\epsilon_0} Z(\mathcal{B})/Z(\mathcal{B})$.

Zeros of the partition function are poles of $\eta_0(\mathcal{B})$ and are indicated by dark spots, which influence the value of the ground-state occupation number at real temperatures impres-

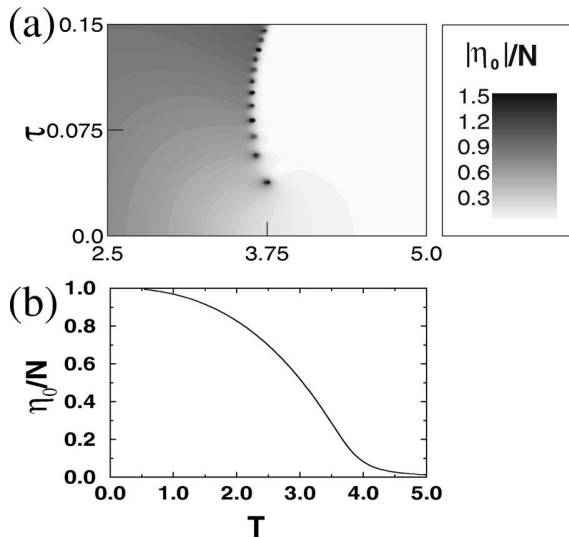


FIG. 3. Comparison of (a) $|\eta_0|/N$ with (b) the appropriate value of η_0 at real temperatures for a 120-particle harmonically trapped ideal Bose gas (note that $\hbar=k_B=\omega=1$).

sively. Every pole seems to *radiate* onto the real axis and therefore determines the occupation number at real temperatures. This *radiation* extends over a broad temperature range so that the occupation number for real temperatures does not show a discontinuity but rather a smoothed curve. A closer look at Eq. (2.3) gives the mathematical explanation for this effect. The discrete distribution of zeros, i.e., $\tau_1 > 0$, inhibits the specific heat and all other thermodynamic properties to show a divergency at some critical temperature because the denominators of the arguments of the sum remain finite.

Without going into a detailed analysis, we note that in the thermodynamic limit the parameter α is connected to the critical index for the specific heat by

$$C_V \sim (\beta - \beta_c)^{\alpha-1}. \quad (2.6)$$

However, since critical indices are used to describe the shape of a divergency at the critical point, an extension to small systems seems to be more or less academic.

The introduction of complex temperatures might seem artificial at first sight, but, in fact, the imaginary parts τ_k of the complex zeros \mathcal{B}_k have an obvious quantum-mechanical interpretation. We write the quantum-mechanical partition function as

$$Z(\beta + i\tau/\hbar) = \text{Tr}(\exp(-i\tau\hat{H}/\hbar)\exp(-\beta\hat{H})) \quad (2.7)$$

$$= \langle \Psi_{\text{can}} | \exp(-i\tau\hat{H}/\hbar) | \Psi_{\text{can}} \rangle \quad (2.8)$$

$$= \langle \Psi_{\text{can}}(t=0) | \Psi_{\text{can}}(t=\tau) \rangle, \quad (2.9)$$

introducing a *canonical state* as a sum over Boltzmann-weighted eigenstates $|\Psi_{\text{can}}\rangle = \sum_k \exp(-\beta\epsilon_k/2) |\phi_k\rangle$. We explicitly write the imaginary part as τ/\hbar since the dimension is $1/[\text{energy}]$ and the imaginary part therefore can be interpreted as time. Then the imaginary parts τ_k of the zeros resemble those times for which the overlap of the initial canonical state with the time-evolved state vanishes. However, they are not connected to a single system but to a whole ensemble of identical systems in a heat bath with an initial Boltzmann distribution.

III. BEC IN POWER-LAW TRAPS

In this section, we assume a continuous single-particle density of states $\Omega(E) = E^{d-1}$ as an approximation for a d -dimensional harmonic oscillator or a $2d$ -dimensional ideal gas. For example, for the harmonic oscillator this corresponds to the limit of $\hbar\omega \rightarrow 0$ and taking only the leading term of the degeneracy of the single-particle energy levels. The one-particle partition function is given by the Laplace transformation

$$Z_1(\mathcal{B}) = \int dE E^{d-1} \exp(-BE) = (d-1)! \mathcal{B}^{-d}. \quad (3.1)$$

The canonical partition function for N noninteracting bosons can be calculated by the following recursion [6]:

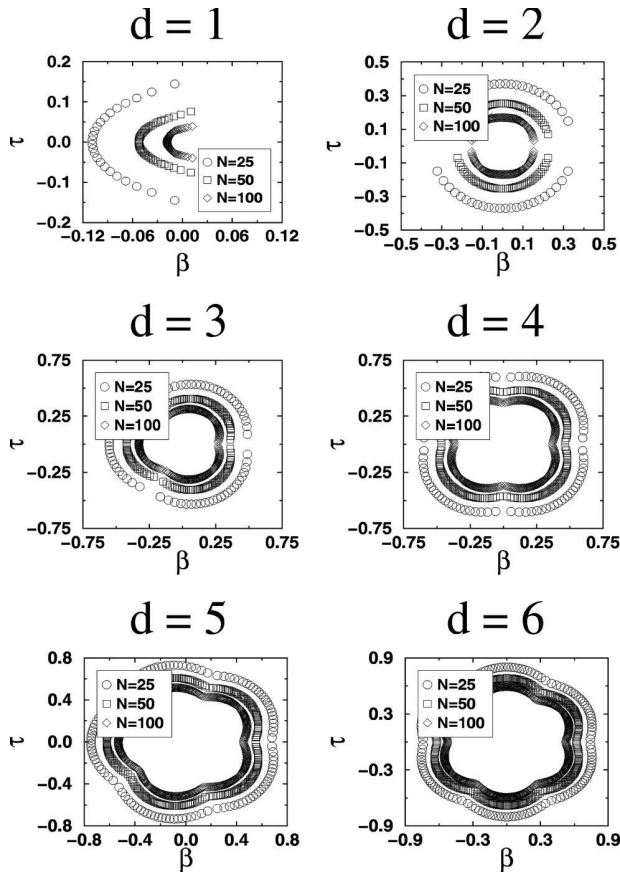


FIG. 4. Distribution of zeros for Bose-Einstein condensates with continuous one-particle density of states $\Omega(E) = E^{d-1}$ for $d=1-6$.

$$Z_N(\mathcal{B}) = \frac{1}{N} \sum_{k=1}^N Z_1(k\mathcal{B}) Z_{N-k}(\mathcal{B}), \quad (3.2)$$

where $Z_1(k\mathcal{B}) = \sum_i \exp(-k\mathcal{B}\epsilon_i)$ is the one-particle partition function at temperature $k\mathcal{B}$ and $Z_0(\mathcal{B}) = 1$. For small particle numbers, this recursion works fine, even though its numerical effort grows proportional to N^2 .

With Eq. (3.1) as Z_1 , Eq. (3.2) leads to a polynomial of order N in $(1/\mathcal{B})^d$ for Z_N , which can be easily generated using MAPLE or MATHEMATICA. The zeros of this polynomial can be found by standard numerical methods.

Figure 4 displays the zeros of the N -particle partition function for $d=1-6$ in the complex temperature plane for particle numbers $N=25, 50$, and 100 . For $d=2-6$, the zeros approach the positive real axis with increasing particle number and are shifted to higher temperatures, which is already an indicator of phase transitions. For $d=1$, the zeros approach the real axis only at negative temperature. This behavior is consistent with the usual prediction that there is no Bose-Einstein condensation for the one-dimensional harmonic oscillator and the two-dimensional ideal Bose gas [10].

The symmetry of the distributions of zeros is due to the fact that Z_N is a polynomial in \mathcal{B}^{-d} . For this reason, it can be inferred that for $d \rightarrow \infty$ the zeros lie on a perfect circle.

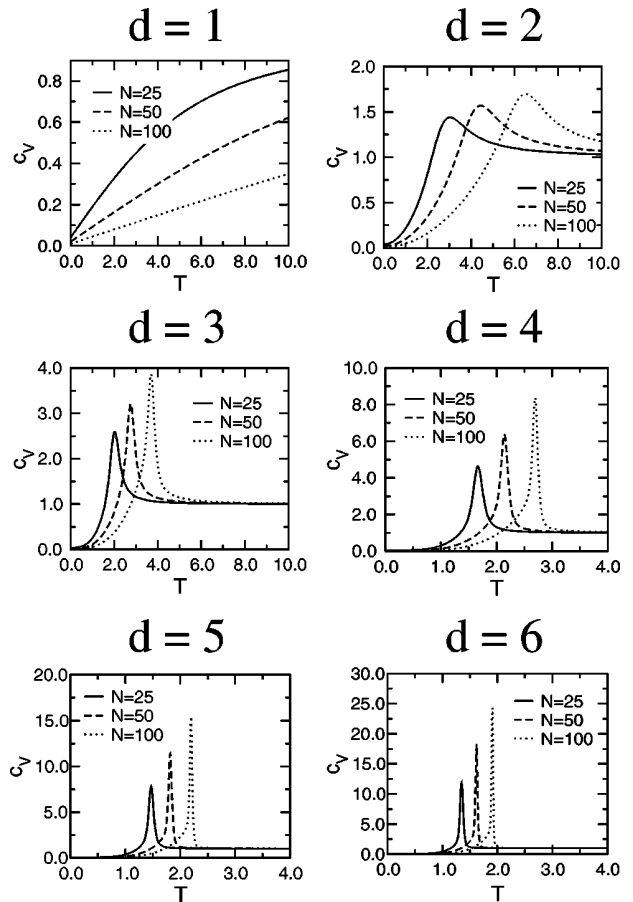


FIG. 5. Specific heat scaled by dN of Bose-Einstein condensates with continuous one-particle density of states for $d=1-6$.

Figure 5 shows the corresponding specific heats calculated using Eq. (2.3). As expected, for $d=1$ the specific heat has no hump and approaches with increasing temperature the classical value. We therefore exclude the analysis of $d=1$ from the discussions below. For $d=2-6$, the specific heats show humps or peaks, which get sharper with increasing d and increasing particle number. However, from these smooth curves the orders of the phase transition cannot be deduced.

In Fig. 6, the classification parameters α, γ, τ_1 defined above are plotted for two to six dimensions and particle numbers up to $N=100$. For all values of d , the parameter α is only a slightly varying function of N and approaches very fast an almost constant value. Since α is the primary classification parameter, from Fig. 6(a) we can directly infer that the $d=2$ system exhibits a third-order phase transition ($\alpha > 1$) while the transition for all higher dimensions is of second order ($0 \leq \alpha \leq 1$). For $N=50$, the dependence of α on d is plotted in Fig. 7(a). Since α decreases rather rapidly with increasing d , it can be speculated that systems corresponding to a large d exhibit a phase transition that is almost of first order. As mentioned above, for finite systems even values $\alpha \leq 0$ cannot be excluded for mathematical reasons. We note that two-dimensional Bose gases are an interesting and growing field of research. As is well known, the ideal free Bose gas in two dimensions ($d=1$) does not show a phase

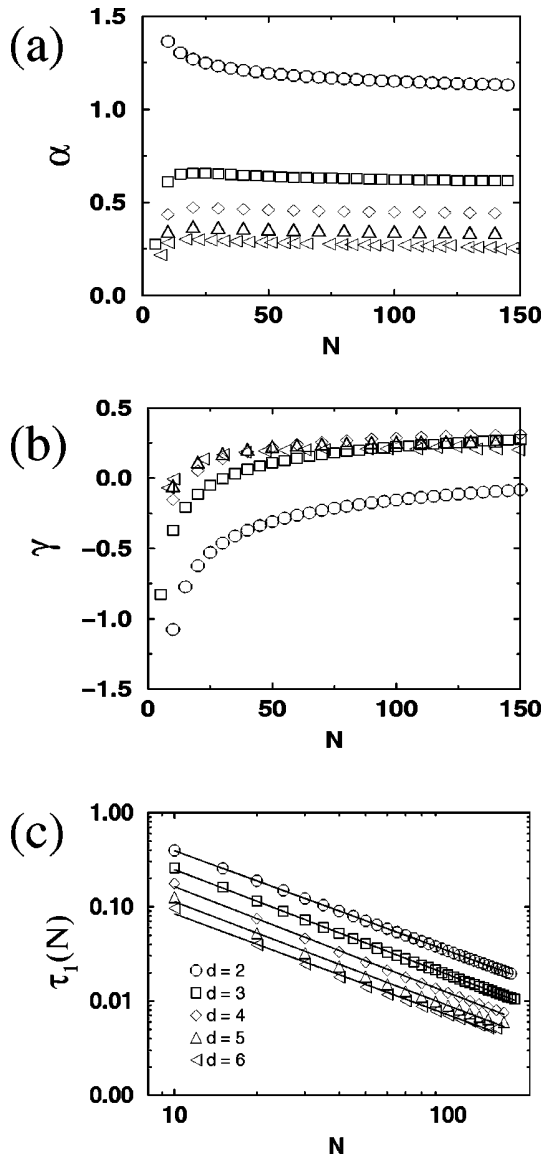


FIG. 6. Classification parameters α , γ , and τ_1 for $d=2-6$ versus particle numbers N .

transition due to thermal fluctuations that destabilize the condensate [14]. Switching on a confining potential greatly influences the properties of the gas, the thermal fluctuations are suppressed, and the gas will show Bose-Einstein condensation. Recent experiments [12] have shown that Bose-Einstein

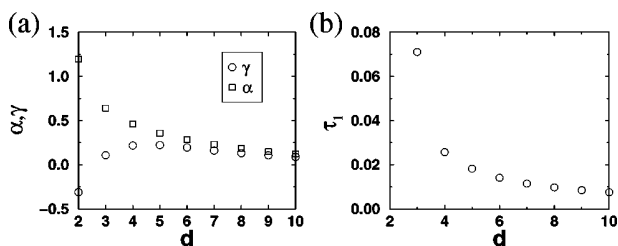


FIG. 7. Classification parameters for $N=50$ for different densities of states $\Omega(E)=E^{d-1}$ and $d=2-10$.

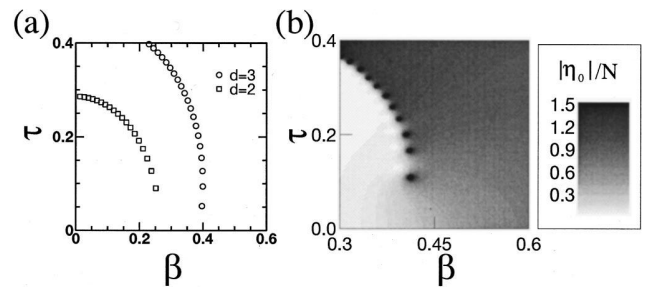


FIG. 8. Comparison between calculated zeros of the canonical partition function for three-dimensional trap geometries with (a) a continuous single-particle density of states and (b) discrete energy levels for $N=40$.

condensation is possible even though it is called a quasicondensate. In our notion, the quasicondensate is just a third-order phase transition. Thus, our results are in complete agreement with recent experiments and earlier theoretical work. An interesting question in this respect is whether the order of the transition changes for $d=2$ in the limit $N \rightarrow \infty$. Additional calculations for larger N , which are not printed in Fig. 6, indicate that α approaches 1 or might even get smaller. Note that $d=2$ is equivalent to a hypothetical four-dimensional ideal Bose gas or bosons confined in a two-dimensional parabolic trap. Our results indicate that the order of the phase transition depends sensitively on d for values around 2. This might be the reason why phase transitions in three space dimensions are sometimes classified as second- and sometimes as third-order phase transitions.

The parameter τ_1 is a measure of the finite size of the system, i.e., the scaling behavior of τ_1 as a function of N is a measure of how fast a system approaches a true n th-order phase transition in the Ehrenfest sense. The N dependence of τ_1 is displayed in Fig. 6(c). The scaling behavior can be approximated by $\tau_1 \sim N^{-\delta}$ with δ ranging between 1.06 and 1.12 for $d=2-6$.

The d dependence of the classification parameter is visualized in Fig. 7 for 50 particles. For this system size, we found $\alpha \sim d^{-4/3}$ and $\tau_1 \sim d^{-4/3}$.

The results presented above for continuous single-particle densities of states $\Omega(E)=E^{d-1}$ are obtained within semianalytical calculations. In order to compare these results to systems with a discrete level density, we adopt as a reference system the three-dimensional harmonic oscillator with the partition function given by

$$Z(\mathcal{B}) = \sum_{n=0}^{\infty} \frac{(n+2)(n+1)}{2} \exp(-\mathcal{B}(n+3/2)), \quad (3.3)$$

with $\hbar = \omega = k_B = 1$.

Figure 8(a) displays the zeros of the partition function (3.1) for $d=2$ and $d=3$. Figure 8(b) displays a contour plot of the absolute value of the ground-state occupation number $\eta_0(\mathcal{B}) = -(1/\mathcal{B}) \partial_{\epsilon_0} Z(\mathcal{B})/Z(\mathcal{B})$ with Z given by Eq. (3.3) calculated using an alternative recursion formula [4]. The zeros of Z are poles of η_0 and are indicated by dark spots in this figure.

Analyzing the distribution of zeros consolidates our speculation that the order of the phase transition depends sensitively on d . The distribution of zeros behaves like the above calculated values for $d=2$ but quantitatively like $d=3$. Since the degeneracy of the three-dimensional harmonically confined ideal Bose gas is a second-order polynomial, the quadratic term is not the only term that must be taken into account. The linear term becomes dominant for lower temperatures, so for very low temperatures the best approximation of a continuous one-particle density of states is $\Omega(E)=E$. The parameter α supports this statement [9], i.e., α resides in a region above 1, whereas the parameter γ behaves like the $d=3$ case. Finally, the parameter τ_1 , which is a measure for the discreteness of the system, shows a $\tau_1 \sim N^{-0.96}$ dependence that is comparable to the one for $d=2$. Thus, for small systems the phase transition is of third order; it can be speculated whether it becomes a second-order transition in the thermodynamic limit.

Our calculations are in very good agreement with recent theoretical works, not only qualitatively but also quantitatively [15,16]. Comparing the *critical* temperature, which we defined in Sec. II, with the usually utilized temperature of the peak of the specific heat $\beta(C_{V,\max})$ or the grand canonically calculated $T_C \sim N^{1/3}$ confirms our approach. In Fig. 9, three possible definitions of the critical temperature are given that all coincide in the thermodynamic limit. All definitions show a $\beta \sim N^{-\rho}$ dependence with ρ ranging between $\frac{2}{5}$ and $\frac{1}{3}$.

IV. CONCLUSION

Starting with the old ideas of Yang and Lee and Grossmann *et al.*, we have developed a classification scheme for phase transitions in finite systems. Based on the analytic continuation of the inverse temperature β into the complex

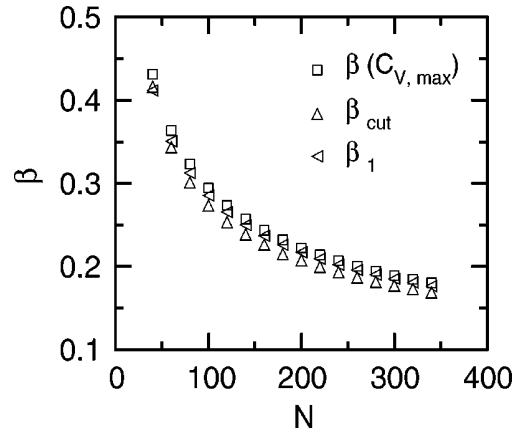


FIG. 9. Comparison between three different approaches to define a critical temperature for phase transitions in finite systems.

plane, we have shown the advantages of this approach. The distribution of the so-called Fisher zeros \mathcal{B}_k draws enlightening pictures even for small systems, whereas the usually referred to thermodynamic properties such as the specific heat fail to classify the phase transitions properly. The classification scheme presented in this paper enables us to name the order of the transition in a nonambiguous way. The complex parts τ_k of the zeros \mathcal{B}_k resemble times for which a whole ensemble of identical systems under consideration in a heat bath with an initial Boltzmann distribution loses its memory.

We have applied this to ideal noninteracting Bose gases confined in power-law traps. We have found that the order of the phase transition sensitively depends on the single-particle density of states generated by the confining potential. The distribution of zeros exactly reveals the order of the phase transition in finite systems.

-
- [1] S. Bose, Z. Phys. **26**, 178 (1924); A. Einstein, Sitzungsber. K. Preuss. Akad. Wiss. **1925**, 3 (1925).
- [2] M. H. Anderson, J. R. Ensher, M. R. Matthews, C. E. Wieman, and E. A. Cornell, Science **269**, 198 (1995); C. C. Bradley, C. A. Sackett, J. J. Tollett, and R. G. Hulet, Phys. Rev. Lett. **75**, 1687 (1995); K. B. Davis, M.-O. Mewes, M. R. Andrews, N. J. van Druten, D. S. Durfee, D. M. Kurn, and W. Ketterle, *ibid.* **75**, 3969 (1995).
- [3] D. Stamper-Kurn, M. R. Andrews, A. P. Chikkatur, S. Inouye, H.-J. Miesner, J. Stenger, and W. Ketterle, Phys. Rev. Lett. **80**, 2027 (1998).
- [4] P. Borrmann, J. Harting, O. Mülken, and E. Hilf, Phys. Rev. A **60**, 1519 (1999).
- [5] S. Grossmann and M. Holthaus, Phys. Rev. Lett. **79**, 3557 (1997); S. Grossmann and M. Holthaus, Opt. Express **1**, 262 (1997); P. Navez *et al.*, Phys. Rev. Lett. **79**, 1789 (1997); M. Gajda and K. Razazewski, *ibid.* **78**, 2686 (1997).
- [6] P. Borrmann and G. Franke, J. Chem. Phys. **98**, 2484 (1993).
- [7] S. Grossmann and W. Rosenhauer, Z. Phys. **207**, 138 (1967); **218**, 437 (1969); S. Grossmann and W. Rosenhauer, *ibid.* **218**, 449 (1969).
- [8] M. E. Fisher, in *Lectures in Theoretical Physics*, edited by W. E. Brittin (University of Colorado Press, Boulder, 1965), Vol. 7c.
- [9] P. Borrmann, O. Mülken, and J. Harting, Phys. Rev. Lett. **84**, 3511 (2000).
- [10] V. Bagnato and D. Kleppner, Phys. Rev. A **44**, 7439 (1991).
- [11] H. Perez Rojas, Phys. Lett. A **234**, 13 (1997); S. Pearson, T. Pang, and C. Chen, Phys. Rev. A **58**, 4811 (1998); Z. Yan, *ibid.* **59**, 4657 (1999).
- [12] A. I. Safonov *et al.*, Phys. Rev. Lett. **81**, 4545 (1998).
- [13] C. N. Yang and T. Lee, Phys. Rev. **97**, 404 (1952); **87**, 410 (1952).
- [14] W. J. Mullin, J. Low Temp. Phys. **106**, 1405 (1997); **110**, 167 (1997); F. Dalfovo, S. Giorgini, L. P. Pitaevskii, and S. Stringari, Rev. Mod. Phys. **71**, 463 (1999).
- [15] N. L. Balazs and T. Bergeman, Phys. Rev. A **58**, 2359 (1998).
- [16] S. Grossmann and M. Holthaus, Z. Naturforsch. A. Phys. Sci. **50**, 921 (1995).

6

Origins of Phase Transitions in Small Systems

**O. Mülken, H. Stamerjohanns
and P. Borrmann**

Physical Review E **64**, 047105 (2001) in press

The Origins of Phase Transitions in Small Systems

Oliver Mülken and Heinrich Stamerjohanns

Department of Physics, Carl von Ossietzky University Oldenburg, D-26111 Oldenburg, Germany

Peter Borrmann

IBM UBG, Am Sandtorkai 73, 20457 Hamburg, Germany

(Dated: June 25, 2001)

The identification and classification of phases in small systems, e.g. nuclei, social and financial networks, clusters, and biological systems, where the traditional definitions of phase transitions are not applicable, is important to obtain a deeper understanding of the phenomena observed in such systems. Within a simple statistical model we investigate the validity and applicability of different classification schemes for phase transitions in small systems. We show that the whole complex temperature plane contains necessary information in order to give a distinct classification.

PACS numbers: 05.70.F, 36.40.E, 64.60.C

The thermodynamics of small systems, e.g. Bose-Einstein condensates in magneto-optical traps [1–3], the nuclear liquid-gas transition observed by multifragmentation in heavy ion reactions [4–6], and the solid-liquid phase transition of sodium clusters [7–9], have gained increasing interest over the last few years. Because these systems are far away from the thermodynamic limit the standard tools for the description of phase transitions are not applicable and new concepts are needed. Within the last few years several classification schemes for phase transitions in finite systems have been proposed [10]. In this Letter we compare these classification schemes by means of a simple statistical models for atomic clusters and show that graveling transitions occurring in these models can only completely understood by considering the whole complex temperature plane.

Among others Gross *et al.* have suggested a microcanonical treatment [10–12], where phase transitions of different order are distinguished by the curvature of the entropy $S = k_B \ln \Omega(E)$. According to their scheme a *back-bending* in the microcanonical caloric curve $T(E) = 1/\partial_E \ln(\Omega(E))$, i.e. the appearance of negative heat capacities, is a mandatory criterion for a first order transition. Caloric curves without back-bending, where the associated specific heat shows a hump, are classified as higher order transitions.

From classical statistical mechanics it is clear that the back-bending feature is forbidden in the thermodynamic limit by the van Hove theorem [13]. Since the canonical and the microcanonical caloric curves must give the same results in this limit and the canonical caloric curve is proportional to the mean-squared energy fluctuations the microcanonical caloric curve cannot exhibit a back-bending. However, in small systems necessary and sufficient conditions for this type of microcanonical caloric curves have been derived by Wales *et al.* [14, 15]. An analysis of thermodynamic stability has gained that a loop in the microcanonical caloric curve with turning points $T_m > T_f$ occurs if the entropy S is bimodal for canonical temperatures in this range. As an equivalent condition the authors showed that neglecting phase space regions

corresponding to intermediate compositions, i.e. solidlike and liquidlike forms, also result in a back-bending.

We have proposed a classification scheme based on the distribution of zeros of the canonical partition function in the complex temperature plane [16]. The classical partition function

$$Z(\beta) = \left(\frac{1}{2\pi\beta} \right)^{3N/2} \int dx^{3N} \exp(-\beta V(x)) \quad (1)$$

can be factored into a product of the kinetic part and a product depending on the zeros $\mathcal{B}_k = \beta_k + i\tau_k$, with $\mathcal{B}_{-k} = \mathcal{B}_k^*$ of this integral function in the complex temperature plane,

$$Z(\beta) = \left(\frac{1}{2\pi\beta} \right)^{3N/2} \prod_{k=-M}^M \left(1 - \frac{\beta}{\mathcal{B}_k} \right) \exp \left(\frac{\beta}{\mathcal{B}_k} \right). \quad (2)$$

Phase transitions then can be classified by a set of three parameters (α, γ, τ_1) , describing the distribution of zeros close to the real axis, where $\gamma = \tan \nu$ is the crossing angle between the real axis and the line of zeros, and α is determined from the approximated density of zeros $\phi(\tau) \sim \tau^\alpha$ on this line. For infinite systems it has been exactly shown that $\alpha = 0$, $\gamma = 0$ and $\tau_1 = 0$ corresponds to a first order phase transition, while $\alpha > 0$ corresponds to a higher order phase transition [17]. For finite systems τ_1 is always greater than zero reflecting the size of the system. The classification scheme can be extended to values of $\alpha < 0$ also being interpreted as first order phase transitions. This scheme sensitively reproduces the space dimension and particle number dependence of the transition order in Bose Einstein condensates [18] and the first order nature of the nuclear multifragmentation phase transition [19].

The differences between both schemes can be revealed within a simple statistical model for atomic clusters. A harmonic superposition of different vibrational densities of states is well established in the cluster literature [20–22]. This multiple normal-modes model describes structural transitions within small noble gas clusters by considering several isomers

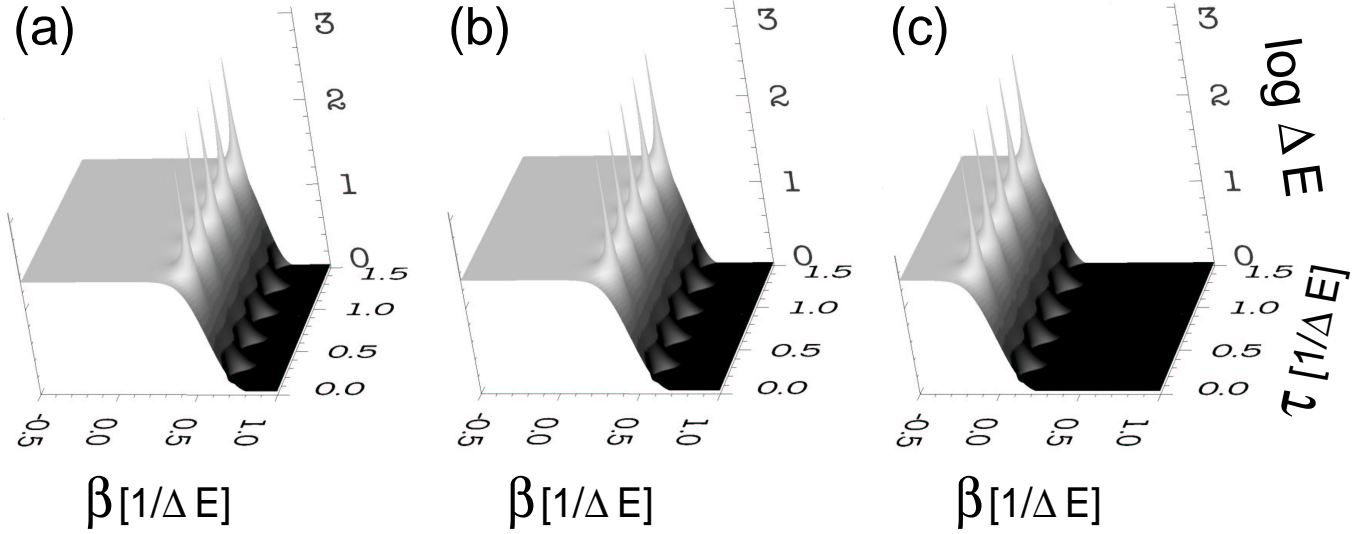


FIG. 1: Logarithm of the canonical potential energy difference expectation value $\log(\langle \Delta E \rangle)$ in the complex temperature plane for (a) $\rho_2/\rho_1 = 50000$, (b) $\rho_2/\rho_1 = 5000$, and (c) $\rho_2/\rho_1 = 0.5$. The location of the zeros of the partition function are signaled by the sharp needles. In all cases the distributions of zeros indicate first order phase transitions.

and the vibrational eigenfrequencies of the isomers. For a two isomer system the partition function can be written as

$$\begin{aligned} Z(\beta) &= \sum_{i=1}^2 \sigma_i \exp(-\beta E_i) \prod_{j=1}^{3N-6} \frac{2\pi}{\beta \omega_{ij}} \\ &= \beta^{-(3N-6)} (\rho_1 \exp(-\beta E_1) + \rho_2 \exp(-\beta E_2)), \end{aligned} \quad (3)$$

where the ω_{ij} are the normal modes of isomer i and the σ_i are the permutational degeneracies of the isomers and $\rho_i = \sigma_i \prod_{j=1}^{3N-6} \frac{2\pi}{\omega_{ij}}$. The zeros of Z

$$\beta_k = (\ln(\rho_2/\rho_1) + i(2k+1)\pi) / \Delta E, \quad (4)$$

lie on a straight line and are equally spaced yielding $\alpha = \gamma = 0$ thus implying a first order phase transition in any case ($\Delta E = E_2 - E_1$) (see Figure 1). It is important to note, that with increasing system size the energy difference between the isomers will also increase, thus τ_1 approaches zero. The microcanonical caloric curve $T(E) = 1/\partial_E \ln(\Omega(E))$ for this model can be calculated via the inverse Laplace transform $\Omega(E) = \mathcal{L}^{-1}\{Z(\beta)\}$. Fig. 2 shows that the back-bending arrogated in the Gross scheme for a first order phase transition can be tuned in an out by variation of the model parameters.

The kinetic part of the partition function $\beta^{-(3N-6)}$ plays the crucial role. If this is taken into account the microcanonical caloric curves change dramatically, whereas this part has no effect on the distribution of zeros (the particle number dependence of the canonical partition function is not only reflected by the kinetic part itself but also implicitly by the ground state energies). The change in the topology of the configuration space or equivalently configurations space regions with significantly changing vibrational entropies seems to be a necessary condition for phase transitions in small systems. Similar results have been pointed out by Franzosi

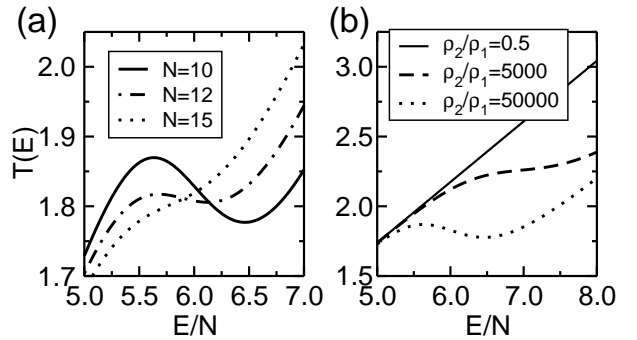


FIG. 2: Microcanonical caloric curves for the multiple normal-modes model with energy difference between the isomers $\Delta E = 20$. For **a**) $N=10, 12$, and 15 and constant $\rho_2/\rho_1 = 50000$ the back-bending is manifest for $N = 10$, can be tuned out by increasing the particle number, and disappears for N as low as $N = 15$. In **b**) for constant $N = 10$ the back-bending can be tuned out by decreasing the ratio ρ_2/ρ_1 .

et al. [23, 24]. Equivalent findings are those of Wales *et al.* [14, 15]. Utilizing also the harmonic superposition of vibrational densities of states and assuming "coexistence" of liquidlike and solidlike phases the loop in the microcanonical caloric curve is also tunable by variations of system-inherent parameters. Especially the mean difference in the potential energy of both phases correspond to variations of ρ_2/ρ_1 in our model.

Within classical statistical mechanics the kinetic part of canonical partition function is separable and the partition function splits up into a kinetic and a potential part which can be handled independently. Within the microcanonical ensemble structural phase transition might be *washed out* or hidden by the kinetic energy contributions to the entropy.

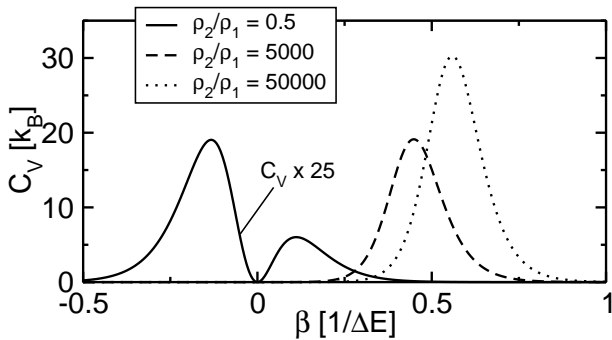


FIG. 3: Canonical specific heat reduced by the kinetic contribution for the same values of ρ_2/ρ_1 as in Figure 1. For values with ρ_2/ρ_1 larger than 1 the expected signals of a first order phase transition are seen. The value $\rho_2/\rho_1=0.5$ corresponds formally to a first order phase transition at negative temperature. This *graveling* transition exhibits at positive temperature a very weak hump in the specific heat (the graph is amplified by a factor of 25).

A very interesting feature of the multiple normal-modes model occurs in the case where the isomer with the lower ground state energy has a larger vibrational entropy (see Fig. 1 (c)). In this case formally a first order phase transition at negative temperatures occurs. The structural transition between the isomers, which occurs when the temperature is increased is accompanied by a drop in the vibrational entropy. This is a *graveling* transition with a significantly smaller signal in the specific heat than that of the *normal* transition (see Fig. 3). Fig.3 and Fig.4 show i) that the zeros in the complex temperature plane sensitively detect phase transitions and ii) it is very important to use β as the natural variable since only this yields continuous pictures of thermodynamic properties.

In conclusion we have found that the classification of phase

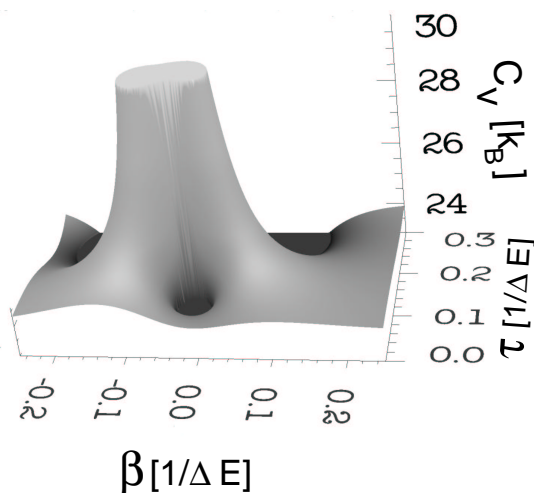


FIG. 4: Specific heat in the complex temperature plane for $\rho_2/\rho_1=0.5$. The figure displays how the interplay of the zero and the pole of the specific heat influences the behaviour of the specific heat curve at positive temperatures.

transitions in small systems based on the curvature of the microcanonical caloric curves seems to be not rigorous enough to make distinct statements about the order. In the *Zero*-classification scheme the potential energy surface characterizes the phase behavior of the system, while in the scheme of Gross the density of states is the characterizing quantity. We have shown that the investigation of the whole complex temperature plane adds a valuable amount of information in order to classify phase transitions in small systems.

REFERENCES

- [1] M. Anderson, et al., *Science* **269**, 198 (1995).
- [2] C. Bradley, C. Sackett, J. Tollett, and R. Hulet, *Phys. Rev. Lett.* **75**(9), 1687 (1995).
- [3] K. Davis, et al., *Phys. Rev. Lett.* **75**(22) (1995).
- [4] R. Nebauer, A. J., and the INDRA collaboration, *Nucl. Phys. A* **658**, 67 (1999), and references therein.
- [5] J. Pochodzalla, et al., *Phys. Rev. Lett.* **75**, 1040 (1995).
- [6] Y.-G. Ma, et al., *Phys. Lett. B* **390**, 41 (1997).
- [7] M. Schmidt, et al., *Phys. Rev. Lett.* **79**, 99 (1997).
- [8] M. Schmidt, B. von Issendorf, and H. Haberland, *Nature* **393**, 238 (1998).
- [9] H. Cheng, X. Li, R. L. Whetten, and R. S. Berry, *Phys. Rev. A* **46**, 791 (1992).
- [10] D. H. E. Gross and E. Votyakov, *E. Phys. J. B* **15**, 115 (2000).
- [11] D. H. E. Gross, *Phys. Rep.* **279**, 119 (1995).
- [12] D. H. E. Gross, M. Madjet, and O. Schapiro, *Z. Phys. D* **39**, 75 (1997).
- [13] L. van Hove, *Physica* **15**, 951 (1949).
- [14] D. J. Wales and R. S. Berry, *Phys. Rev. Lett.* **73**, 2875 (1994).
- [15] D. J. Wales and J. P. K. Doye, *J. Chem. Phys.* **103**, 3061 (1995).
- [16] P. Borrmann, O. Mülken, and J. Harting, *Phys. Rev. Lett.* **84**, 3511 (2000).
- [17] S. Grossmann and W. Rosenhauer, *Z. Phys.* **218**, 437 (1969).
- [18] O. Mülken, P. Borrmann, J. Harting, and H. Stamerjohanns, *Phys. Rev. A* **64**, 013611 (2001).
- [19] O. Mülken and P. Borrmann, *Phys. Rev. C* **63**, 023406 (2001).
- [20] G. Franke, E. Hilf, and P. Borrmann, *J. Chem. Phys.* **98**, 3496 (1993).
- [21] D. J. Wales, J. P. K. Doye, M. A. Miller, P. N. Mortenson, and T. R. Walsh, *Adv. Chem. Phys.* **115**, 1 (2000), and references therein.
- [22] D. J. Wales, *Mol. Phys.* **78**, 151 (1993).
- [23] R. Franzosi, L. Casetti, L. Spinelli, and M. Pettini, *Phys. Rev. E* **60**, 5009 (1999).
- [24] R. Franzosi, M. Pettini, and L. Spinelli, *Phys. Rev. Lett.* **84**, 2774 (1999).

7 **Deceptive Signals of phase transitions in Small Magnetic Clusters**

**H. Stamerjohanns, O. Mülken
and P. Borrmann**

arxiv/cond-mat 0107176 (2001),
to be published in Phys. Rev. Lett.

Deceptive signals of phase transitions in small magnetic clusters

Heinrich Stamerjohanns,¹ Oliver Mülken,¹ and Peter Borrmann²¹Department of Physics, Carl von Ossietzky University Oldenburg, D-26111 Oldenburg, Germany²IBM Unternehmensberatung, Am Sandtorkai 73, 20457 Hamburg, Germany

(Dated: October 9, 2001)

We present an analysis of the thermodynamic properties of small transition metal clusters and show how the commonly used indicators of phase transitions like peaks in the specific heat or magnetic susceptibility can lead to deceptive interpretations of the underlying physics. The analysis of the distribution of zeros of the canonical partition function in the whole complex temperature plane reveals the nature of the transition. We show that signals in the magnetic susceptibility at positive temperatures have their origin at zeros lying at negative temperatures.

PACS numbers: 64.60.-i, 36.40.Ei, 05.70.Fh

Experiments on Bose-Einstein condensation [1–3] or the experimental determination of structural, electronic and thermal properties of clusters [4–6] are prototypes of physical investigations of transitions in small systems. Intuitively phase transitions in such systems do exist. While the atomic structure at low temperatures is more or less rigid, at high temperatures the atoms move resembling a liquid drop. But the theoretical description is complicated since the thermodynamic functions of clusters do not show singularities at the transition point. Phase changes are seen in blurred slopes or humps. To have the physical concept of phase transitions and their properties of bulk material in mind and apply it to interpret the smooth thermodynamic functions for small systems, e.g. clusters, of a given size accordingly and assign a “first” or “second” order phase transition may be inconclusive. Despite the ambiguity in these signals, it is still reasonable to attribute an order to phase changes in small systems because fundamental differences between the kind of the transitions such as the existence of metastabilities for first-order transitions still persist. Therefore, various approaches for the classification of phase transitions in small systems have been developed which have to coincide in the thermodynamic limit and should be mathematically rigorous.

Gross *et al.* have proposed a microcanonical treatment, where phase transitions are distinguished by the curvature of the entropy $S(E)$ [7, 8]. If $S(E)$ has a convex intruder, i.e. the microcanonical caloric curve $T(E)$ shows a backbending, the phase transition is assumed to be of first order. Franzosi *et al.* have started by investigating the topology of the potential energy surface and established a connection between topological changes and phase transitions [9, 10]. However, they are not able to determine the order of the phase transition. Recently we have proposed a classification scheme based on the distribution of zeros of the analytically continued canonical partition function $Z(\mathcal{B})$, with $\mathcal{B} = \beta + i\tau$ ($\beta = 1/T$), in the complex temperature plane [11–14].

The basic principle of the description of phase transitions by the zeros of the partition function is the *product theorem of Weierstrass* and the *theorem of Mittag-Leffler* which relate integral functions to their zeros [15]. Applying these theorems,

the canonical partition function can be written as

$$Z(\beta) = \left(\frac{1}{2\pi\beta}\right)^{3N/2} \int d^{3N}q \exp[-\beta V(q)] \quad (1)$$

$$= \left(\frac{1}{2\pi\beta}\right)^{3N/2} \prod_{k=-M}^M \left(1 - \frac{\beta}{\mathcal{B}_k}\right) \exp\left(\frac{\beta}{\mathcal{B}_k}\right). \quad (2)$$

We assume the zeros to lie on a line with a density $\phi(\tau) \sim \tau^\alpha$ and to have a crossing angle ν with the plummet on the real temperature axis ($\gamma = \tan \nu$). Together with the imaginary part τ_1 of the first zero \mathcal{B}_1 this leads to a distinct classification of phase transitions in small systems. For zeros perpendicular to the real axis with equal or increasing spacing, i.e., $\alpha \leq 0$ and $\gamma = 0$, the transition is of first order, for $0 < \alpha < 1$ and arbitrary γ as well as for $\gamma \neq 0$ and $\alpha \leq 0$ of second order, see Fig. 1. The imaginary part τ_1 reflects the “discreteness” of the system. Thus, in the thermodynamic limit we have $\tau_1 \rightarrow 0$ and our scheme coincides with the scheme given by Grossmann and coworkers [16].

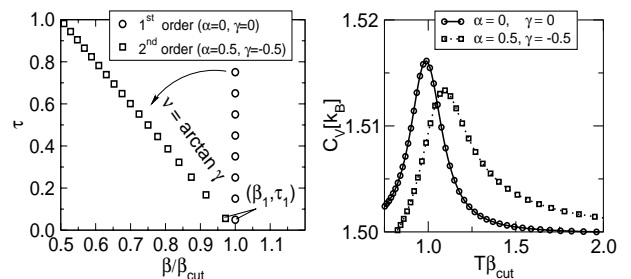


FIG. 1: Examples of distributions of zeros for 1st and 2nd order phase transitions along with the corresponding specific heat, calculated as functions of the zeros.

We utilize small magnetic clusters exposed to an external magnetic field in order to show how the common treatment of phase transitions in small systems like the identification by humps of response functions eventually leads to misinterpretations of physical properties.

Metal clusters have the intriguing property that they occur as different isomers with almost equal ground state energies

but very different magnetic moments and different geometries [17, 18]. For simplicity, we consider in our model two isomers with magnetic moments $\mu_1 = 1\mu_B$ and $\mu_2 = 10\mu_B$, and their ground state energy difference $\Delta E = E_0(2) - E_0(1) = 1$ meV. In the presence of an external magnetic field H pointing in z -direction the partition function reads

$$Z(\beta) = \sum_{i=1}^2 \exp[-\beta E_0(i)] \frac{2}{\beta \mu_i H} \sinh(\beta \mu_i H). \quad (3)$$

We have assumed equal vibrational energies. The two isomers can be identified by their average magnetic moment $\langle \mu \rangle$ which are calculated by standard differentiation of Eq.(3) with regard to the magnetic field

$$\langle \mu \rangle = \beta^{-1} \partial_H \ln Z(\beta) = \sum_i p_i \langle \mu_i \rangle \quad (4)$$

$$= \sum_i p_i [\mu_i \tanh^{-1}(\beta \mu_i H) - 1/(\beta H)], \quad (5)$$

where p_i is the probability of finding isomer i .

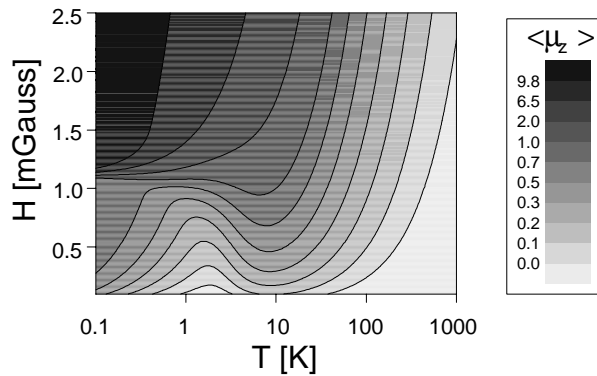


FIG. 2: Contour plot of the average magnetic moment $\langle \mu \rangle$ versus temperature T and magnetic field H . Note the non-linear scale.

This system is driven by two effects, the entropy increase due to thermal excitation and the alignment of the magnetic moments along the magnetic field. For low temperatures, there is a transition from $\langle \mu \rangle \simeq 1$ to $\langle \mu \rangle \simeq 10$ at about 1.1 mGauss, as shown in Fig. 2. At higher temperatures the magnetic field does not align the magnetic moments along the field resulting in a general decrease of $\langle \mu \rangle$.

Figure 3(a) shows the occupation probability of isomer 1 ($\mu_1 = 1\mu_B$) for different magnetic fields. At low magnetic fields, the lower energetic isomer is predominately occupied, while higher magnetic fields lower the ground state energy of isomer 2 ($\mu_2 = 10\mu_B$) and therefore the occupation is reversed. With increasing temperature the probabilities become equal. The contributions of both isomers to the total average magnetic moment $\langle \mu \rangle$ are plotted in Fig.3(b) and (c). At low temperatures, small magnetic fields align the magnetic moment of isomer 1 H . With increasing temperature the mobility of the atoms is raised which decreases the contribution of isomer 1 to $\langle \mu \rangle$.

From Fig. 2 and Fig. 3 we can infer that for temperatures $T \lesssim 1$ K and an increasing magnetic field a transition with a coexistence phase occurs (for coexistence in small systems see [19–22]). As the magnetic field is raised the contributions of both isomers to $\langle \mu \rangle$ are inverted which causes a bimodal probability distribution $P(\mu_z)$ of the order parameter μ_z . The response of the system is observable as a hump in the susceptibility $\chi = \partial_H \langle \mu \rangle$ at about 30 K for $H = 2.0$ mGauss, see Fig. 3(d).

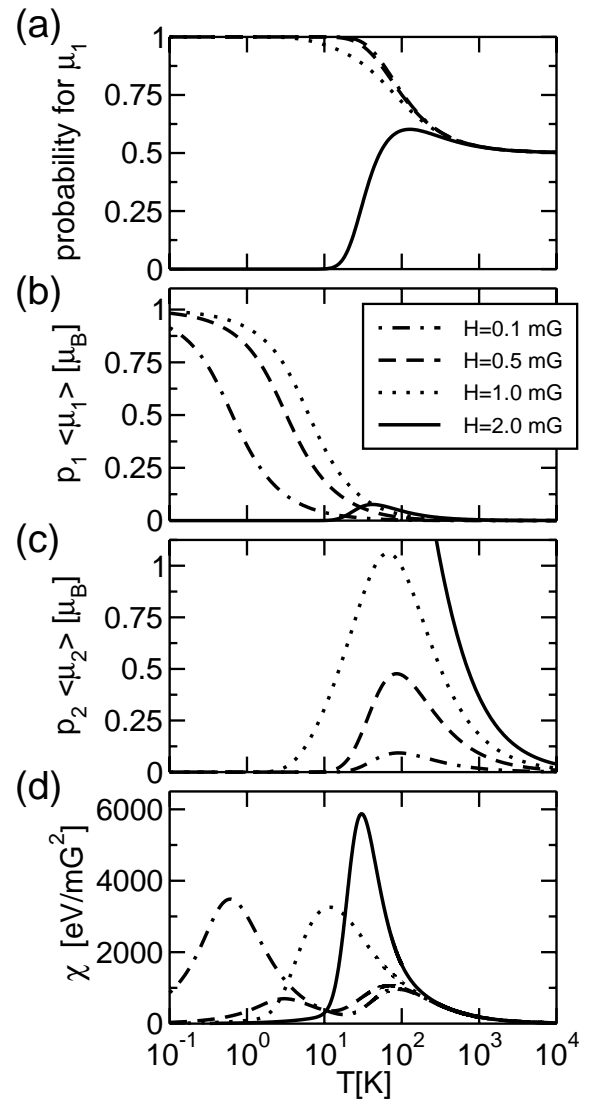


FIG. 3: Plots of physical properties versus temperature T for $H = 0.1, 0.5, 1.0,$ and 2.0 mGauss. (a) Probability for isomer 1. (b) Contribution of isomer 1 and (c) of isomer 2 to the total average magnetic moment $\langle \mu \rangle$. (d) Magnetic susceptibility χ .

However, at temperatures about 10 – 1000 K the situation is a bit more complicated. With increasing temperature and at “intermediate” fields ($H \lesssim 1.0$ mGauss) the contribution of isomer 1 decreases, while the contribution of isomer 2 to $\langle \mu \rangle$ for is raised up to $1 \mu_B$. This also results in humps of the susceptibility χ but $P(\mu_z)$ is unimodal because the magnetic

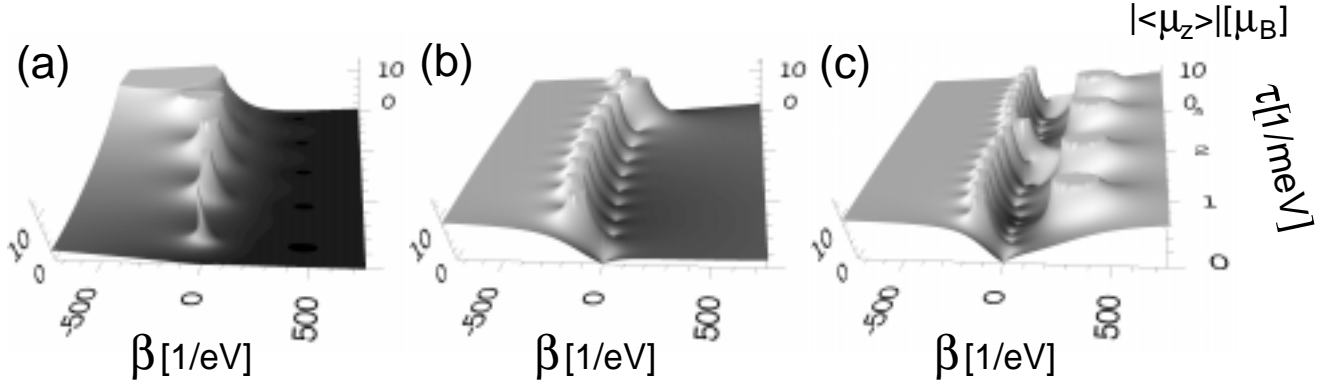


FIG. 4: The absolute value of the average magnetic moment $|\langle\mu\rangle|$ in the complex temperature plane for (a) 0.1mGauss, (b) 1.2 mGauss, and (c) 2.0 mGauss.

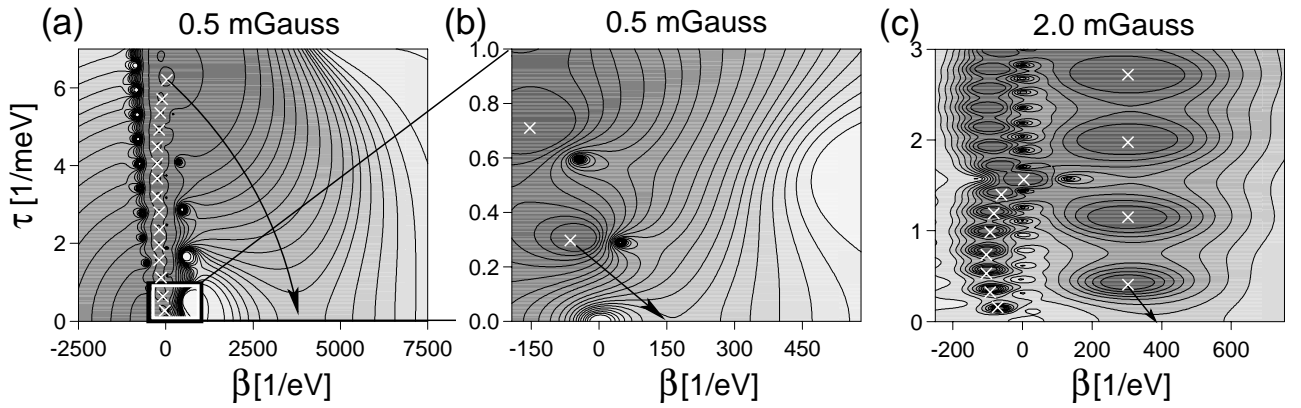


FIG. 5: Contour plot of the magnetic susceptibility χ over the complex temperature plane, (a) for $H = 0.5$ mGauss, (b) displays a close-up of ca. one tenth of this plane, and (c) for $H = 2.0$ mGauss. The white crosses indicate the location of the poles of χ . The arrows are a guide to the eye and visualize the "radiation" of the poles.

moments of the $10\mu_B$ isomer are less aligned along the magnetic field. Since the first effect can be regarded as pure magnetic field driven, it is not clear whether one should attribute the humps for $H \lesssim 1.0$ mGauss to a magnetic field effect or to a temperature effect. The "coexistence" observable in the contributions of both isomers to $\langle\mu\rangle$ is fundamentally different, it would be more correct to associate this with thermal excitation.

Magnetic clusters are finite spin-systems. Such systems, if their energy has an upper limit, can show an inverse change of entropy with respect to energy corresponding to negative inverse temperatures, $\beta = 1/T = \partial_E S(E) = \partial_E \ln \Omega(E)$ with $\Omega(E)$ being the density of states. Note, that negative temperatures are attributed to the *spin temperature* of the system. Negative temperatures have been measured, e.g. in LiF-crystals [23–25] by decoupling the spin temperature from the kinetic energy contribution. The spin-lattice relaxation time is large enough (up to hours) to assure that the spin system is thermally stable and thus can come to equilibrium [26].

Obviously, the above presented indicators of phase transition thwart the classification *and* to some extent the distinction

between different phase transitions. Within the microcanonical ensemble the occurrence of negative temperatures arises naturally because T is an internal parameter in contrast to the canonical ensemble. We consider the positive *and* negative inverse temperatures within the canonical treatment to assure having sufficient information.

Figure 4 shows 3-dimensional images of the distribution of zeros of $Z(\mathcal{B})$ in the complex temperature plane. The poles of $|\langle\mu\rangle|$ coincide with the zeros of the canonical partition function $Z(\mathcal{B})$. For $H = 0.1$ mGauss only one distribution of zeros lying at negative temperatures is present (Fig. 4(a)) corresponding to the inverse occupation of the two isomers at negative temperatures. With increasing magnetic field the shape of the distribution changes (Fig. 4(b)) and the influence of the poles of $|\langle\mu\rangle|$ on the real temperature axis becomes visible. While this effect is hardly seen for $H = 0.1$ mGauss, one is not able to distinguish the isomers due to their real-temperature values of $\langle\mu\rangle$. For $H = 1.2$ mGauss and $\beta > 0$ the average magnetic moment equals $1\mu_B$, whereas we have $\langle\mu\rangle = 10\mu_B$ for negative temperatures. At higher magnetic fields a second distribution of zeros corresponding to the

structural transition between both isomers is seen.

An inspection of both distributions of zeros reveals that the structural transition is of first order, i.e., for the classification parameters we have $\alpha = \gamma = 0$. Whereas for the transition located at negative temperatures we find $\alpha > 0$ and $\gamma \neq 0$, i.e., a second-order transition, unless the magnetic field completely disappears.

Another interesting example for first-order transitions, which become second order with growing size have been found by Proykova et al. [27]. There, two transitions have been found in TeF_6 clusters. They conclude that one of them is supposed to be of first-order, which becomes continuous for larger clusters, because they find two minima in the free energy as a function of an order parameter which merge to one minimum for larger cluster sizes. The arbitrary choice of the order parameter, however, might lead to different results [22].

Figure 5 displays the the magnetic susceptibility χ within the complex temperature plane. The susceptibility is plotted versus the complex inverse temperature. The blurred peaks of χ in Fig. 3(d) can be clearly related to “radiations” of the zeros onto the real axis.

An inspection of the whole complex temperature plane reveals the origin of the two maxima of the susceptibility at $H = 0.5$ mGauss on the real axis (cmp. Fig. 3(d)). For $H = 0.5$ mGauss the hump in χ located at $T \approx 3$ K ($\beta \approx 3800$ 1/eV) has its origin in the distribution of zeros lying at negative temperatures. Also the hump at $T = 80$ K, where earlier calculations have suggested that it is also related to a structural transition [17], has its origin in this distribution of zeros. For 2.0 mGauss the distribution of zeros lying at positive temperatures contributes most to χ for real temperatures at $\beta \approx 400$ 1/eV $\hat{=}$ $T \approx 30$ K corresponding to the structural transition seen in Fig. 3(d).

Since the distribution of poles of the considered thermodynamic function (the distribution of zeros of $Z(\mathcal{B})$) is discrete the influences on the real axis might be shielded by zeros of these function. For example, the distributions of poles of $\langle \mu \rangle$ and χ are surrounded by distributions of zeros which are different for $\langle \mu \rangle$ and χ . These thermodynamic functions are analytic everywhere except at the poles and zeros. Thus, if there is a zero in the vicinity of a pole near the real axis the decrease of $\langle \mu \rangle$ or χ cannot be compensated.

In conclusion we have shown that the use of the complex inverse temperature plane has advantages to common investigations of thermodynamic functions. Within our classification scheme the order of a transition can be clearly identified. By means of a simple two-isomer model for small magnetic clus-

ters we are able to identify two different types of phase transitions. Furthermore, we found that signals in the magnetic susceptibility at positive temperatures might have their origin at negative temperatures. This also indicates that the inverse temperature is analytic at $\beta = 1/T = 0$ and therefore should be used in calculations of thermodynamic properties.

We thank E. R. Hilf for fruitful discussions and valuable comments.

-
- [1] M. Anderson, et al., *Science* **269**, 198 (1995).
 - [2] C. Bradley, C. Sackett, J. Tollett, and R. Hulet, *Phys. Rev. Lett.* **75**(9), 1687 (1995).
 - [3] K. Davis, et al., *Phys. Rev. Lett.* **75**(22) (1995).
 - [4] M. Schmidt, et al., *Phys. Rev. Lett.* **79**, 99 (1997).
 - [5] M. Schmidt, B. von Issendorf, and H. Haberland, *Nature* **393**, 238 (1998).
 - [6] M. Schmidt, et al., *Phys. Rev. Lett.* **86**, 1191 (2001).
 - [7] D. H. E. Gross, *Phys. Rep.* **279**, 119 (1995).
 - [8] D. H. E. Gross and E. Votyakov, *E. Phys. J. B* **15**, 115 (2000).
 - [9] R. Franzosi, L. Casetti, L. Spinelli, and M. Pettini, *Phys. Rev. E* **60**, 5009 (1999).
 - [10] R. Franzosi, M. Pettini, and L. Spinelli, *Phys. Rev. Lett.* **84**, 2774 (1999).
 - [11] P. Borrmann, O. Mülken, and J. Harting, *Phys. Rev. Lett.* **84**, 3511 (2000).
 - [12] O. Mülken, P. Borrmann, J. Harting, and H. Stamerjohanns, *Phys. Rev. A* **64**, 013611 (2001).
 - [13] O. Mülken and P. Borrmann, *Phys. Rev. C* **63**, 023406 (2000).
 - [14] O. Mülken, H. Stamerjohanns, and P. Borrmann, *Phys. Rev. E* **64**, 047105 (2001).
 - [15] E. Titchmarsh, *The Theory of Functions* (Oxford University Press, 1964).
 - [16] S. Grossmann and W. Rosenhauer, *Z. Phys.* **207**, 138 (1967); **218**, 437 (1969); S. Grossmann and V. Lehmann, *ibid.* **218**, 449 (1969).
 - [17] P. Borrmann, B. Diekmann, E. R. Hilf, and D. Tománek, *Surface Review and Letters* **3**, 463 (1996).
 - [18] P. Borrmann, et al., *J. Chem. Phys.* **111**, 10689 (1999).
 - [19] D. J. Wales and R. S. Berry, *Phys. Rev. Lett.* **73**, 2875 (1994).
 - [20] D. J. Wales and J. P. K. Doye, *J. Chem. Phys.* **103**, 3061 (1995).
 - [21] R. S. Berry, in *Theory of Atomic and Molecular Clusters*, edited by J. Jellinek (Springer, Berlin, 1999).
 - [22] D. J. Wales, et al., *Adv. Chem. Phys.* **115**, 1 (2000).
 - [23] E. Purcell and R. Pound, *Phys. Rev.* **81**, 279 (1951).
 - [24] N. Ramsey, *Phys. Rev.* **103**, 20 (1956).
 - [25] P. T. Landsberg, *Phys. Rev.* **115**, 518 (1959).
 - [26] A. Abragam and W. G. Proctor, *Phys. Rev.* **109**, 1441 (1958).
 - [27] A. Proykova, R. Radev, F.-Y. Li, and R. S. Berry, *Jour. Chem. Phys.* **110**, 3887 (1999).

Curriculum Vitae

Personal Data

Name: Heinrich Stamerjohanns
Academic degree: Dipl.-Phys.
Date of Birth: June 6th, 1968
Place of Birth: Brake/Unterweser
Nationality: German
Marital status: unmarried
Address: Hindenburgstr. 3
26122 Oldenburg
(0441) 76819
Telephone:
E-Mail: heinrich@stamerjohanns.de



Time Overview

1974 - 1988 School, Abitur, grade 1.6.
1988 - 1990 Civilian Service as emergency paramedic.
1990 - 1991 Work as programmer in Southern Germany and Canada.
1991 - 1997 University of Oldenburg (Dipl. Physics), grade "gut".
1997 - 2001 Scientific Assistant at the University Oldenburg / Institute for Science Networking.

School

1974 - 1978 Elementary School Kleibrok, Rastede.
1978 - 1980 School: Orientierungsstufe Feldbreite, Rastede.
1980 - 1984 School: Gymnasium of the KGS Rastede.
1984 - 1985 Belleville-West High School in Belleville, Illinois (USA) as foreign exchange student.
1985 - 1988 High School: Gymn. Oberstufe at KGS Rastede.
Degree: Abitur (grade: 1.6).

Work

- 8/1988 - 4/1990 Civilian service at the Johanniter-Unfall-Hilfe in Oldenburg as emergency paramedic and first aid teacher.
- 4/1990 - 10/1991 Work as programmer at the Company Franke in Donauwörth / Augsburg and Québec, Canada.
- 11/1997 - 12/2000 Scientific Assistant in the project of the Bundesministerium für Forschung und Bildung (BMBF) *Global Info, The German Digital Library*.
- 1/2001 - Scientific Assistant in the project of the Deutsche Forschungsgesellschaft (DFG) / National Science Foundation of the USA (NSF) *Open Archives* at the Institute for Science Networking, Oldenburg.

University

- 10/1991 - 7/1997 Diploma studies of physics with subsidiary subject computer science at the Carl-von-Ossietzky University Oldenburg.
Degree: Diploma Physicist (grade: gut).
- 8/1997- 9/2001 Phd studies at Prof. Dr. Dr. E. R. Hilf and Priv. Doz. Dr. Peter Borrmann, University Oldenburg.

Erklärung gemäß §8(2) der Promotionsordnung

Hiermit versichere ich, dass ich diese Arbeit selbständig verfasst und keine anderen als die angegebenen Quellen und Hilfsmittel verwandt habe.

(Heinrich Stamerjohanns)